COMPRESSED SENSING BASED IMAGE DENOISING: NOVEL PATCH-BASED COLLABORATIVE ALGORITHMS

BY

MUZAMMIL BEHZAD

A Thesis Presented to the

DEANSHIP OF GRADUATE STUDIES

KING FAHD UNIVERSITY OF PETROLEUM & MINERALS

DHAHRAN, SAUDI ARABIA

In Partial Fulfillment of the
Requirements for the Degree of

MASTER OF SCIENCE

In

ELECTRICAL ENGINEERING

January 2017

KING FAHD UNIVERSITY OF PETROLEUM & MINERALS
DHAHRAN 31261, SAUDI ARABIA

DEANSHIP OF GRADUATE STUDIES

This thesis, written by **MUZAMMIL BEHZAD** under the direction of his thesis adviser and approved by his thesis committee, has been presented to and accepted by the Dean of Graduate Studies, in partial fulfillment of the requirements for the degree of **MASTER OF SCIENCE IN ELECTRICAL ENGINEERING**.

Thesis Committee

Dr. Wail A. Mousa (Adviser)

Dr. Tareq Y. Al-Naffouri (Member)

Dr. Ali Ahmad Al-Shaikhi (Member)

Dr. Ali Ahmad Al-Shaikhi
Department Chairman

Dr. Salam A. Zummo
Dean of Graduate Studies

12/1/17
Date

"You will not enter Paradise until you believe and you will not believe until you love each other. Shall I show you something that, if you did, you would love each other? Spread peace between yourselves."

Prophet Muhammad (Peace Be Upon Him) [Sahih Muslim: Hadees No. 54]

To My Father, Mother and Siblings,
for their Endless Support, Continuous Encouragement and Unmatchable Love.

ACKNOWLEDGMENTS

First of all, I am greatly thankful to Almighty Allah *subhanahu-wa-taala*, the Most Compassionate and the Most Merciful, for making me capable of starting and completing this work. I pray to Him that the work I have done and the skills and qualities I have developed at King Fahd University of Petroleum and Minerals (KFUPM) will be used in His holy cause *inshaAllah*.

I deeply thank KFUPM for providing me the amazing opportunity to study at such a prestigious institute of great reputation and extremely high caliber. The facilities and support I have received here has greatly strengthened my skills and have helped me a lot in accomplishing my goals. I would also like to thank the Research Institute (RI) at KFUPM for partly funding my research work.

I truly acknowledge the faculty at KFUPM for their precious and valuable interaction with me. The experience of having interesting brainstorming discussions and quality learnings, both academic and non-academic, from professors of their class was absolutely awesome. I am greatly thankful to them for motivating me every time I needed.

I would also like to acknowledge the support and initial boost provided by COMSATS Institute of Information Technology (CIIT), Islamabad, Pakistan, by

giving me top notch and strong undergraduate educational background. Specifically, the guidance given by and learnings from Prof. Raja Ali Riaz, Prof. Mahmood Ashraf Khan and other faculty members played a key role in my research work here at KFUPM.

Most importantly, I would like to express my deepest gratitude to my mentor Prof. Tareq Y. Al-Nafforui for the continuous motivation, help and trust that I received from him. He always helped me in various phases of my stay at KFUPM and pushed me hard from time to time in order to reach high standards. Along with his brilliant academic skills, he is also a very humble, kind and magnificent human being and I have been profoundly enriched with his kind self. The precious lessons I learned from him will always keep me motivated and focused while achieving my goals. I would also like to deeply thank Prof. Tareq for organizing a number of funded research visits to have various interactive sessions with his research group in King Abdullah University of Science and Technology (KAUST). The experience I gathered there has also improved my skills both academically as well as socially.

I would also like to pay my kind regards and acknowledge the efforts of my respected adviser Dr. Wail A. Mousa and the chairman of electrical engineering department Dr. Ali Ahmad Al-Shaikhi for their strong support and careful reviews throughout my degree tenure that ultimately led me to write this thesis work. I am thankful to my entire thesis committee for their positive and helpful criticism that enabled me to prepare a more sharpened and polished presentation of my

work.

The milestones I have achieved with my research work would not have been possible without the help of several faculty members and colleagues. In this regard, I would like to thank Dr. Azeddine Beghdadi (University of Paris 13), Dr. Maha Shadaydeh (Hungarian Academy of Sciences) and a number of researchers from the Visual Computing Center (VCC) at KAUST. I would like to specially and deeply thank Dr. Mudassir Masood (KFUPM) and Dr. Tarig Ballal (KAUST) for their great support throughout my research phase. This research work contain a large effort put by them via their thorough reviews and suggestions.

I am thankful to my friends at KFUPM and KAUST for making this experience very beautiful and memorable for me. The extended cultural interaction I had with many friends from all around the world is cherishing for me. The unplanned sudden outings, beach sports, shopping tours and food gatherings will always remain a valuable part of memory.

I am infinitely thankful to my parents for their unmatchable love, care and support that they passed down to me. I am also grateful to my entire family and friends for their constant encouragement throughout my degree. Without this support from all you, I would not be able to complete this degree.

TABLE OF CONTENTS

LIST OF TABLES

LIST OF FIGURES

THESIS ABSTRACT

NAME: Muzammil Behzad

TITLE OF STUDY: Compressed Sensing Based Image Denoising: Novel Patch-Based Collaborative Algorithms

MAJOR FIELD: Electrical Engineering

DATE OF DEGREE: January, 2017

In this thesis, we propose novel patch-based image denoising algorithms to take care of the undesired additive white Gaussian noise (AWGN) components introduced in an image. Our algorithms are broadly classified into grayscale and color image denoising. We propose to utilize normalized Euclidean distance and correlation based grouping of patches in our algorithms. Such grouping of patches is an effective way for collaborative support-agnostic sparse reconstruction to denoise a noisy patch. For the collaboration, we stack similarly structured patches via distance and correlation based intensity-invariant approach. The key idea is that since similar patches share the same support in the transformed domain, these supports can be used as probabilities of active taps to refine the sparse estimates. This ultimately yields a very good patch estimate and therefore increases the qual-

ity of recovered image by discarding the noise-causing components. For the smooth regions of an image, a specially developed post-processor is then applied to further increase the quality of the denoised image. Comparison results from extensive simulations against the existing state-of-the-art algorithms in terms of PNSR and SSIM over a wide range of scenarios demonstrate the superiority of our proposed algorithms.

ملخص الرسالة

الاسم الكامل: مزمل بهزاد

عنوان الرسالة: الإستشعار المضغوظ لحد الضجيج بالصورة :خوارزميات التصحيح التعاوني

التخصص: الهندسة الكهربائية

تاريخ الدرجة العلمية: يناير 2017

في هذا البحث ، تم إقتراح خوارزمية القائمة على تصحيح والحد من ضجيج الصورة مع الأخذ بالاعتبار ضجيج جاوس المضاف والغير مرغوب به في مكونات الصورة. الخوارزميات المقترحة يتم تصنيفها في الصورة قليلة الضجيج الرمادية والملونة. تم اقتراح الاستفادة من تطبيع مسافة يوكولديان والعلاقة القائمة على مجموعة من الأجزاء في الخوارزميات. هذه المجموعة من الأجزاء هو وسيلة فعالة للحصول على الدعم التعاوني-اللأدري متفرق لإعادة الإعمار إلى تقليل أجزاء من الضجيج. من أجل هذا الترابط في الخوارزميات،تم حزم مجموعة مماثلة من الأجزاء المنظمة مقابل المسافة والتصحيح اعتمادا على نهج الكثافة الثابتة. الفكرة الرئيسية هي أنه بما أن الأجزاء المتماثلة تتشارك الدعم في مجال التحويل، هذا الدعم يمكن استخدامه كاحتماليات المناطق النشطة لتحسين متفرق التقديرات. هذا في نهاية المطاف ينتج تصحيح جيد تقديريا وبالتالي يزيد من جودة تعافى الصورة عن طريق التخلص من الضوضاء المتسببة من مكوناتها. من أجل المناطق السلسة في الصورة، تم وضع وتطبيق معالج متخصص لزيادة جودة التصحيح للصورة. تم مقارنة النتائج في برنامج المحاكاة مع أواخر الخوارزميات من خلال ذروة الإشارة إلى نسبة الضوضاء والتشابه الهيكلي على مجموعة واسعة من السيناريوهات مع إظهار تفوق الخوارزميات المقترحة.

CHAPTER 1

INTRODUCTION

Digital images play a vital role in a number of real world disciplines with various applications. These disciplines range from daily life applications, such as television and satellite broadcasting, to research and engineering technology including but not limited to computer vision, pattern recognition, geographical information systems, seismology and bio-medical processing. In order to obtain required data in the form of a 2D image, several tools and techniques from image processing areas are applied. Such image processing techniques provide the critical information of interest that can be then used depending upon the nature of applications.

1.1 Motivation

With the advent of latest technologies, adaptive and automatic ways of learning innovative techniques have evolved leading to tremendous developments in daily life applications. Since such practical applications are always based on processing the available information efficiently, image processing plays a backbone role.

With the help of acquired images, a number of smart applications have come into existence thereby providing the ease of access.

For example, the concept of smart cars have been recently implemented for practical scenarios. These smart cars are autonomous, driverless and self-driving vehicles having the ability to sense its environment. They are also capable of navigating without the need of an input via human driver. The fundamental technique on which these cars rely on is that of image processing which helps them getting the environmental data in the form of images and then processing them based on the required action. An example of these latest smart cars have been shown in Fig. 1.1.

Moreover, the applications involving image-based processing also extend to the field of security surveillance. This includes the mega-level security systems, like satellite surveillance of particular earth areas, to the micro-level security systems such as retina or fingerprint detection based security. Similarly, there is a huge number of applications in seismic signal processing where the required data is usually received in the form of images and is then processed to extract the desired information.

Additionally, the digital images also pay a key role in medical sciences and the field of microscopic life. For example, the detection of tiny organisms, like bacteria and viruses, in the form of digital images have been made possible only due to the advancement in the field of image processing. Apart from this, a number of applications in bio-medical image processing has led to effective ways of saving

(a)

(b)

(c)

(d)

Figure 1.1: (a) Waymo Smart Car (b) Google Car (c) Audi TT Pikes Peak (d) Mercedes Benz F 015

humans lives. This include detection of tumors and other diseases that ultimately help doctors to diagnose and suggest proper treatments. An example of such images taken from online databases[1,2] has been shown in Fig. 1.2.

Importantly, there is a tremendously increasing interest towards the field of computer vision and automation that led to the development of many smart machines providing ease of access to end users. Such increasing interest seeded the growth of applications like efficient motion and gesture recognition. Extending its applications towards future, the concept of future computers has been put into

[1] `http://www.imageprocessingplace.com/`
[2] `http://www.sciencephoto.com/`

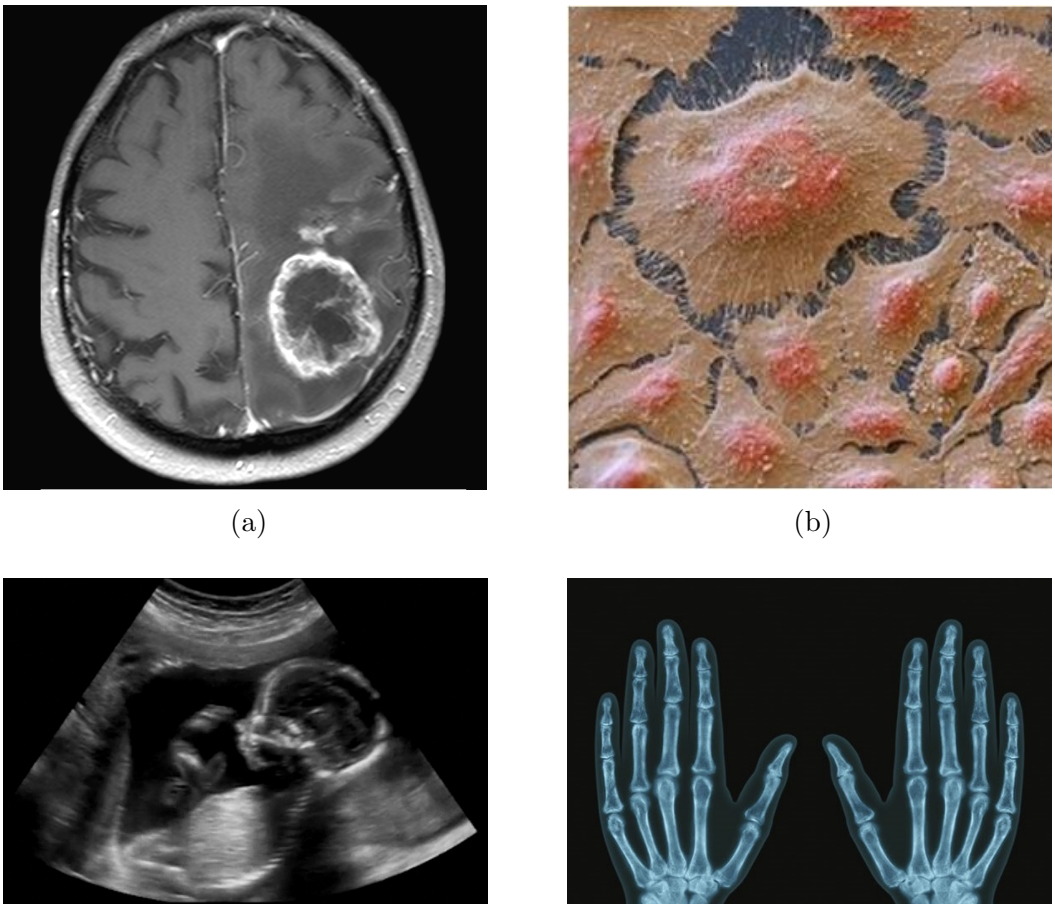

(a) (b)

(c) (d)

Figure 1.2: (a) Brain Tumor (b) Cancer Cells (c) Ultrasound (d) X-Ray

practice where the signals, mainly in the form of images, from brain, finger prints and eye blinks etc. will be translated to perform required actions.

Since these images contain very important information, the process of acquiring these images should be ideal as much as possible in order to avoid the loss of information due to some unavoidable factors. However, the information collected while capturing these images is generally contaminated by various degradation processes like blurring, noise contamination etc. as the process of acquiring these images is always non-ideal and imperfect due to some extrinsic and intrinsic factors [1]. Such image contamination may happen due to inefficient image acquisition,

poor or imperfect instruments and interfering natural phenomena, etc.

During image acquisition, performance of sensors in the imaging system is greatly effected by numerous factors such as environmental and atmospheric conditions, and also by the quality of sensing elements. As in the case of obtaining images using a CCD (charge-coupled device) camera, light and sensor's temperature levels are major contributors towards contaminating the image pixels. Whereas in the case of transmission, poor channel and resultant interference are the principle factors for introducing degradation that leads to image corruption. For instance, a transmitted image using any wireless channel might be contaminated as a result of lightening or other atmospheric disturbance [1].

Since the discussed factors can never be controlled, as these comprise of random phenomenon, an image always go through degradation leading to destroying the useful information it contains. Within such contamination processes, one of the main degradation that a digital image generally suffers from is the presence of noise. As discussed, the source of such noise in these images arise while capturing images using some acquisition system. Furthermore, transmission of the image may also involve noise introduction leading to image degradation. In Fig. 1.3, we show how an MRI (magnetic resonance imaging) image of brain tumor has been corrupted severely due to uncontrollable presence of noise. As shown, the amount of noise introduced in the image usually destroys very critical amount of information, such degradation can be as severe as life threatening.

The noise being introduced in these digital images can be of many types like

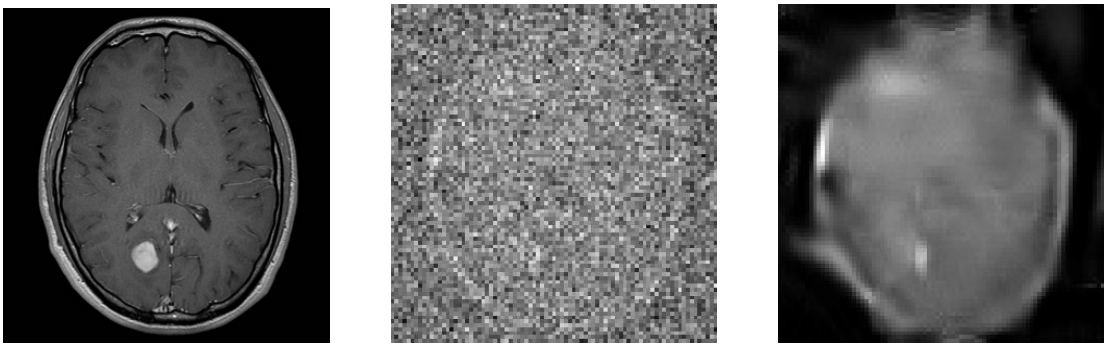

Figure 1.3: (a) Clean Image (b) Noisy Image (c) Denoised Image

Gaussian noise, Salt-and-pepper noise, Shot or Poisson noise, Speckle noise, etc. However, the most general type of noise that an image gets contaminated by is the Gaussian noise. In order to tackle this Gaussian noise, it is generally assumed to be zero mean additive but signal dependent in classical models [2]. To discard the noisy component, traditional mathematical approaches are applied to get the signal independent version of the Gaussian noise as a first step. A nonlinear transformation [3] serves as one of the best ways to get an independent additive noise model.

As this Gaussian noise produces undesirable effects such as artefacts, disturbed corners, unrealistic edges, blurred objects and disturbs background scenes. All the effects make the images difficult, and sometime impossible, to read. Since these images may carry critically important information as discussed already, there is a need to denoise them in order to recover the hidden information successfully. We have shown an example of original and Gaussian added noisy Cameraman images in Fig. 1.4. It is clear that in case of high noise, critical data information can be lost. Since such data can be very crucial in many situations like bio-medical and battlefield applications, this serves as a motivation for us to pursue this research

Figure 1.4: (a) Original Image (b) Noisy Image

work.

Consequently, the contribution of this thesis will be to design image denoising algorithms. For that, we will utilize compressed sensing techniques since sparsity is a characteristic that is found abundantly in many natural as well as man-made signals such as speech, images, videos, seismic activity, galactic activities and frequency hopping. In this research study, we will seek to remove the noise from a noisy image while retaining the original image features. Generally, the properties of any image in a given neighborhood do not change. We will use this fact to develop a method in which the image pixels (or group of pixels), in a well defined neighborhood, will collaborate to reach a consensus about their values. As a result, the unwanted added noise components would be discarded and the degradation would be minimized to a much greater extent that will be depicted in terms of improved peak signal-to-noise ratio (PSNR) as well as structure similarity (SSIM) index.

Generally, this process of degradation due to noise is modeled as a linear

system [4]. Consequently, many tools from matrix and algebra can be applied on it for analysis. The system model of noise introduction is shown in Fig. 1.5 which indicates that the degradation process of additive noise term $j(n, m)$, operates on a clean image $f(n, m)$ to yield a corrupted image $g(n, m)$. Here, n and m corresponds to the row and column pixels, respectively. As this noise introduction process is assumed to be spatially invariant [5], so we can express the system model shown in Fig. 1.5 as:

$$g(n, m) = f(n, m) + j(n, m) \tag{1.1}$$

Here, $g(n, m)$, $f(n, m)$ and $j(n, m)$ are the discrete representations. Given $g(n, m)$

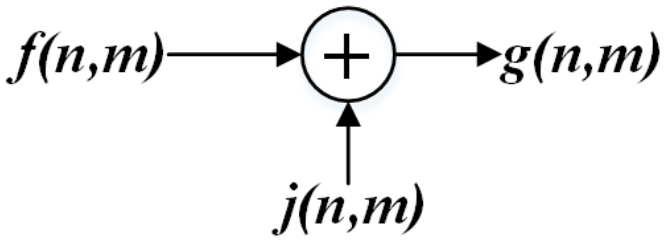

Figure 1.5: Noise Degradation Model

and some prior knowledge about the additive noise $j(n, m)$, like mean and variance, the objective is to denoise the noisy image as close as possible to its clean form, i.e. $\hat{f}(n, m) \approxeq f(n, m)$, where $\hat{f}(n, m)$ represents the discrete representation of the denoised image.

The contribution of noise $j(n, m)$ introduces difficulty in extraction of useful data from the image. Removing it is of extreme importance in many applications, and this paves the way for wide interest in this inevitable problem and its solution. Being one of the increasingly interesting inverse problems, the field of

image denoising has been explored a lot. However, there is still a lot of room for improvements because of the amazingly adopted techniques likes compressive sensing, domain transformation, exploiting correlation in the neighborhoods, etc., as these techniques provide a convenient platform over which many of the image processing tools and techniques can be applied [6].

1.2 Research Objectives

Digital images often suffer from noise corruption as the process of acquiring these images is inevitably random. These noise contamination destroys the useful information that these images carry and consequently make them unable to read. The process of such noise introduction is generally assumed to be linear and various tools and techniques can then be applied to denoise these image.

A significant amount of attention has been given to the problem of noise in 1D signals. However, as traditional 1D signal processing techniques did not take into account the correlation that exists in the neighboring signals, it resulted in inefficient schemes that were not very effective. In case of image pixels, one of the ways to discard the unwanted noise added components is to use collaboration among the pixel neighbors since they are correlated. Since the information in the correlated pixels or group of pixels would be similar, this serves as a good tool to handle the problem. However, since Gaussian noise is added in the image pixels, the chances of collaborating with dissimilar neighbors pixels increase. Hence, efficient choice of the neighbors and efficient collaboration is required.

For efficient collaboration, patch-based approaches have emerged out to be more effective as opposed to pixel-based approaches. This includes the division of a noisy image into various patches followed by searching for similar patches. This is usually followed by spatial-domain or transformed domain techniques where an image patch is transformed into other domain and then processed. Since sparsity is abundant in natural signals, this property of sparsity is exploited in many approaches to ensure efficient collaboration. One of the ways is to use compressed sensing (CS) where a signal is represented as a linear representation using some pre-determined dictionary. However, in doing so, most of the algorithms implement hard thresholding in which smaller sparse coefficients are discarded which might correspond to image details and may be mistaken as noise. Besides, choice of an appropriate dictionary is also a key factor to ensure improved performance both in terms of PSNR and SSIM. Consequently, the main objective of our work is to design efficient image denoising algorithms that will not only take care of the noise components but will also avoid the blur effects, artefacts, etc.

1.3 Contributions of Thesis

In this work, we have proposed novel image denoising algorithms to take care of the additive white Gaussian noise meanwhile preserving the details of an image. The algorithms work by first computing the overlapping patches and then finding structurally similar patches for all patches. Using compressed sensing (CS), we find the sparse estimates of all the patches. A collaborative step is then

performed in the sparse transformed domain to compute *apriori* information of the likelihood of the active taps. This information helps us to get a refined estimates of patches via refined estimation step. For finding similar patches, we used normalized Euclidean distance as the similarity measure for collaboration. This enables us finding those patches that share similar inherent sparse structure and thus helps us isolate the noisy components. The nature of this algorithm motivates us to name it as *collaborative support-agnostic recovery* (CSAR).

Additionally, since the collaboration in our method is a key step to take care of the unwanted noise, it is strongly dependent on the way similar patches are grouped and thus greatly affects the denoising performance. For further improvements in the denoising performance, we use correlation coefficient based similarity and then pass the denoised results to a specially developed post-processor that take care of the smooth and non-smooth regions separately. Based on this, we call our second algorithm *Advanced collaborative support-agnostic recovery* (ACSAR). Our contribution for this research work has been summarized as follows:

1. An overlapping patch-based scheme is implemented that utilizes information from both spatial as well as transform-domain.

2. Unlike other existing approaches, we propose two ways to find similarity among patches: we use 1) normalized Euclidean distance based similarity, and 2) correlation coefficient based similarity to compute similarly structured patches.

3. The probability vectors of active taps for each patch is computed.

4. Such probability vectors of patches are then stacked together in similar groups that collaborate in the sparse domain to find refined probabilities.

5. These refined probabilities are then used as *apriori* information to obtain refined sparse estimates, as explained in detail in Section 4.3.

6. With the help of a pre-determined dictionary, the denoised patches are computed.

7. Based on smooth region detection and region growing, a specially developed post-processor is designed to further eliminate the noisy components.

The key features of our algorithm are as follows:

1. A Bayesian approach is used to recover the sparse estimates of patches with significant improvements by incorporating any available *apriori* information.

2. Instead of going for similar intensity patches, we use an intensity-invariant approach. We hunt similar structured patches that helps us perform better collaboration in the transformed domain.

3. Our proposed denoising method lends itself a computationally-simple implementation.

1.4 Thesis Outline

The rest of the thesis is organized as follows: in Chapter 2, we present the literature survey of the relevant and famous image denoising techniques used and

applied globally. This is followed by Chapter 3 where we give some overview of the topics that are used in this research work. In Chapter 4 and 5, we describe in detail how we are tackling the image denoising problem. These chapters also contain the detailed description of how we use various tools and techniques to improve the image quality and produce efficient results. The extension of proposed algorithms to color image denoising is given in Chapter 6. Here, we discuss the key idea that is used in three different channels of a color image for a much better denoising performance. In Chapter 7, we present, analyze and compare the results of our proposed image denoising algorithms with state-of-the-art algorithms. Results from extensive simulations are presented using various parameters and scenarios where we show that our algorithms outperform other state-of-the-art algorithms both in terms PSNR and SSIM. Finally, we conclude the work and present some interesting future directions in Chapter 8.

1.5 Notations

In the rest of the thesis, we represent all the vectors used in our work with small case and bold face letters (e.g. $\mathbf{y}$), all the scalars with small case normal font letters (e.g. y). We reserve upper case and bold face letters (e.g. $\mathbf{Y}$) for matrices. For sets, we use calligraphic notation (e.g. $\mathcal{N}$). We use $\mathbf{y}_i$, $y(j)$ and $\mathcal{N}_k$ to denote ith column of matrix $\mathbf{Y}$, jth element of vector $\mathbf{y}$ and a subset of $\mathcal{N}$, respectively.

CHAPTER 2

RELATED WORK

Image denoising has been explored extensively over the past decades because of its tremendous importance towards many applications like computer vision, image processing, machine intelligence, robotics, artificial intelligence and statistical/seismic signal processing, etc. The amount of noise in images plays a backbone role for the analysis of image reliability and is of a major interest during the image acquisition phase in image processing [7]. In such scenarios, the objective is to find an estimate $\widehat{\mathbf{X}}$ of original image $\mathbf{X}$ corrupted by the signal independent AWGN noise as $\mathbf{Y} = \mathbf{X} + \mathbf{W}$, where the noise $\mathbf{W} \sim \mathcal{N}(0, \sigma_w^2 \mathbf{I})$.

Since image denoising is an ill-posed problem, that's why theoretically it is really hard to accurately restore a denoised version of the image from the noisy one since it's a highly under-constrained problem [8]. However, over the past few decades, a number of intelligent algorithms have been designed to tackle this problem. This covers pixel based filtering techniques to patch based approaches. The existing denoising methods are further classified into the following two main

categories: spatial-domain based methods and transform-domain based methods. We now discuss them in the following sections.

2.1 Pixel-Based versus Patch-Based Approaches

Traditionally, the pixel based filtering techniques, such as Gaussian filtering, bilateral filtering, total variation regularization, etc. have been developed to improved the denoising performance. In such methods, a pixel is taken as a reference and then processed to denoise it. One of its representative approaches is the non-local means (NL-means) [31]. This approach uses a pixel based technique where a reference pixels is replaced by the weighted average of the similar pixels. Despite an improved performance, the algorithm is costly in terms of time since processing each pixel is time consuming.

On the other hand, the patch based methods have shown to produce amazingly better results and have outperformed many traditional pixel based denoising methods that existed previously [9]. This not only reduced the time of processing, since group of pixels is processed as opposed to a single pixel, but also yielded better results when signal processing techniques were applied to exploit correlation among neighboring patches. Since then, a significant number of patch based methods have been used not only specifically in denoising but also in the broad range of computer vision, pattern recognition and image processing application.

For instance, J. Boulanger, et al. [10] proposed a method for image restoration using a space-time patch-based approach. Based on the local analysis of

the variance, the authors have implemented an adaptive statistical estimation framework. They demonstrated quantitative evaluations on standard artificially noise-corrupted images and have also reported convincing results on real images. Similarly, a general signal and image denoising algorithm has been proposed by the authors in [11], where the process of denoising is formulated as a process of partial differential equation with spatially varying time.

Additionally, the authors in [12] proposed a hashed non-locals means method for rapid image filtering using a patch-based approach. They report significant speed gains as opposed to existing non-local means methods. P. Chatterjee, et al. [13] come up with an image denoising algorithm by implementing a patch-based Wiener filter exploiting the patch redundancy. They used both the geometrical as well as the photometric similarity for the estimation of various filter parameters. Similarly, the authors in [14] have introduced a new patch based image denoising algorithm using dual domain image denoising (DDID). This leads to the development of non-local dual image denoising (NLDD) that is three times faster than DDID. S. H. Chan, et al. proposed a new algorithm named as Expectation-Maximization (EM) adaptation in [15]. Their work focus on finding the image patch-priors effectively to get sufficient performance gains in denoising.

Based on the under discussion patch-based approach, A. Buades, et al. present a novel image sequence denoising in [16]. In this approach, they exploit the similarity as well as the redundancy in the adjacent video frames. The authors in [17] introduced a soft threshold to take care of the small weights associated

with dissimilar patches in non-local means. This patch based approach then uses a simple averaging filter for further improvements in denoising performance. To further explore the denoising, the authors in [18] worked on how to get non-local self similarity (NSS) of the clean image. They proposed a patch group based NSS prior learning mechanism. This ultimately increases the PSNR of the output image yielding a more improved denoising performance.

Apart from the discussed patch-based approaches in the field of denoising, there are a number of articles that span the area of deblurring [19, 20], segmentation [21, 22], detection and tracking [23, 24] and bio-medical applications [25, 26, 27] using the patch-based approaches. Such extraction of patches from images or frames not only produces efficient and speedy processing but also helps to improve the processing performance. This performance improvement can usually be achieved by finding and processing similar patches both spatially as well as in the transformed domain.

2.2 Spatial-Domain versus Transform-Domain Based Methods

The existing denoising methods are further classified into the following two main categories: spatial-domain based methods and transformed-domain based methods. Among the spatial-domain based denoising approaches, P. Getreuer presented a total variation (TV) minimization method in [28] for the image denoising

problem. They implemented the TV regularized technique for denoising a noisy image to a very good extent.

Similarity, some recently developed methods exploited the spatial self-similarity in the images and have showed promising results. This includes the research work carried out in [29] where the authors proposed a novel adaptive approach for denoising images. The method is based on a pointwise selection of small image patches in the variable neighborhood of each pixel. They associated a reference pixel with the weighted sum of points within an adaptive neighborhood. Similarly, J. R. Chang, et al. proposed a propagation filter for denoising in [30]. The goal in this work is to denoise an image via smoothing over neighboring image pixels meanwhile not relying on explicit spatial kernel functions. They report improved denoising performance and have shown to outperform various image filters.

The non-local means (NL-means) [31] is the first of its kind method to take advantage of the spatial self-similarity within an image itself. This algorithm replaces a reference pixel by the weighted average of other pixels having a similar neighborhood. The similarity in the neighborhood of each pixel with that of a reference pixel is taken as a self-similarity measure.

On the contrary, the transform-domain based techniques rely on an underlying image regularity assumption and process the data in that domain. Generally, they use the idea of thresholding/compressing of coefficients in the transformed domain. In this regard, D. Gnanadurai, et al. described a way of image pro-

cessing in the transformed domain [34]. Since threshold selection is an important factor while denoising images in the transformed domain, they used double density wavelet transform (DDWT) as an adaptive way of threshold estimation. An observed image is first decomposed into various levels to get various frequency bands using DDWT. Thresholding based denoising is then applied using the threshold attained from their proposed method. In a similar fashion, J. Starck [33] introduced taking image components into Fourier domain. They showed impressive results of processing a corrupt image in the transformed-domain.

A sparse representation based 2D nonlocal image denoising scheme has been proposed in [32]. The authors developed a framework in which a dictionary learning method has been presented that decomposes groups of similar noisy patches on subsets of dictionaries. H. Li, et al. in [35] discussed the advantages and disadvantages of wavelet and curvelet transforms. The authors combine both transforms to deal with noisy images. The reported results show that the proposed approach outperforms the methods that use wavelet and curvelet transforms only.

A higher order singular value decomposition (HOSVD) based denoising algorithm is presented in [36]. The technique groups similar patches in a 3D stack followed by computing the HOSVD coefficients of the stack. The coefficients are then processed via hard thresholding and the invert HOSVD is applied afterwards to get the final denoised image.

N. Pierazzo, et al. proposed data adaptive dual domain denoising (DA3D) [37], where a frequency domain shrinkage on shape and data-adaptive patches is

performed. However, such approach makes the algorithm require more computational time in order to denoise images. Similarly, the authors in [38] used an adaptive signal modeling and soft thresholding technique to propose a novel image denoising algorithm. The image quality is improved by using regularization of all the image patches in the transformed domain.

However, over the recent years, algorithms introducing sparse representation of the image patches via dictionaries are proposed that outperform the existing algorithms and yield optimized results. To do so, compressed sensing (CS) algorithms are applied to recover the sparse coefficients of a given vectorized patch. One of the important works in this category include the algorithm K-SVD proposed by Elad et al. [39] for dictionary learning. This algorithm computes a highly overcomplete dictionary using a preliminary training method. A similar work by Mairal et al. [40, 41], Lebrun et al. [42], Yu et al. [43] and Guo et al. [44] have also significantly contributed towards this domain of research. However, a strong practical limitation of these algorithms is that these impose a very high computational burden.

The currently developed image denoising algorithms takes into account the critical information from both spatial as well as the transform domain and use that as an important piece of information to yield amazingly better results (e.g. see [45, 46, 47]). One of the most efficient algorithms to date is the block-matching 3D filtering (BM3D) proposed by Dabov et al. in [48], which is considered the current state-of-the-art algorithm in image denoising. This algorithm operates at

the patch level and first collects the similar patches (or blocks as they call it) in the spatial domain and then stacking them in 3D arrays. Afterwards, they apply hard thresholding in the transformed domain producing an initial denoised estimate of the image. Finally, the results are further refined by a specially developed Wiener filter. A fundamental drawback of this algorithm is the introduction of blur due to over smoothing. Since the details in image carry important information, the blur can destroy the critical details that reside in the image. Consequently, there is a need for more effective ways of denoising images.

2.3 Current Efficient Algorithms

As discussed above, the current state-of-the-art algorithms like NL-means [31] and BM3D [48] produce near to optimal results when tested on natural images as shown by Levin et al. [49] and Chaterjee et al. [50]. However, denoising still remains a challenging problem that has room for improvements in many directions specially in the case of large noise. For example, while majority of these algorithms manage to separate the noise from image to a good extent, they tend to blur out the recovered patches thus removing image details.

2.3.1 Challenges in Image Denoising

With reference to the discussion above, following are a number of challenges that the recently developed image denoising algorithms are competing for:

1. The perceptually smooth areas of an image should be kept as flat as possible

and noise should be removed completely from such regions.

2. The boundaries in an image should be well preserved since the generally used averaging approach results in blurring out those details.

3. The texture details of an image should not be removed as these details are of extreme importance and have key information. This is one of the most challenging task in image denoising where majority of the algorithms can't perform well and tend to blur out the images that results in loosing texture details.

4. Artefacts should not appear in the denoised image specifically at very high noise levels.

CHAPTER 3

TECHNICAL OVERVIEW

3.1 Sparse Reconstruction

As majority of the observed signals and images are usually sparse in nature, CS algorithms can be used to recover these using under-determined model of linear equations

$$\mathbf{y} = \mathbf{A}\mathbf{h} + \mathbf{w}, \tag{3.1}$$

where $\mathbf{y}$, $\mathbf{A}$, $\mathbf{h}$ and $\mathbf{w}$ represents noisy observation signal, an overcomplete dictionary, sparse representation of the clean signal and the noise vector, respectively. The objective is to restore the degraded image, as shown in 1.4, by some restoration processes, as close as possible to its original form, i.e. $\widehat{\mathbf{X}} \approx \mathbf{X}$. For this restoration, we use the model of (3.1), a depiction of which is shown in Fig. 3.1.

As we can see from Fig. 3.1, the number of unknown elements in such a scenario are usually much larger than the number of observations. With CS, a

true signal can be reconstructed by linear projections of the sparse signal using ℓ_1-optimization with high probability [51]. Many algorithms are proposed in the literature that compete to provide a better estimate of the sparse vector. We will be specifically interested in utilizing a Bayesian scheme that enjoys low computational burden and outperforms currently existing sparse reconstruction techniques. In particular, a good estimate of the sparse vector can be provided even when there is no *apriori* knowledge about signal support. More importantly, such sparse recovery algorithms are agnostic to support distribution and hence there is no need to estimate distribution parameters.

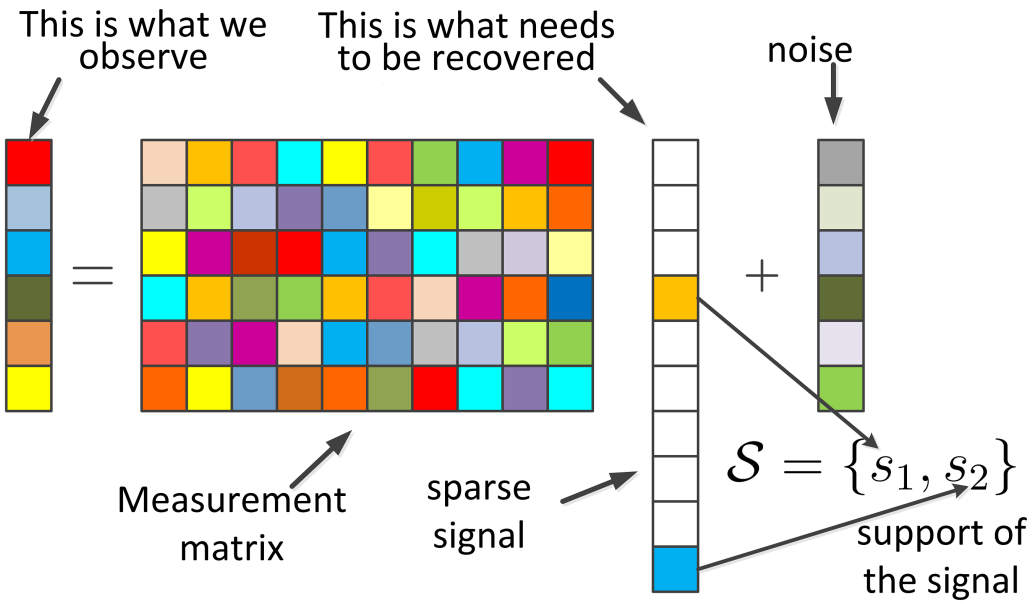

Figure 3.1: Sparse Model

3.2 Sparse Recovery Algorithm Selection

Our proposed image denoising algorithms involve estimation of the sparse vectors $\widehat{\mathbf{h}}_k$ and $\bar{\mathbf{h}}_k$ as will be discussed in detail in the following chapters. Even though there exist a number of algorithms for sparse recovery that provide the estimate efficiently, we have to be cautious in our selection for such sparse recovery algorithm. In particular, the nature of our way of tackling the denoising problem dictates that such algorithm should:

- not pose strict conditions on the dictionary matrix $\mathbf{A}$,
- be able to estimate parameters such as sparsity and variance of unknown vectors if not provided,
- be invariant to the distribution of unknowns, and
- be capable of utilizing any available *a priori* info.

Several number of sparse algorithms are proposed in the literature that provides the aforementioned attributes. However, very few have all of the mentioned attributes. Among such sparse recovery methods, we are interested specifically in the support agnostic Bayesian matching pursuit (SABMP) algorithm [51] due to its nature of fulfilling our requirements. This algorithm is capable of MMSE estimation even in the case when the probability distribution of the unknown vector is unavailable. Additionally, it also provides active taps probabilities along with the estimated sparse vector which is one of the main advantages our proposed algorithm is benefiting from.

3.3 Dictionary Selection

Since we will be using the sparse estimates from collaborative filtering in the transform domain to denoise the patches, the use of an appropriate dictionary also serves as a key step. Generally, the dictionary mainly consist of basis vectors through which any random patch can be represented as a linear combination of the basis elements. In our case, we will be representing any patch using the obtained sparse vector and the dictionary as already shown in Fig. 3.1.

3.3.1 Dictionary De-correlation

Each patch can be written as linear combination of basis elements from the dictionary. The columns of this dictionary are derived from wavelet basis and are normalized to have unit norms. Prior finding support sets of $\widehat{\mathbf{h}}_k$ via sparse estimation of patches, we will reduce the correlation between dictionary columns for a robust computational and performance ability. Consequently, we remove weak supports by rejecting highly correlated columns as the information they encode could easily be encoded by other columns which correlate with them.

$$\mathbf{A} = \Gamma_\beta(\mathbf{A}') \tag{3.2}$$

where $\Gamma_\beta(.)$ is the de-correlation operator that removes all the columns of $\mathbf{A}'$ with correlation greater than β.

CHAPTER 4

COLLABORATIVE SUPPORT-AGNOSTIC RECOVERY (CSAR)

In this chapter, we present our first proposed image denoising algorithm based on collaborative CS in a sparse transform domain. The proposed algorithm is named *collaborative support-agnostic recovery* (CSAR) because of its nature as mentioned in earlier chapters. In the proposed algorithm, the sparse coefficients of an image patch are computed and refined via collaboration with similarly structured patches. This collaboration process in computing the supports of the patches results in a more accurate sparse representation of these patches, which in turn produce an enhanced image denoising performance. We now present a detailed description of our proposed method.

4.1 System Model

The system model under observation is assumed to be linear and spatially invariant [5]. Let $\mathbf{X} \in \mathbb{R}^{R \times C}$ represent the matrix version of a clean noiseless image, where R and C denotes the number of rows and columns, respectively. Our aim is to find an estimate of the clean image matrix $\mathbf{X}$ from its noise contaminated observations $\mathbf{Y}$ given by,

$$\mathbf{Y} = \mathbf{X} + \mathbf{W}, \tag{4.1}$$

where, $\mathbf{W}$ is the matrix version of the noise whose entries are independent and identically distributed (i.i.d.) random variables taken from a Gaussian distribution having zero mean and variance σ_w^2, i.e., $\mathbf{W} \sim \mathcal{N}(0, \sigma_w^2 \mathbf{I})$. Let us denote the estimated/denoised image by $\widehat{\mathbf{X}}$. To find the denoised image $\widehat{\mathbf{X}}$, we use the three main steps as explained in the subsequent sections.

4.2 First Step: Formation and Grouping of Image Patches

We form $N \times N$ square patches around each pixel in the image where N is selected to be an odd number.[1] Further, to accommodate the border pixels, we pad the image borders with $\lfloor \frac{N}{2} \rfloor$ pixels via symmetrical padding. This results in a total

[1]Our algorithm applies to the general case where patches could be rectangular or even linear. However, for simplicity and convenience we focus on the special case of square patches in this work.

number of $K = RC$ patches as

$$\mathbf{Y}_k = \mathbf{X}_k + \mathbf{W}_k, \quad \forall k \in \mathcal{K}, \tag{4.2}$$

where $\mathcal{K} = \{1, 2, \ldots, K\}$. Note that for computational convenience, we represent patches in (4.2) in vectorized form and use the resulting notation in the rest of the thesis. So we have

$$\widetilde{\mathbf{y}}_k = \widetilde{\mathbf{x}}_k + \widetilde{\mathbf{w}}_k, \quad \forall k \in \mathcal{K}, \tag{4.3}$$

where $\widetilde{\mathbf{y}}_k, \widetilde{\mathbf{x}}_k$ and $\widetilde{\mathbf{w}}_k, \forall k$ are vectors of length N^2.

The next step is to group each patch with similar patches as shown in STAGE 01 of Fig. 4.1. The aim is to group all patches with similar underlying image structure irrespective of their intensity levels. More importantly, this intensity-invariant grouping requires normalization of the image patches as follows

$$\mathbf{y}_k = \eta(\widetilde{\mathbf{y}}_k) = \begin{cases} \frac{\widetilde{\mathbf{y}}_k}{\|\widetilde{\mathbf{y}}_k\|}, & \|\widetilde{\mathbf{y}}_k\| \neq 0 \\ \widetilde{\mathbf{y}}_k, & \text{otherwise} \end{cases}, \quad \forall k \in \mathcal{K}, \tag{4.4}$$

where $\eta(\cdot)$ represents the normalization operator and $\mathbf{y}_k$ is the normalized version of $\widetilde{\mathbf{y}}_k$. As a result, we have

$$\mathbf{y}_k = \mathbf{x}_k + \mathbf{w}_k, \quad \forall k \in \mathcal{K}. \tag{4.5}$$

Thus, patch $\mathbf{y}_k$ and those among all other patches that lie within a distance of, say ϵ, from $\mathbf{y}_k$ are grouped together. We call these the *neighbors* of the kth patch i.e., $\mathbf{y}_k$. Therefore,

$$\mathcal{N}_k = \{i : d(\mathbf{y}_k, \mathbf{y}_i) \leq \epsilon\}, \quad \forall k \in \mathcal{K} \tag{4.6}$$

denotes a set of indices of all neighbors of patch k and the index k itself. Here, $d(\cdot)$ could be any feasible distance measure, such as the Euclidean distance. Note that by virtue of the definition above, the set of neighbors need not be spatial neighbors and the set of neighbors $\mathcal{N}_k, \forall k \in \mathcal{K}$ are not disjoint. The upshot of such grouping is that it yields a higher number of neighbors for each patch which is beneficial for our collaborative approach as described in the following section.

4.3 Second Step: Collaborative Denoising

It is a well-known fact that images are sparse in the wavelet domain. We use this property to find sparse representation of each patch as follows

$$\mathbf{y}_k = \mathbf{A}\mathbf{h}_k + \mathbf{w}_k, \quad \forall k \in \mathcal{K} \tag{4.7}$$

where $\mathbf{A} \in \mathbb{R}^{N^2 \times M}$, $M \gg N^2$ is an overcomplete wavelet dictionary. Moreover, $\mathbf{h}_k \in \mathbb{R}^M$ is the sparse representation of $\mathbf{x}_k$ i.e., $\mathbf{x}_k = \mathbf{A}\mathbf{h}_k$. Let $\widehat{\mathbf{h}}_k$ represent an estimate of the sparse vector obtained through a sparse recovery algorithm and let $\mathcal{S}_k$ be its support set. Note that in an ideal scenario $\mathcal{S}_k = \mathcal{S}_i, \forall i \in \mathcal{N}_k$ should hold

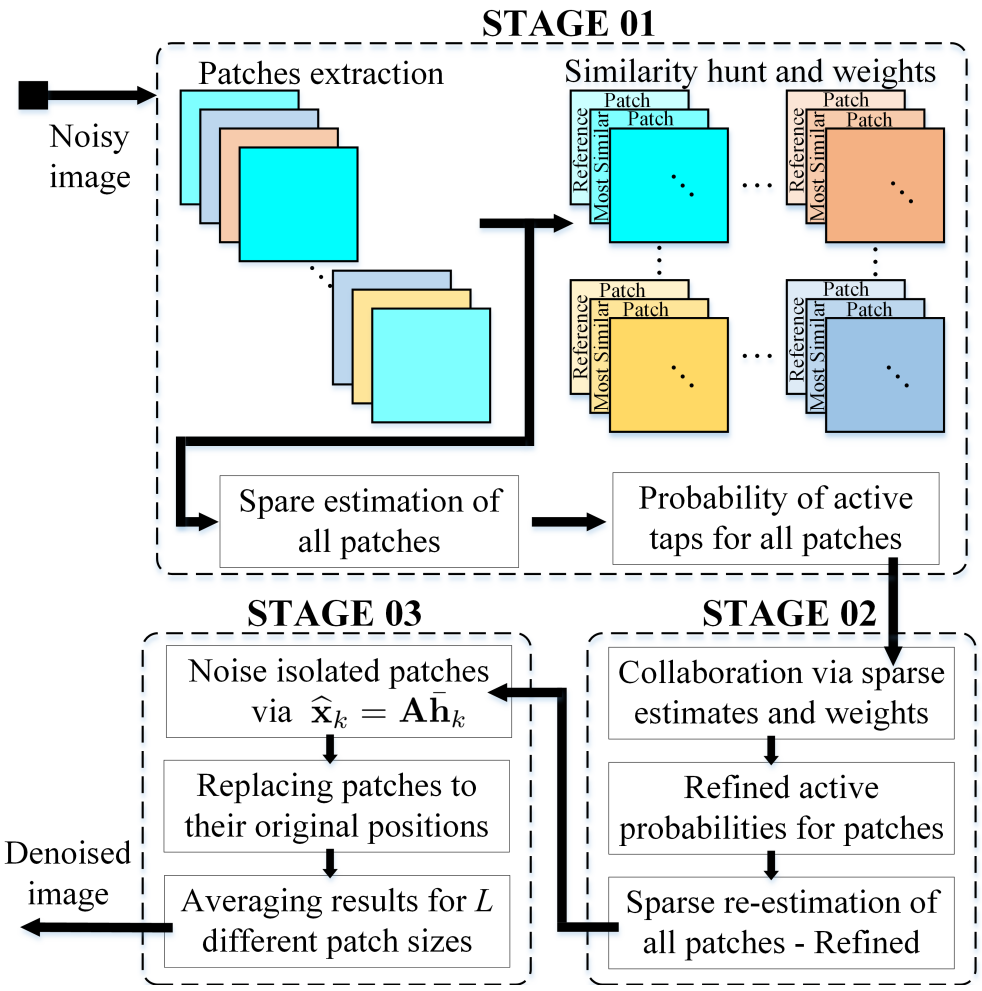

Figure 4.1: Flowchart of proposed CSAR denoising algorithm

true for all $k \in \mathcal{K}$. This observation motivates us to use the sparse representation of patches to devise a collaborative denoising method. However, note that in reality the supports may not match exactly as $\mathcal{N}_k$ is a function of a non-zero ϵ as well as $\mathbf{w}_k$. The threshold ϵ could be selected such that it guarantees high similarity among the group members. However, the perturbations due to noise would remain and result in a disagreement among the supports of similar patches. Here we would like to stress that this disagreement is a blessing in disguise. Given sufficiently small ϵ, most of the outliers $\mathcal{V}_k = \bigcup_{i \in \mathcal{N}_k} \mathcal{S}_i \setminus \bigcap_{i \in \mathcal{N}_k} \mathcal{S}_i$ in the support

are there, with high probability, due to noise. This helps us identify and take care of the noise-causing components in the estimate $\widehat{\mathbf{h}}_k$. One naive approach could be to eliminate the non-zero components of $\widehat{\mathbf{h}}_k$ located at $\mathcal{V}_k$ and use the resulting sparse vector to form an estimate $\widehat{\mathbf{x}}_k = \mathbf{A}\widehat{\mathbf{h}}_k$. However, this could result in destroying useful information especially in high noise cases as some legitimate non-zero locations could be mistaken for noise-causing components. In view of this, we resort to a much moderate approach.

In this approach, we utilize active probabilities of the non-zero locations of $\mathbf{h}_k$. The idea is that similar patches will have similar support and the legitimate non-zero locations among these will have high active probabilities. Thus, we propose that collaboration among patches take place in the sparse domain as shown in STAGE 02 of Fig. 4.1. Specifically, for the kth patch, let $\boldsymbol{\lambda}_k \in \mathbb{R}^M$ represent the vector of active probabilities for the estimate $\widehat{\mathbf{h}}_k$. We compute the weighted average

$$\boldsymbol{\lambda}'_k = \frac{1}{\mathcal{N}_k} \sum_{j \in \mathcal{N}_k} \alpha_{j,k} \boldsymbol{\lambda}_j, \quad \forall k \in \mathcal{K}, \tag{4.8}$$

as an estimate of the active probability vector of *clean* $\mathbf{h}_k$. The weighting factor

$$\alpha_{j,k} \propto \frac{1}{d(\mathbf{y}_j, \mathbf{y}_k)}, \quad j \neq k. \tag{4.9}$$

This simple process allows us to gracefully downgrade the contribution of solitary active taps while preserving the values for locations that are common to most of

the patches in $\mathcal{N}_k$. Moreover, by virtue of the law of large numbers, we expect that (4.8) will result in a good estimate especially because $|\mathcal{N}_k|$ is large due to the intensity-invariant grouping approach. The derived clean $\boldsymbol{\lambda}'_k$ is a valuable piece of information which approximates the *a priori* information about the active locations of true or clean sparse representation of the kth patch $\mathbf{x}_k$. This *a priori* information could be provided to a sparse recovery algorithm, as shown in STAGE 02 of Fig. 4.1, to find an estimate of true $\mathbf{h}_k$ (let us call it $\bar{\mathbf{h}}_k$) and thus an estimate of true (and denoised) kth patch which we denote as $\widehat{\mathbf{x}}_k$, where

$$\widehat{\mathbf{x}}_k = \begin{cases} \eta^{-1}(\mathbf{A}\bar{\mathbf{h}}_k) = \mathbf{A}\bar{\mathbf{h}}_k\|\widetilde{\mathbf{y}}_k\| & \|\widetilde{\mathbf{y}}_k\| \neq 0 \\ \eta^{-1}(\mathbf{A}\bar{\mathbf{h}}_k) = \mathbf{A}\bar{\mathbf{h}}_k & \text{otherwise} \end{cases}, \quad \forall k \in \mathcal{K}. \tag{4.10}$$

4.4 Third Step: Formation of Final Denoised Image

As described in Sec. 4.2, we form overlapping patches. As a result, each image pixel is present in N^2 patches and therefore has as many estimated values. In order to reconstruct the denoised image $\widehat{\mathbf{X}}$, we simply average the N^2 estimates of each pixel. In this way, the final image formation adds another level of averaging out impurities. Lastly, we average the denoising results using L different odd patch sizes, STAGE 03 of Fig. 4.1, that significantly improves the denoising performance.

CHAPTER 5

ADVANCED COLLABORATIVE SUPPORT-AGNOSTIC RECOVERY (ACSAR)

In this chapter, we present a detailed description of the methodology that we used for designing our second image denoising algorithm named *Advanced collaborative support-agnostic recovery* (ACSAR). Our proposed method has two major blocks of working: 1) the denoiser and 2) the post-processor as discussed separately in the following sections. The denoiser consists of the following major steps. First of all, an observed image is decomposed into several overlapping patches, and similarly structured patches are computed. Afterwards, a sparse domain based collaborative approach is used on the similarly grouped image patches to refine the

patch estimates. Finally, the patches are placed back to their original positions. For further improvement in the results, we ultimately pass the denoised image to a post-processor that takes care of the smooth region and produces promising results. This process has also been summarized as a block diagram in Fig. 5.1 each stage of which we'll discuss in the following sections. Since the observed system model is same as described in Section 4.1, we proceed to first explain in detail how the denoiser block of this algorithm works. The methodology of the denoiser block is explained in the subsequent sections. A detailed description of our post-processor block is then described afterwards.

5.1 Image Decomposition

For a given noisy image, we first of all form $N \times N$ size squared patches around every pixel where N is always an odd number for proper processing[1]. Such decomposition results in overlapping patches that are useful to mitigate the effect of noise. Moreover, to facilitate the border pixels without introducing any artifacts, we pad the given image's border first with $\lfloor \frac{N}{2} \rfloor$ pixels, before processing. This step yields a total number of $K = RC$ patches, where R and C denote the number of rows and columns of the image, respectively. The patches are thus represented

[1]Our proposed image denoising algorithm is able to process the general case where patches can be non-squared, i.e., rectangular or even linear. However, for convenience and simplicity, we present the special case of squared patches in this work.

as

$$\mathbf{Y}_k = \mathbf{X}_k + \mathbf{W}_k, \quad \forall k \in \mathcal{K}, \tag{5.1}$$

where $\mathcal{K} = \{1, 2, 3, \ldots, K-1, K\}$. In order to have computational simplicity and convenience, we denote the patches in (5.1) as vectors/1D signals and will be utilizing this notation in the coming sections of the thesis. The vectorized representation of the patches is given as

$$\widetilde{\mathbf{y}}_k = \widetilde{\mathbf{x}}_k + \widetilde{\mathbf{w}}_k, \quad \forall k \in \mathcal{K}, \tag{5.2}$$

where $\widetilde{\mathbf{y}}_k, \widetilde{\mathbf{x}}_k$ and $\widetilde{\mathbf{w}}_k, \forall k$ are vectors of length N^2.

5.2 Similar Patches Hunt: Distance vs. Correlation

Once the overlapping patches are formed, the next step is to find a certain number of similar patches, for each patch, that would be used later during collaboration. Since the patches we process are in their vectorized 1D signal format, we aim to find similarity among the 1D signals. The grouping of patches in such a way using a similarity measure has led to a number significant improvements in a wide range of application like signal/image/bio-medical processing, computer vision, machine intelligence, etc. (see e.g. [52, 53, 54, 55, 56]).

A number of techniques for similarity based grouping of patches have been proposed in the literature. Some of those include self-organizing maps [57], vector quantization [58], fuzzy clustering [59] and a review on these [60]. The recently developed denoising algorithms use a distance based measure where similarity between different signals are realized in terms of the inverse of the point-wise distance between them. Therefore, a smaller distance between the signals would imply a higher similarity and vice versa. The generally used distance based similarity measure is the Euclidean distance as used by the state-of-the-art denoising algorithms like NL-means [31], BM3D [48], etc.

However, despite being an effective way of finding similarity, Euclidean distance based similar-intensity grouping has a limitation; it limits the search for number of similar patches. For instance, even though natural images have some similarity in their structure, the number of similar patches vary. Consequently, in an image having a smaller number of similar patches, the collaboration is not that effective thereby disturbing the performance of denoising, especially in case of high noise. This creates a bottleneck specifically for lower resolution images where finding similar-intensity patches becomes a hard job as will be shown in the results section of this work.

To tackle this case and have a similarity measure that can be used globally even in lower resolution images or images having a smaller number of similar-intensity patches, novel methods are being proposed to find better ways of collaboration by using efficient grouping of similar patches. For example, the authors in [61]

search the similar patches by using not only a patch itself but the noise too where they propose the concept of noise similarity, while the authors in [62] propose sequence-to-sequence similarity (SSS) which is an essential way of preserving the edge information.

In our case, we take care of the aforementioned problem by introducing intensity-invariant grouping. The idea is to stack all the patches that have a similar inherent structure without relying on the intensity values as shown in the STAGE 01 of Fig. 5.1. The correlation coefficient serves as the best tool to be utilized for the said purpose. For two signals $\mathbf{y}_k$ and $\mathbf{y}_i$, the correlation coefficient is given as,

$$r(\mathbf{y}_k, \mathbf{y}_i) = \frac{cov(\mathbf{y}_k, \mathbf{y}_i)}{\sigma_{\mathbf{y}_k}\sigma_{\mathbf{y}_i}}, \tag{5.3}$$

where $-1 \leq r(\mathbf{y}_k, \mathbf{y}_i) \leq 1$. A value close to 1 or -1 means larger positive and negative correlation, respectively, while a value close to 0 means smaller correlation. We are using the correlation coefficient for finding the similar patches because this method efficiently identifies the signals/patches having similar structure.

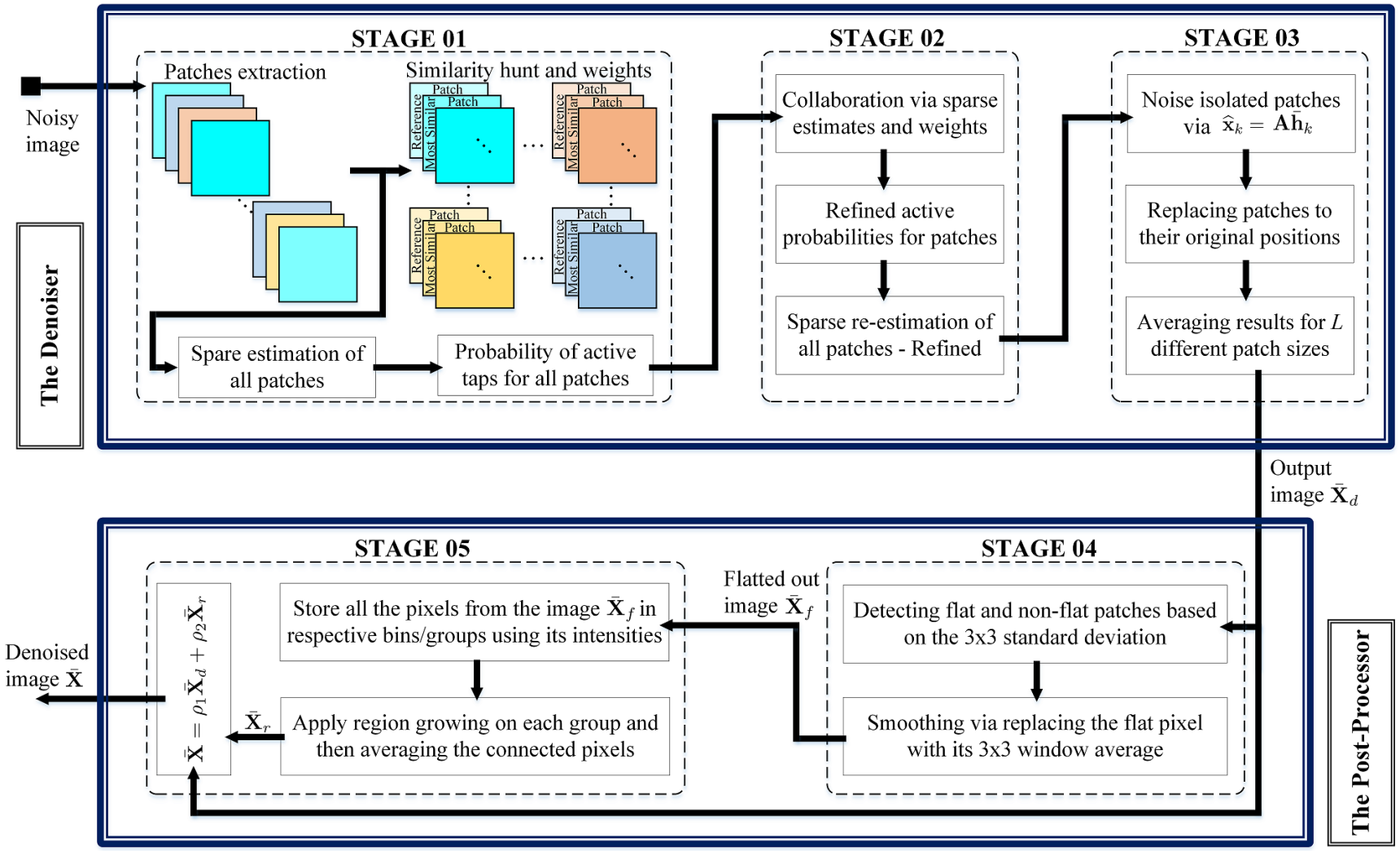

Figure 5.1: Flowchart of proposed denoising algorithm

Importantly, since the underlying structure would be reflected in the sparse domain, as we'll explain in the following sections, we place those patches in the similarity group that have a positive correlation (near $+1$) as well as a negative correlation (near -1). This is because we search for the patches that have similar structure independent of the sign of correlation coefficient since the signs would be absorbed in the sparse domain. Most importantly, to make such a method work more efficiently, the normalization of patches is needed. Therefore, we normalize the patches in (5.2) to get the following equivalent representation,

$$\mathbf{y}_k = \eta(\widetilde{\mathbf{y}}_k) = \begin{cases} \frac{\widetilde{\mathbf{y}}_k}{\|\widetilde{\mathbf{y}}_k\|}, & \|\widetilde{\mathbf{y}}_k\| \neq 0 \\ \widetilde{\mathbf{y}}_k, & \text{otherwise} \end{cases}, \quad \forall k \in \mathcal{K}, \tag{5.4}$$

where $\eta(\cdot)$ denotes the operator for normalization and $\mathbf{y}_k$ is a normalized representation of the patch $\widetilde{\mathbf{y}}_k$. Consequently, we have the following relationship

$$\mathbf{y}_k = \mathbf{x}_k + \mathbf{w}_k, \quad \forall k \in \mathcal{K}. \tag{5.5}$$

Hence, a patch $\mathbf{y}_k$ and those among all other patches that have an absolute correlation coefficient greater than, say ϵ, from $\mathbf{y}_k$ are placed together in a group. We name these the *neighbors* of the kth patch i.e., $\mathbf{y}_k$. Therefore,

$$\mathcal{N}_k = \{i : r(\mathbf{y}_k, \mathbf{y}_i) \geq \epsilon\}, \quad \forall k \in \mathcal{K}, \tag{5.6}$$

represents a set of indices for all neighbors of patch $\mathbf{y}_k$ and the index k itself.

(a) Observed Image

(b) Euclidean Distance

(c) Corr. Coefficient

Figure 5.2: Sail boats image from Kodak gallery

Here, $r(\cdot)$ is the correlation coefficient based similarity measure that we are using.

To understand this completely, consider the natural images shown in Fig. 5.2 and 5.3 taken from Kodak© gallery[2]. Here, we bring the focus towards the limitation of finding Euclidean distance based similar-intensity patches as shown in 5.2b. As a result, such distance based techniques limits the performance of algorithms. A similar scenario is presented in Fig 5.3 where we take a portion of the image, shown in 5.3b, and show that distance based measures suffer limitations. Such cases becomes severe when processing images contaminated by high noise.

On the other hand, when we apply the intensity-invariant and correlation

[2]http://r0k.us/graphics/kodak/.

(a) Observed Image

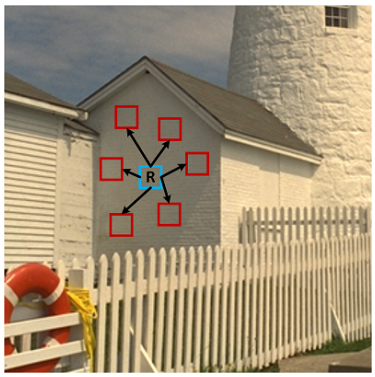

(b) Euclidean Distance

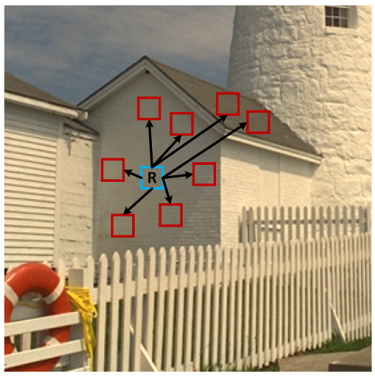

(c) Corr. Coefficient.

Figure 5.3: Light home image from Kodak gallery

coefficient based similar measure, then we have a higher number of patches to collaborate with. This is because not only such measure will give us the same intensity patches[3], but it will also consider the patches as similar that have a similar underlying structure. This is shown in Fig. 5.2c and Fig. 5.3c where a reference patch has access to similar structure patches throughout the image and is significantly less-constrained.

For much better understanding, we present a comparison of the Euclidean distance and correlation coefficient based similar patches in Fig. 5.4. We chose a

[3]By intensity-invariant, we mean that we don't specifically look for similar intensity patches rather we aim to find the patches that have a similar underlying structure. This will of course include the patches that are similar intensity-wise but will also group those patches that are similar structure-wise.

random patch as reference from the standard *Cameraman* image and then searched for the most similar patches. For both methods, we show the top 3 similar patches. As shown in Fig. 5.4a, a reference patch hunt for distance based similar intensity patches in which case it would accept even those patches which have different pixel values at some locations that may correspond to an edge information. As a result in that case, the edge information will vanish and the details will blur out due to improper collaboration.

On the contrary, a result of similar structured patches has been shown in Fig. 5.4b. As stated before, we are interested even in those patches that have negative but larger correlation. That is why the first and the third most similar patches in this case are negatively oriented corresponding to negative correlation but their underlying structure is of critical importance to our algorithm since the negative sign would be absorbed in the transformed domain.

Furthermore, it's worth noting that by virtue of the above presented definition in (5.6), the set of neighbors $\mathcal{N}_k$ are not restricted to be spatial neighbors and the set of neighbors $\mathcal{N}_k, \forall k \in \mathcal{K}$ are not disjoint. The upshot of this novel patches grouping is that it produces a higher number of neighbors for each patch which is beneficial for our sparse-domain based collaborative approach as discussed above already and explained further in the following section.

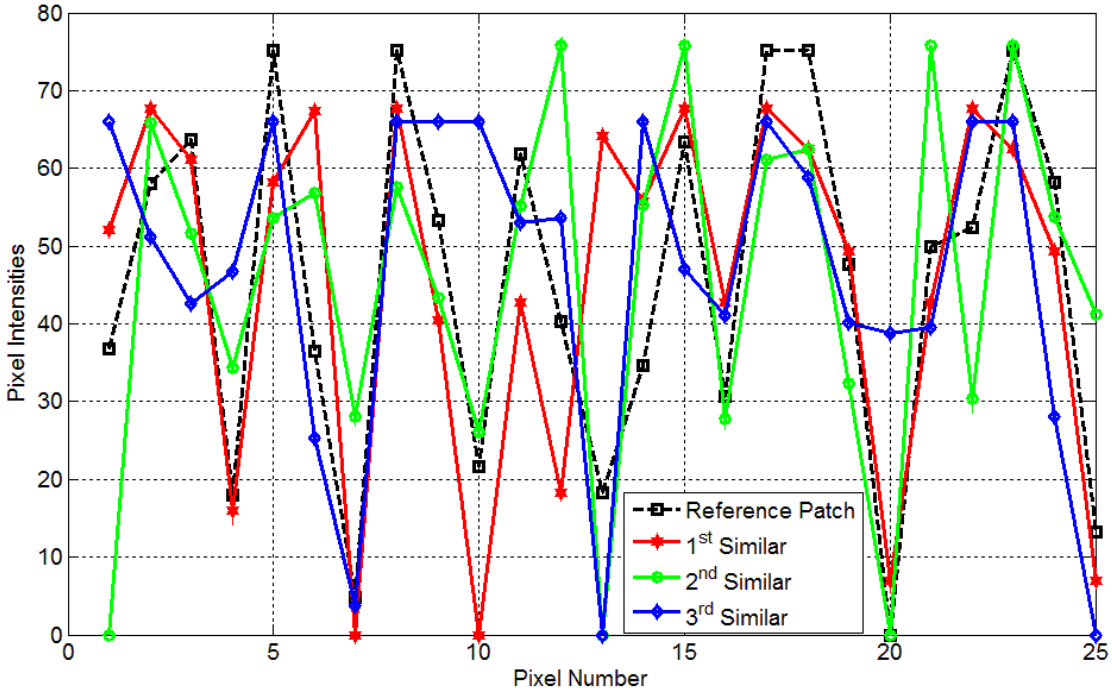

(a) Euclidean Distance Based Similarity

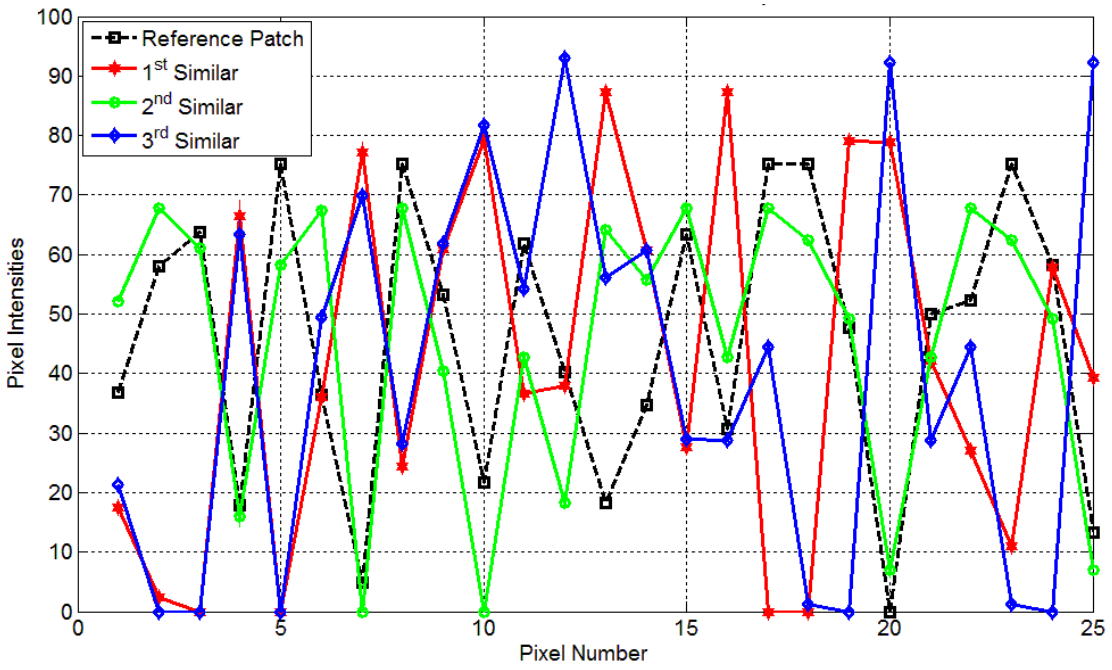

(b) Correlation Coefficient Based Similarity

Figure 5.4: Comparison of top 3 similar patches for a random vectorized 5×5 patch of *Cameraman* image

5.3 Estimation Via Collaborative Denoising

From the theory of image processing and sparse reconstruction, we know that a key property of the images is that they are inherently sparse in the wavelet transformed-domain. To take advantage of this property, we aim to transform the patches in (5.5) to find the corresponding sparse equivalent representations. For this purpose, we use the following equation:

$$\mathbf{y}_k = \mathbf{A}\mathbf{h}_k + \mathbf{w}_k, \quad \forall k \in \mathcal{K}, \tag{5.7}$$

where $\mathbf{A} \in \mathbb{R}^{N^2 \times M}$, $M \gg N^2$ is an overcomplete dictionary having wavelet basis. Furthermore, $\mathbf{h}_k \in \mathbb{R}^M$ is the equivalent sparse representation of the spatial-domain patch $\mathbf{x}_k$ i.e., $\mathbf{x}_k = \mathbf{A}\mathbf{h}_k$.

For the sparse reconstruction, we let $\widehat{\mathbf{h}}_k$ denote a recovered estimate of the sparse vector $\mathbf{h}_k$ obtained via a sparse recovery algorithm and let $\mathcal{S}_k$ represent the set of active indices in the sparse vector i.e., its support set. In order to isolate noise, we process each patch individually. It is worth noting that in an ideal situation, $\mathcal{S}_k = \mathcal{S}_i, \forall i \in \mathcal{N}_k$ should hold true for all $k \in \mathcal{K}$ i.e., the support sets of similar patches should be similar in general.

This motivates us to utilize the transformed-domain representation of the patches to devise a sparse-domain based collaborative denoising algorithm. However, this may not be the case in reality and the support sets of similar patches may have some differences since $\mathcal{N}_k$ is a function of a non-zero ϵ as well as $\mathbf{w}_k$.

Based on this, the value of the threshold ϵ serves as a key parameter in the collaborative approach which is why it should be selected properly. This is the main reason why we are using the correlation coefficient based similarity approach, i.e. so that higher similarity between the groups can be guaranteed.

Even though the correlation coefficient based approach would result in identifying the similar structured patches, the disturbances caused by the noise introduction would still persist yielding a disagreement among the support sets of similarly grouped patches. However, we would like to bring to attention here that this disagreement is actually a blessing in disguise. Provided an adequately large ϵ, majority of the outliers $\mathcal{V}_k = \bigcup_{i \in \mathcal{N}_k} \mathcal{S}_i \backslash \bigcap_{i \in \mathcal{N}_k} \mathcal{S}_i$ in the support sets are there, with high probability, due to noise. Such information ultimately guides us to find and take care of the noise-producing locations in the recovered estimate $\widehat{\mathbf{h}}_k$. One naive tactic is to diminish the contribution of the non-zero components of $\widehat{\mathbf{h}}_k$ located at $\mathcal{V}_k$ by eliminating it and using this resulting sparse vector estimate to compute an estimate of the denoised spatial-domain patch using $\widehat{\mathbf{x}}_k = \mathbf{A}\widehat{\mathbf{h}}_k$, as used in the majority of the sparse domain based denoising algorithms in the literature. However, this would basically result in discarding significantly critical information specifically in the high noise regime since some legitimate non-zero components may be mistaken for noise-producing components. In view of the stated problem, we resort to a much moderate method to tackle this case efficiently.

In this method, we take advantage by using the active taps probabilities of $\mathbf{h}_k$ i.e., the non-zero locations of the sparse vector. The approach is that since

the similar patches are grouped together and their support would be similar, so the legitimate non-zero active locations of their corresponding sparse vectors will have high probabilities of being active as presented in STAGE 02 of Fig. 5.1. Consequently, we propose this novel sparse-domain based collaboration among similar patches via active probabilities. In particular, for the kth patch, we let $\boldsymbol{\lambda}_k \in \mathbb{R}^M$ denote the active probabilities vector for the estimate $\widehat{\mathbf{h}}_k$. As a result, we find the weighted average as follows:

$$\boldsymbol{\lambda}'_k = \frac{1}{\mathcal{N}_k} \sum_{j \in \mathcal{N}_k} \alpha_{j,k} \boldsymbol{\lambda}_j, \quad \forall k \in \mathcal{K}. \tag{5.8}$$

This serves as a refined estimate of the vector corresponding to the active probability of *clean* $\mathbf{h}_k$. Here, the weighting factor is proportional to the similarity between the patches and hence the probability vectors

$$\alpha_{j,k} \propto r(\mathbf{y}_j, \mathbf{y}_k), \quad j \neq k. \tag{5.9}$$

This simple yet effective approach makes us capable of significantly reducing the contribution of solitary active locations while keeping the information on the active taps common to most of the similar patches in $\mathcal{N}_k$. Additionally, by virtue of the law of large numbers, we believe that (5.8) will produce a better refined estimate specifically since $|\mathcal{N}_k|$ is large due to the intensity-invariant correlation coefficient based grouping method as discussed in the previous sections.

The obtained clean $\boldsymbol{\lambda}'_k$ is a valuable piece of information that serves as a guide

for the *a priori* information about the active taps locations of true or clean sparse-domain representation of the kth patch $\mathbf{x}_k$. This *a priori* information would be supplied to a sparse recovery algorithm to compute a refined estimate of true $\mathbf{h}_k$, let's denote it by $\bar{\mathbf{h}}_k$, and thus an estimate of true as well as denoised kth patch that we represent as $\widehat{\mathbf{x}}_k$. To get the denoised patch, we de-normalize the noise-removed patch as follows:

$$\widehat{\mathbf{x}}_k = \begin{cases} \eta^{-1}(\mathbf{A}\bar{\mathbf{h}}_k) = \mathbf{A}\bar{\mathbf{h}}_k\|\widetilde{\mathbf{y}}_k\| & \|\widetilde{\mathbf{y}}_k\| \neq 0 \\ \eta^{-1}(\mathbf{A}\bar{\mathbf{h}}_k) = \mathbf{A}\bar{\mathbf{h}}_k & \text{otherwise} \end{cases}, \quad \forall k \in \mathcal{K}. \tag{5.10}$$

5.4 Formation of Denoised Image

As explained in Section 5.1, we decompose an image to form overlapping patches for a much better performance. Consequently, every pixel in the image is present in N^2 due to the overlapping approach and therefore, each pixel has the same number of estimated denoised intensity values. To place the patches back to their original positions and reconstruct the denoised image $\widehat{\mathbf{X}^a}$, we average the results of N^2 pixels for each pixel which in turn provides another level of denoising impurities. To increase the performance further, we implement a weighted average approach for the denoising results based on different L patch sizes. As a result, we get the further purified restored image from the denoiser, as shown in STAGE 03 of Fig.

Algorithm 1 The Denoiser

procedure COLLABORATIVE SPARSE RECOVERY BASED DENOISING
  for ith odd patch size, $i = 3, 5, 7, 9$ **do**
    Extract patches $\widetilde{\mathbf{y}}_k, \forall k \in \mathcal{K}$
    for each kth patch $\widetilde{\mathbf{y}}_k$ **do**
      Normalize patches and find $\mathcal{N}_k = \{i : r(\mathbf{y}_k, \mathbf{y}_i) \geq \epsilon\}$
      Find weighting matrix containing $\alpha_{j,k}$ entries
      Run SABMP for each patch to find active probabilities $\boldsymbol{\lambda}_k$ via $\widehat{\mathbf{h}}_k$
      Refining probabilities to find $\boldsymbol{\lambda}'_k = \frac{1}{\mathcal{N}_k} \sum_{j \in \mathcal{N}_k} \alpha_{j,k} \boldsymbol{\lambda}_j$
      Refining sparse estimates via SABMP using $\boldsymbol{\lambda}'_k$ to find $\bar{\mathbf{h}}_k$
      Find denoised patch $\widehat{\mathbf{x}}_k = \eta^{-1}(\mathbf{A}\bar{\mathbf{h}}_k)$
    end for
    Restore all the denoised patches to from $\widehat{\mathbf{X}^a}_i$
  end for
  Average the results $\bar{\mathbf{X}}_d = \sum_i \gamma_i \widehat{\mathbf{X}^a}_i$
end procedure

5.1, block as follows:

$$\bar{\mathbf{X}}_d = \sum_i \gamma_i \widehat{\mathbf{X}^a} i, \quad i = 3, 5, 7 \ldots, \tag{5.11}$$

where γ_i and $\widehat{\mathbf{X}^a}_i$ are the weights and image from the denoiser block based on the ith odd patch size, respectively. The aforementioned steps of the denoiser block have also been presented in Algorithm 1.

5.5 The Post-Processor

Once we have the denoised image from the denoiser block $\bar{\mathbf{X}}_d$, we pass it to the post-processor block to further take care of the smooth regions and remove the remaining noise-components, if any. The post-processor block has two major steps to tackle the remaining noise elements: 1) detecting and processing flat/smooth

patches, and 2) region growing based enhancement of the smoother regions. Both of these steps are discussed as follows.

5.5.1 Detecting Flatness

For the detection of flat regions, we use the most commonly used standard deviation based detection method, an example of which has been shown in Fig. 5.5 where, in Fig. 5.5a, we show a clean noiseless 512×512 *Cameraman* image, while in Fig. 5.5b, we show its standard deviation version. In this method, an image has to be padded first to accommodate the border pixels. Then, a 3×3 window based neighborhood approach is applied to find out the flatness of the patch centered at the reference pixel. The standard deviation of this 3×3 patch serves as the decider whether to label it as a flat or non-flat region i.e, a small standard deviation value would correspond to a flat region, while a larger value would mean that it's a non-flat region and has edge details.

As can be seen in Fig. 5.5b that the edges have been separated properly and the flat regions have been segmented out. Now, this of course yield quite promising detection for clean images but might miss out some flat patches in the noisy image. For this reason, we denoise our image first to have a properly details recovered image and then pass it to the post-processor to perform the stated operations. The threshold ζ to decide whether a patch, centered at a reference pixel, should be labeled as smooth or non-smooth has been set based on observing a number of natural as well as synthetic images.

(a) 512 × 512 Cameraman (b) Standard Deviation

Figure 5.5: An example of detecting flat regions of *Cameraman* image using standard deviation of a 3 × 3 neighborhood as the detection measure.

Once the patches are detected and labeled as flat, we then proceed to smooth these out for discarding the remaining noisy components hidden in the flat regions, as shown in STAGE 04 of Fig. 5.1. For a flat patch, we replace the center reference pixel by the average value of the pixels in its 3 × 3 neighborhood. As a result, we get the refined flat pixels[4] that we put back to their original positions to reconstruct the image as follows:

$$\bar{\mathbf{X}}_f(z) = \begin{cases} \bar{\mathbf{x}}_k^f(z) \;\; = \frac{1}{|\bar{\mathbf{x}}_k^d|} \sum_{j=1}^{|\bar{\mathbf{x}}_k^d|} \bar{\mathbf{x}}_k^d(j) & \sigma(\bar{\mathbf{x}}_k^d) \leq \zeta \\ \bar{\mathbf{x}}_k^{nf}(z) = \bar{\mathbf{x}}_k^d(z) & \text{otherwise} \end{cases}, \forall k \in \mathcal{K}, \tag{5.12}$$

where $\bar{\mathbf{x}}_k^d$ is the kth patch extracted from the output image $\bar{\mathbf{X}}_d$ of the denoiser block and z represent the index location of each pixel. The superscripts f and

[4]By flat pixel, we mean a pixel whose neighborhood has been detected as flat. In our case, if the standard deviation of the 3 × 3 neighborhood of a reference pixel is smaller than ζ, then it's called as a flat pixel.

nf in the terms $\bar{\mathbf{x}}_k^f(z)$ and $\bar{\mathbf{x}}_k^{nf}(z)$ correspond to the processed flat and non-flat pixel, respectively, and $\bar{\mathbf{X}}_f(z)$ represents the zth pixel of the flatted/smoothed out image $\bar{\mathbf{X}}_f$ using the aforementioned process.

5.5.2 Region Growing

As a final step for removing out the noisy components from the image, we perform region growing method on the image $\bar{\mathbf{X}}_f$ resulted from the previous process. For the image $\bar{\mathbf{X}}_f$, we store the pixels in different number of bins based on their intensity levels. For instance, we assign group 1 to the pixels that have, let's say, intensity range from 0-3, group 2 to intensities from 4-7 and so on. We do this for all the pixels and as a result we create different bins with pixels and their locations stored within those bin groups. We show an example of applying such intensity-leveling on *Cameraman* image in Fig. 5.6. In this figure, we display all the intensity groups/bins as binary images where the white pixels correspond to the pixels of the *Cameraman* image belonging to the relevant group.

For each bin, we apply the region growing algorithm to find the connected pixels within that bin. This means that the local similar intensity pixels are identified first. Afterwards, if the number of connected pixels in each bin exceed a certain threshold, then we replace those connected pixels by their mean. Similarly, we repeat this process for all the bins which ultimately provides us with the region growing processed image that we denote by $\bar{\mathbf{X}}_r$. Finally, we get our final denoised image $\bar{\mathbf{X}}$, STAGE 05 of Fig. 5.1, using the weighted average of the image $\bar{\mathbf{X}}_d$ from

denoiser and the region growing processed image $\bar{\mathbf{X}}_r$ as follows

$$\bar{\mathbf{X}} = \rho_1 \bar{\mathbf{X}}_d + \rho_2 \bar{\mathbf{X}}_r, \tag{5.13}$$

where ρ_1 and ρ_2 are the weights which are a function of the noise variance. We also present the steps of our post-processor in the Algorithm 2.

Algorithm 2 The Post-Processor

procedure REGION GROWING BASED AVERAGING
    Extract patches $\bar{\mathbf{x}}_k^d, \forall k \in \mathcal{K}$
    for each kth patch $\bar{\mathbf{x}}_k^d$ **do**
        if $\sigma(\bar{\mathbf{x}}_k^d) \leq \zeta$ **then**
            $\bar{\mathbf{x}}_k^f(z) = \frac{1}{|\bar{\mathbf{x}}_k^d|} \sum_{j=1}^{|\bar{\mathbf{x}}_k^d|} \bar{\mathbf{x}}_k^d(j)$
        end if
    end for
    Restore the patches to form $\bar{\mathbf{X}}_f$
    Form pixel intensity based bin groups
    Apply region growing to find connected pixels
    Refine connected pixels
    $\bar{\mathbf{X}} = \rho_1 \bar{\mathbf{X}}_d + \rho_2 \bar{\mathbf{X}}_r$
end procedure

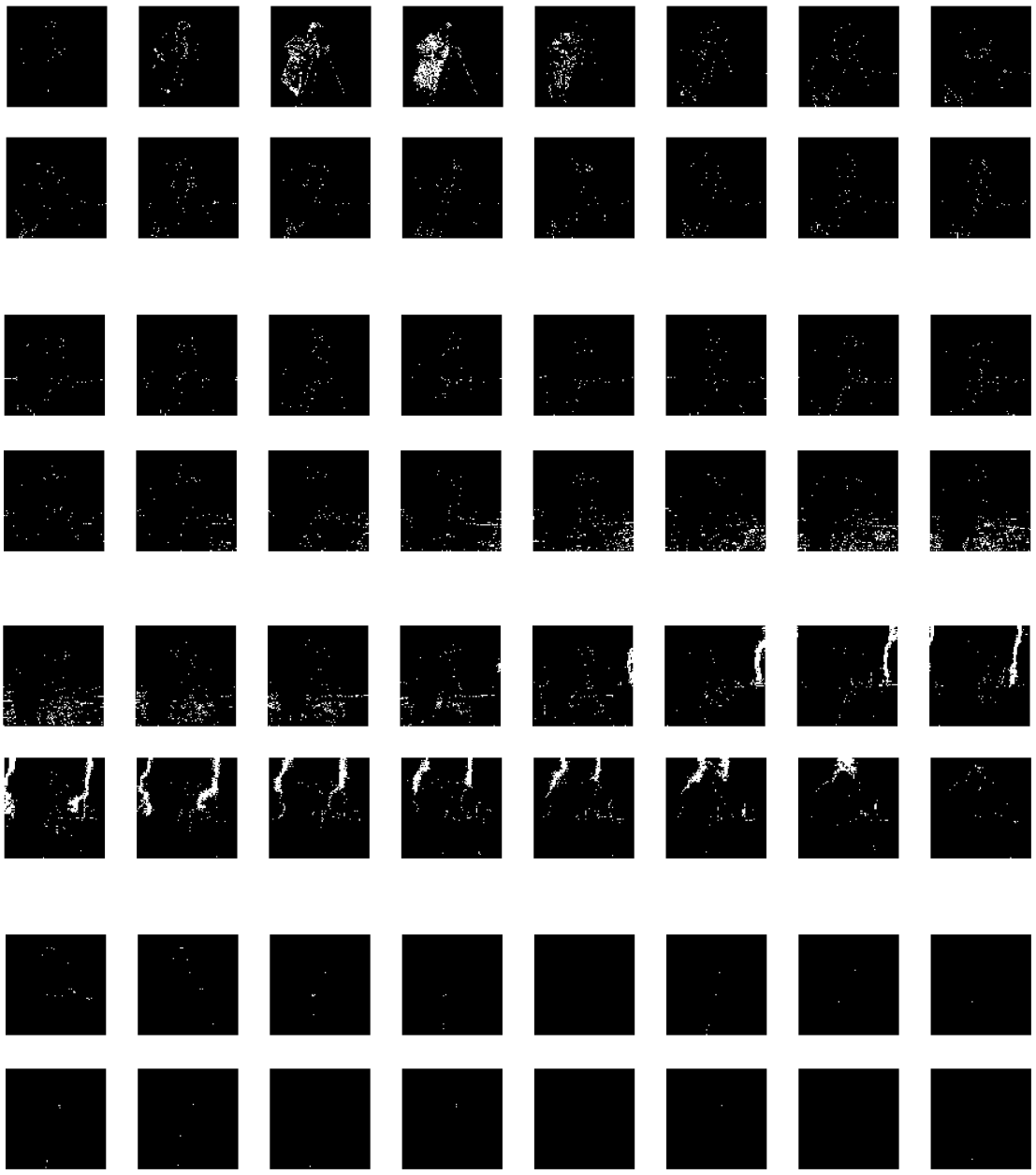

Figure 5.6: An example of dividing the *Cameraman* image into 64 different groups/bins (left to right): first row; group 1-8, second row; group 2-16, third row; group 17-24, fourth row; group 25-32, fifth row; group 33-40, sixth row; group 41-48, seventh row; group 49-56, 8th row; group 57-64

CHAPTER 6

COLOR IMAGE DENOISING

6.1 Color Images

In this chapter, we present our proposed image denoising algorithm for denoising the color images contaminated by additive white Gaussian noise. As opposed to the grayscale images that have only one channel, the color images have 3 channels denoted as R (red), G (green) and B (blue) channels as shown in Fig. 6.1. These channels combinely give the colored appearance to an image scene. We show examples of few color images in Fig. 6.2.

The color images contain the color information for each pixel in 3 different channels. This information representation is done in order to give a more visually acceptable look to a scene so that the resulting digital image can more accurately represent the true information of a natural scene. Consequently, the three channels are used for each pixel that are interpreted as coordinates in some color space.

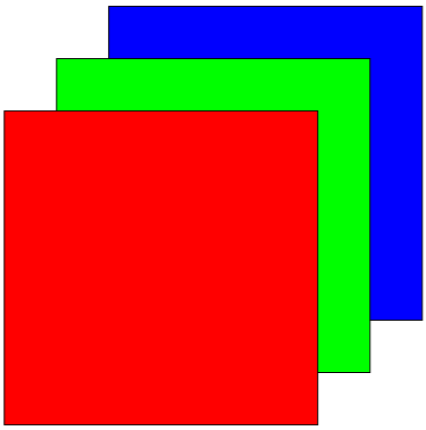

Figure 6.1: R, G and B channels of a color image

(a)

(b)

(c)

(d)

Figure 6.2: (a) Mandrill (b) Islamia College, Peshawar, Pakistan (c) Faisal Masjid, Islamabad, Pakistan (d) Butterfly

6.2 Effective Collaboration Using RGB Channels of Color Images

As opposed to the case of grayscale single channel images, color images having three RGB channels provide a more advanced way through which the patches can collaborate. Since finding similar patches using more effective approaches is the key for such collaboration, the three channels of a color images supply an important piece of information in the form of the channel correlation that can be used to identify similar patches.

(a) (b) (c)

Figure 6.3: (a) Red channel, (b) Green channel, and (c) Blue channel of the Mandrill color image.

To understand this, consider the three R, G and B channels of the standard Mandrill test image as shown in Fig. 6.3 as separate images. Since the additive white Gaussian noise is independent in all three channels of the image, we denoise the color image by denoising each channel separately. This results in formation of rectangular patches for all three channels. To denoise a patch in a specific channel of the observed color image, once the patches are extracted, similar patches are grouped together by taking into account information from both reference channel

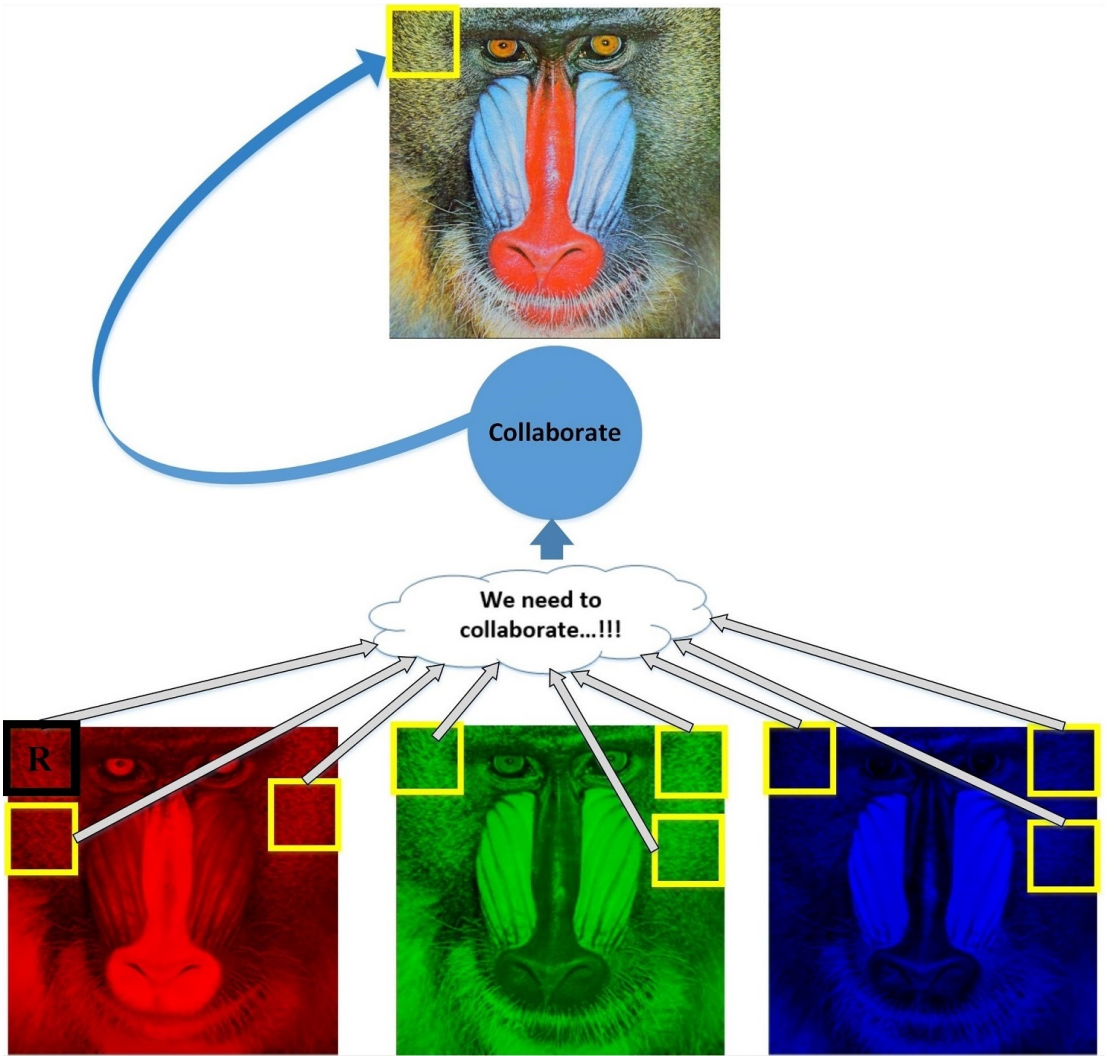

Figure 6.4: A depiction of collaboration among patches across all three channels

and the other two channels.

For example in Fig. 6.4, to denoise the reference patch, denoted by 'R', from the red channel, similar patches are grouped together from the red channel firstly. This ensures the identification of patches as similar and gives a set containing the information of similar patch numbers. Using this set from the red channel, the similar patches from other channels for this specific patch are also identified. Then, the reference patch in the red channel may collaborate with the patches from all

channels. Since the idea is to refine the probabilities of active taps by using the sparse vectors that may share the same support, finding similar patches using all three channels can be very effective. These grouped patches for all channels can then ultimately be used to effectively estimate the sparse vectors that are in turn used to obtain denoised patches. These steps are performed for all the patches in all the three channels which ultimately provide us with a denoised color image.

CHAPTER 7

SIMULATIONS RESULTS

7.1 Results of CSAR

In this section, we compare the proposed CSAR algorithm with two state-of-the-art algorithms, namely, NL-means [31] and BM3D [48]. Comparisons with NL-means and BM3D validate the superior performance of CSAR and prove that our algorithm is even robust to situations where these cannot perform well.

For the simulations, we used various grayscale standard test images. For a more challenging competition, an SNR range including very high noise levels were used providing higher chances of confusing signal components with noise. The entries of dictionary were derived from wavelet as well as DCT basis. Square patch sizes of 3, 5, 7 and 9, i.e., $L = 4$, were used and the denoising results were averaged.

Fig. 7.1 compares the performance of denoising the peppers image by proposed CSAR with BM3D and NL-means algorithms. The peppers image is specifically

selected for its *detailed rich* nature making the comparison more interesting. It is obvious that the proposed algorithm outperforms the other two algorithms across the considered SNR range. Apart from outperforming in terms of PSNR, the SSIM performance of CSAR is also much better than other competing algorithms.

The comparison of denoising *Cameraman* is provided in Fig. 7.2. This experimental results taken at SNR = 5 dB depict that our algorithm outperforms state-of-the-art algorithms. Another comparison of *Mandrill* at SNR = 0 dB and 5 dB is illustrated in Fig. 7.3. These figures emphasize the importance of preserving feature rich portions, as done by CSAR, which are more likely to get destroyed in the presence of noise.

Specifically, we show in Fig. 7.2 that our results are not blurred at high noise of SNR = 5 dB, while in Fig. 7.3 we show that we are good at preserving the details. For instance in Fig. 7.3, note that the face details are blurred out both at SNR = 0 and 5 dB in BM3D but exist in CSAR denoised image. This degradation due to blurring or removal of feature rich components can have critical consequences e.g. detecting tumors in bio-medical applications, that can be life threatening if detections go wrong. Detailed results are provided in Table 7.2 for a number of test images widely used in the denoising literature. These extensive results demonstrate the superiority and efficacy of our approach over images of different types.

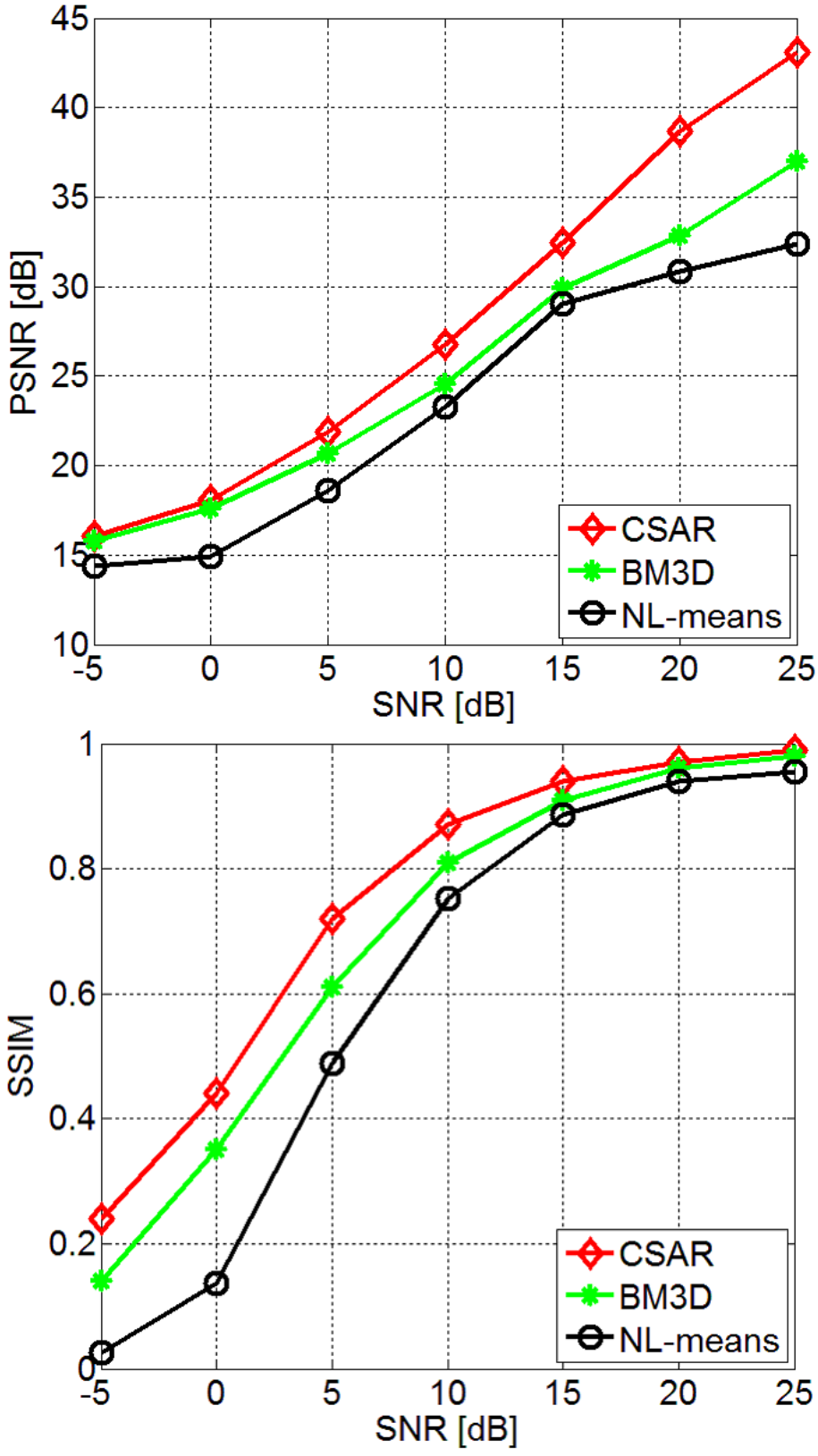

Figure 7.1: PSNR and SSIM comparison of *Peppers* image

Figure 7.2: Left to right: original and noisy *Cameraman*, denoised by: NL-means, BM3D and CSAR at $\mathrm{SNR}_{dB}/\sigma = 5/33$

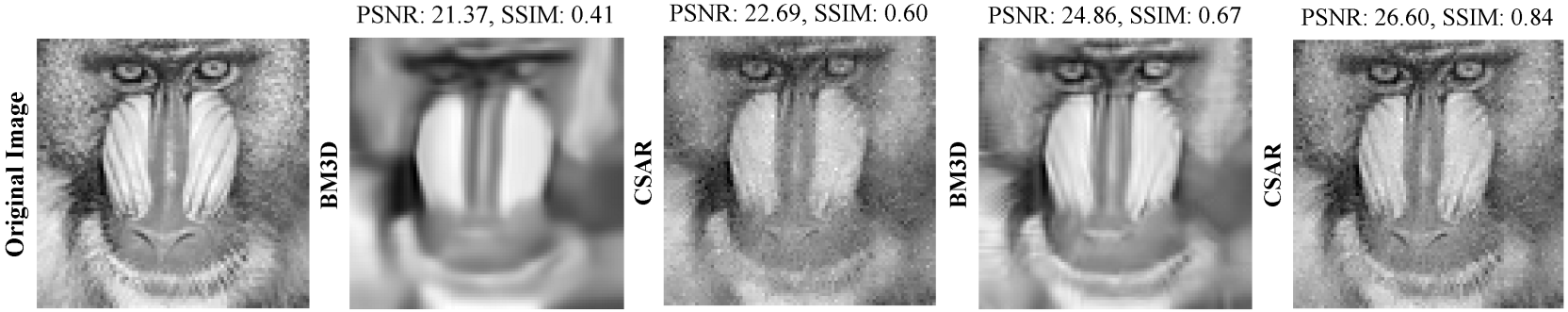

Figure 7.3: Left to right: original *Mandrill*, denoised by BM3D and CSAR at $\mathrm{SNR}_{dB}/\sigma = 0/58$ and $5/33$

SNR [dB] / σ		Cameraman	Lena	Barbara	House	Peppers	Living Room	Boat
-5/103	CSAR	**14.88/0.12**	**16.61/0.26**	**15.20/0.22**	**16.79/0.17**	**16.07/0.24**	**17.70/0.25**	**17.34/0.22**
	BM3D	14.73/0.10	16.37/0.19	14.87/0.11	16.07/0.11	15.80/0.14	16.64/0.14	16.95/0.09
0/58	CSAR	**16.57/0.24**	**19.32/0.50**	**16.99/0.43**	**19.29/0.32**	**18.06/0.44**	**19.81/0.45**	**19.49/0.41**
	BM3D	16.57/0.22	18.94/0.43	16.86/0.34	19.26/0.28	17.60/0.35	18.60/0.29	17.97/0.24
5/33	CSAR	**18.02/0.42**	**24.95/0.77**	**21.13/0.75**	**24.39/0.50**	**21.86/0.72**	**23.24/0.74**	**21.97/0.67**
	BM3D	17.59/0.40	23.91/0.71	20.55/0.67	22.98/0.48	20.68/0.61	21.21/0.58	19.68/0.50
10/18	CSAR	**22.60/0.58**	**26.90/0.87**	**27.34/0.92**	**30.34/0.60**	**26.78/0.87**	**32.46/0.91**	**24.06/0.86**
	BM3D	22.32/0.57	25.04/0.86	26.40/0.88	28.37/0.60	24.53/0.81	29.24/0.86	22.47/0.76
15/10	CSAR	**27.45/0.71**	**28.97/0.91**	**35.22/0.97**	**37.78/0.70**	**32.47/0.94**	**36.92/0.96**	**25.53/0.94**
	BM3D	27.07/0.71	27.45/0.90	31.84/0.95	36.12/0.67	29.93/0.91	32.86/0.93	24.50/0.89
20/6	CSAR	**33.55/0.83**	**33.03/0.94**	**39.84/0.98**	**42.25/0.78**	**38.68/0.97**	**41.55/0.98**	**26.80/0.97**
	BM3D	31.84/0.79	32.33/0.92	35.49/0.97	39.34/0.73	32.87/0.96	36.79/0.97	25.45/0.94
25/3	CSAR	**39.78/0.91**	**33.91/0.96**	**44.55/0.99**	**46.70/0.85**	**43.09/0.99**	**46.27/0.99**	**28.12/0.98**
	BM3D	37.08/0.87	33.01/0.94	39.49/0.98	42.82/0.79	36.97/0.98	41.01/0.98	27.30/0.97

Table 7.1: Comparison of denoising grayscale images using CSAR and BM3D both in terms of PSNR [dB] and SSIM

Further, the results of proposed CSAR algorithm and the competing BM3D algorithm were compared over a large number of standard test images using a wide range of noise levels. For this purpose, we show all the original standard test images in Fig. 7.4 used for the extensive simulations. The noisy and the resulting denoised images using BM3D and proposed CSAR algorithms are shown in Fig. 7.5 to Fig. 7.24. We show in these figures that our proposed algorithm is capable of both preserving smooth regions of the image as well as the details in the image, which is in fact one of the most challenging tasks while denoising since many denoising algorithms tend to blur out the details. Also as we have compared the results using a wide range of noise levels, this validates that our algorithm is superior to the state-of-the-art algorithm BM3D and is better in terms of both objective and subjective measures.

Figure 7.4: First column top to bottom: original Mandrill, Peppers, Barbara and Boat images. Second column top to bottom: original Cameraman, House and Lake images. Third column top to bottom: original Lena, Living Room and Man images.

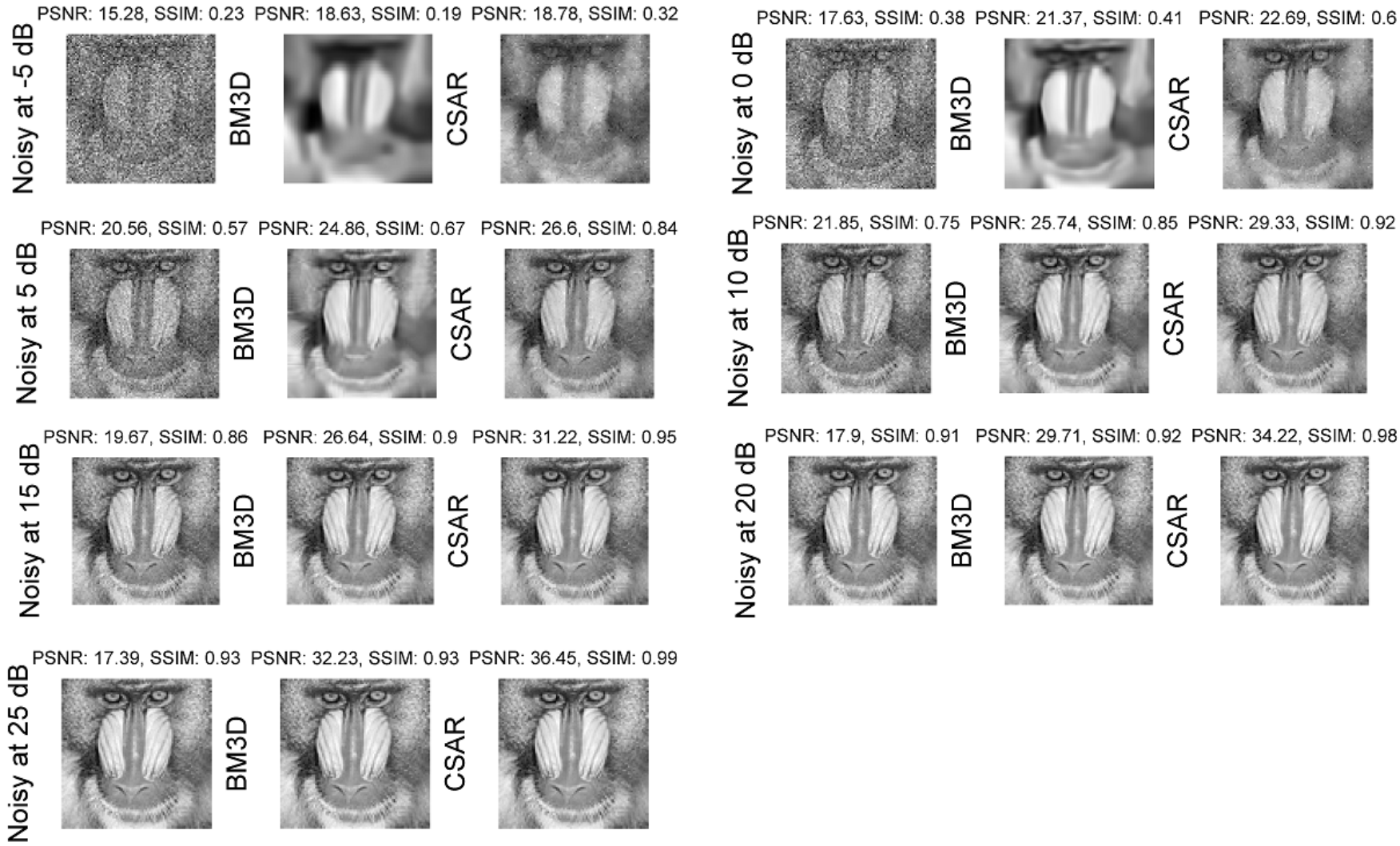

Figure 7.5: A comparison of BM3D and CSAR algorithm's based denoising results of Mandrill standard test image over an extensive SNR range of -5 dB to 25 dB.

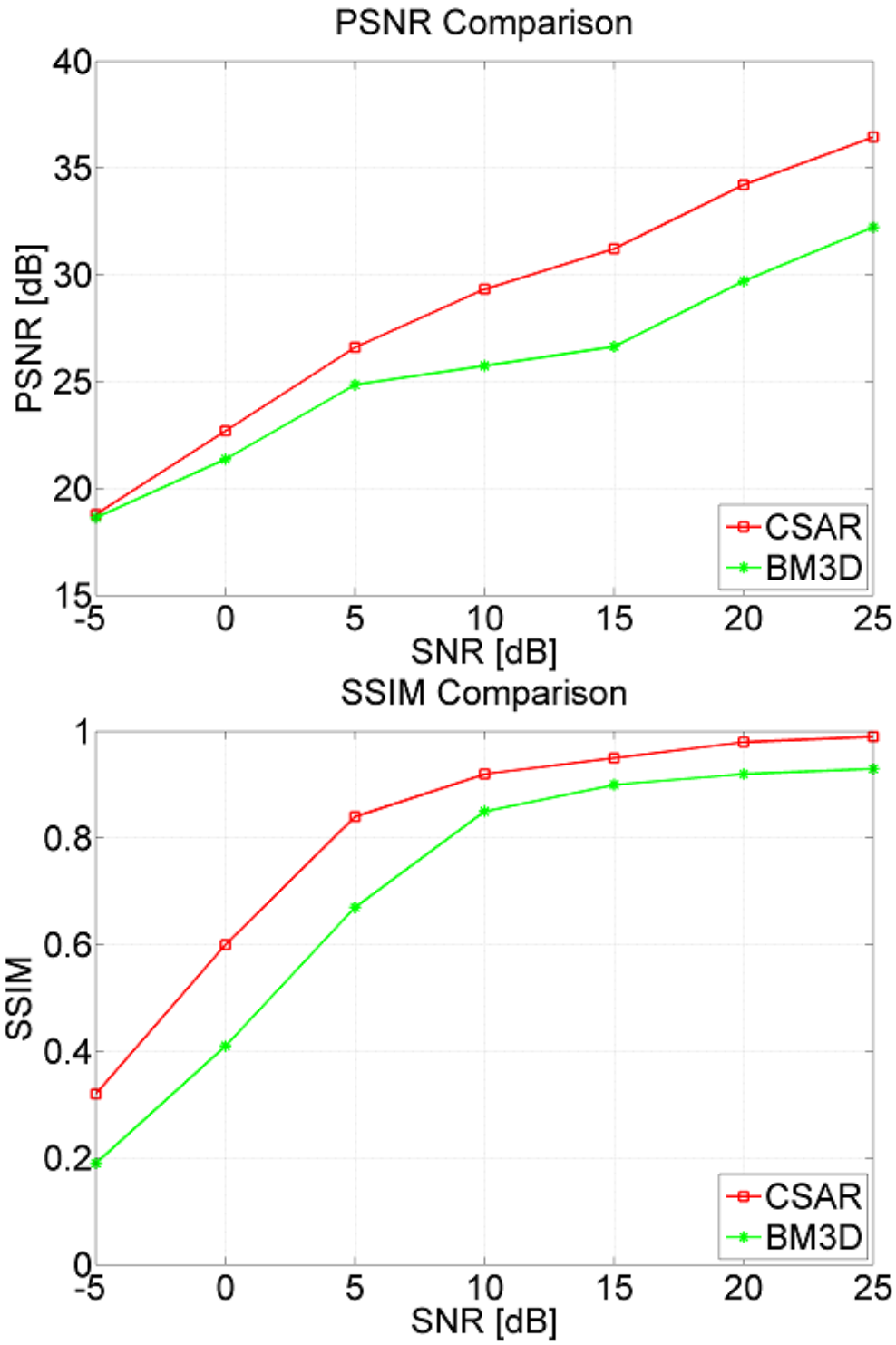

Figure 7.6: A graphical comparison of BM3D and CSAR algorithm's based denoising results of Mandrill standard test image.

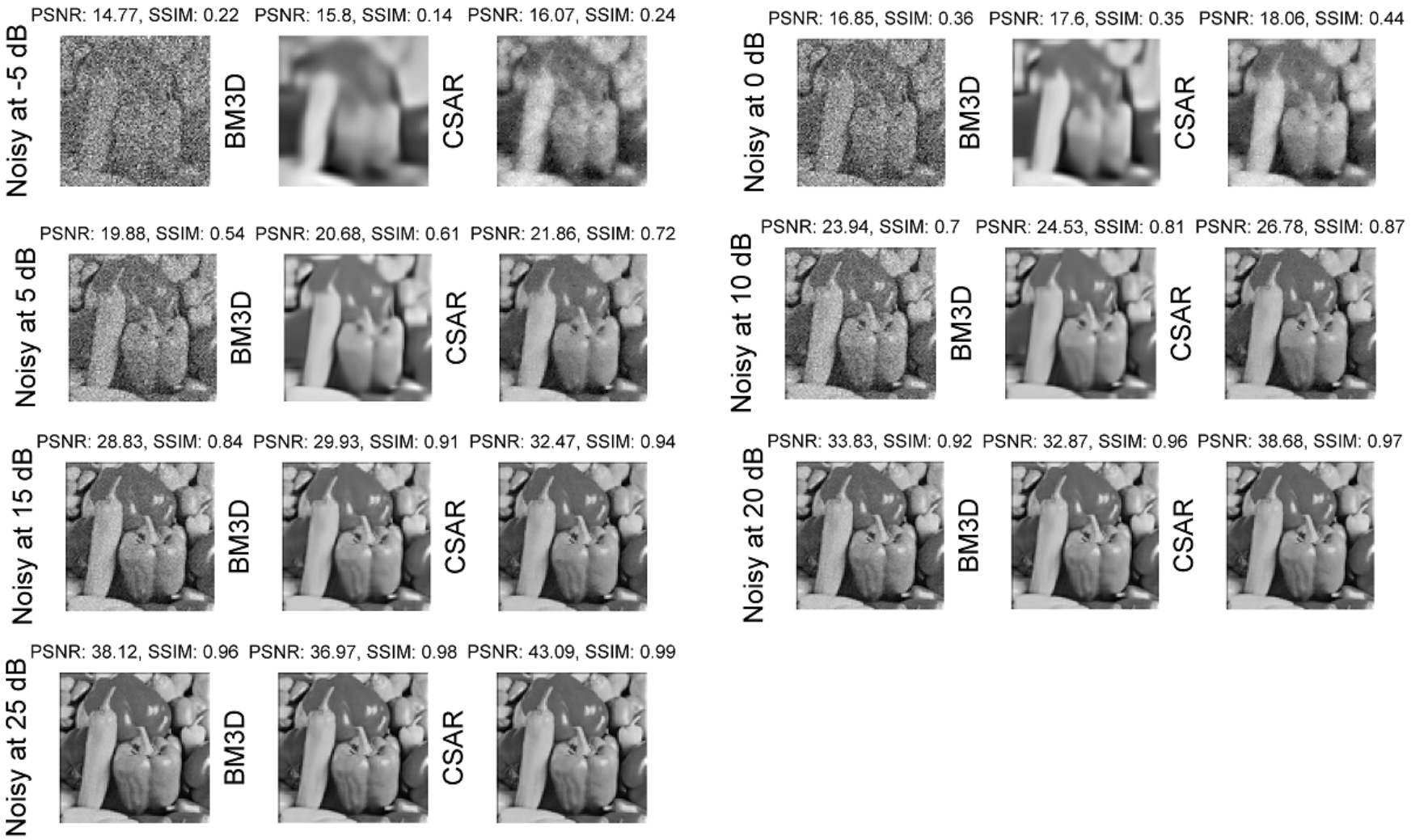

Figure 7.7: A comparison of BM3D and CSAR algorithm's based denoising results of Peppers standard test image over an extensive SNR range of -5 dB to 25 dB.

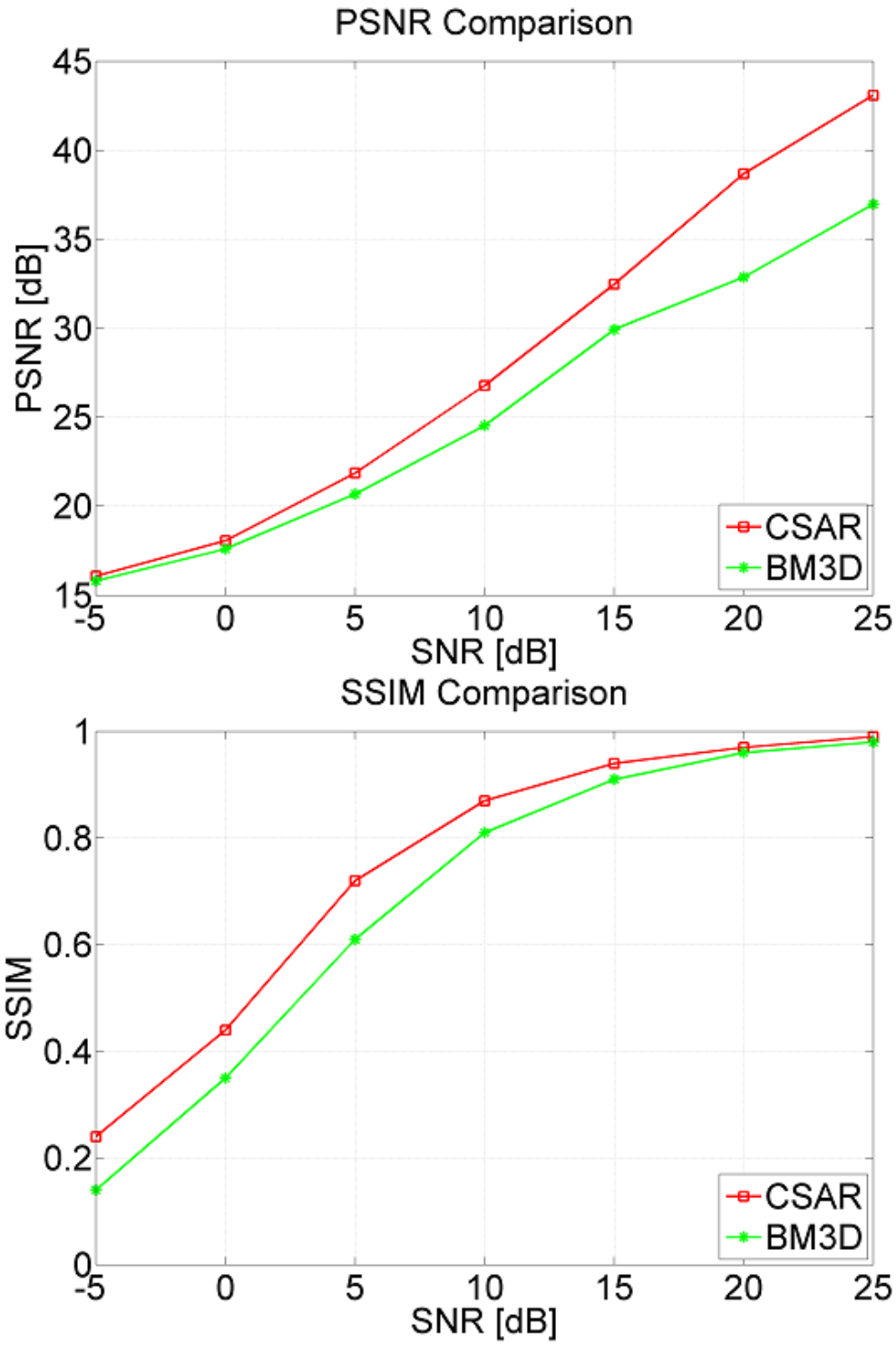

Figure 7.8: A graphical comparison of BM3D and CSAR algorithm's based denoising results of Peppers standard test image.

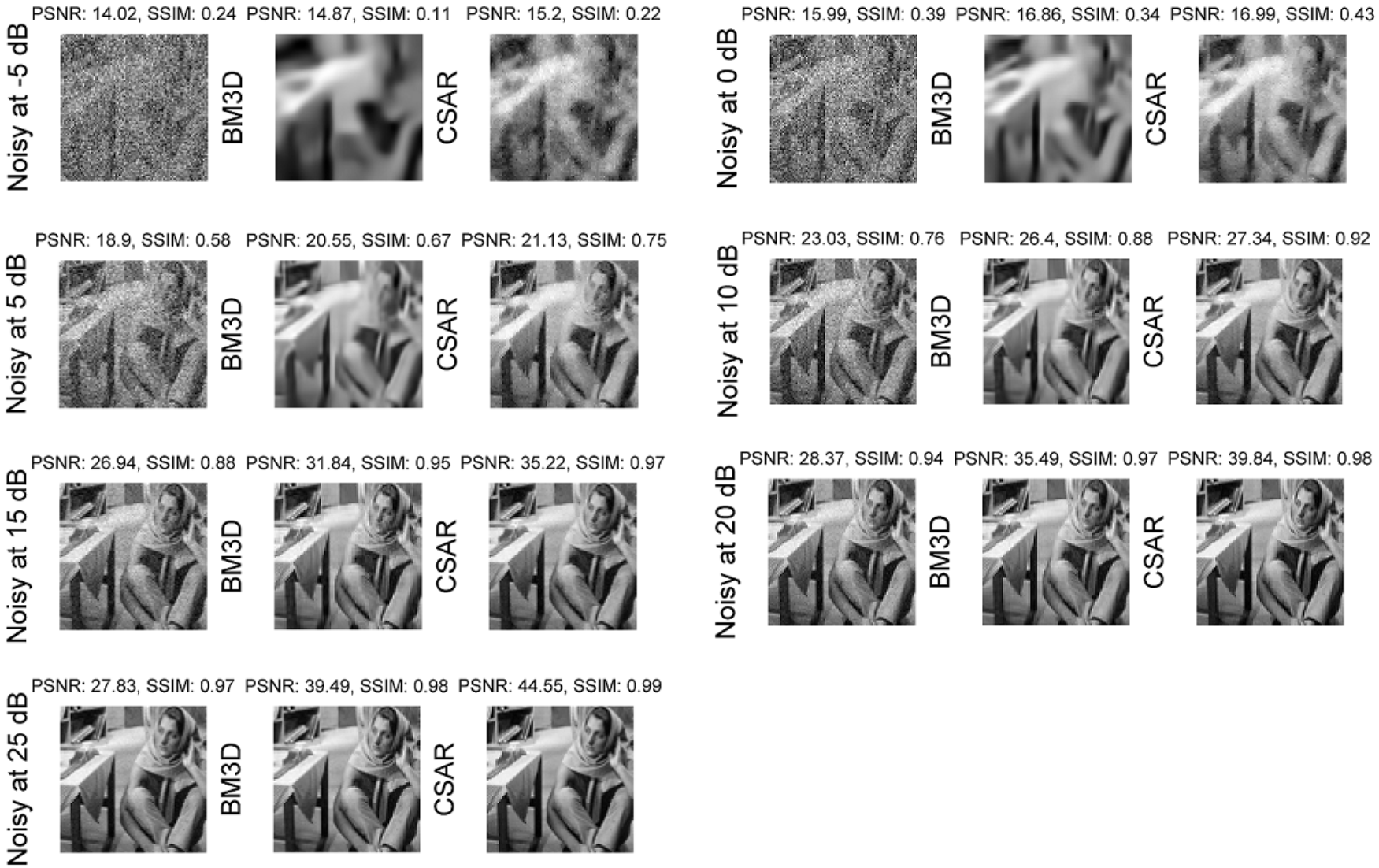

Figure 7.9: A comparison of BM3D and CSAR algorithm's based denoising results of Barbara standard test image over an extensive SNR range of -5 dB to 25 dB.

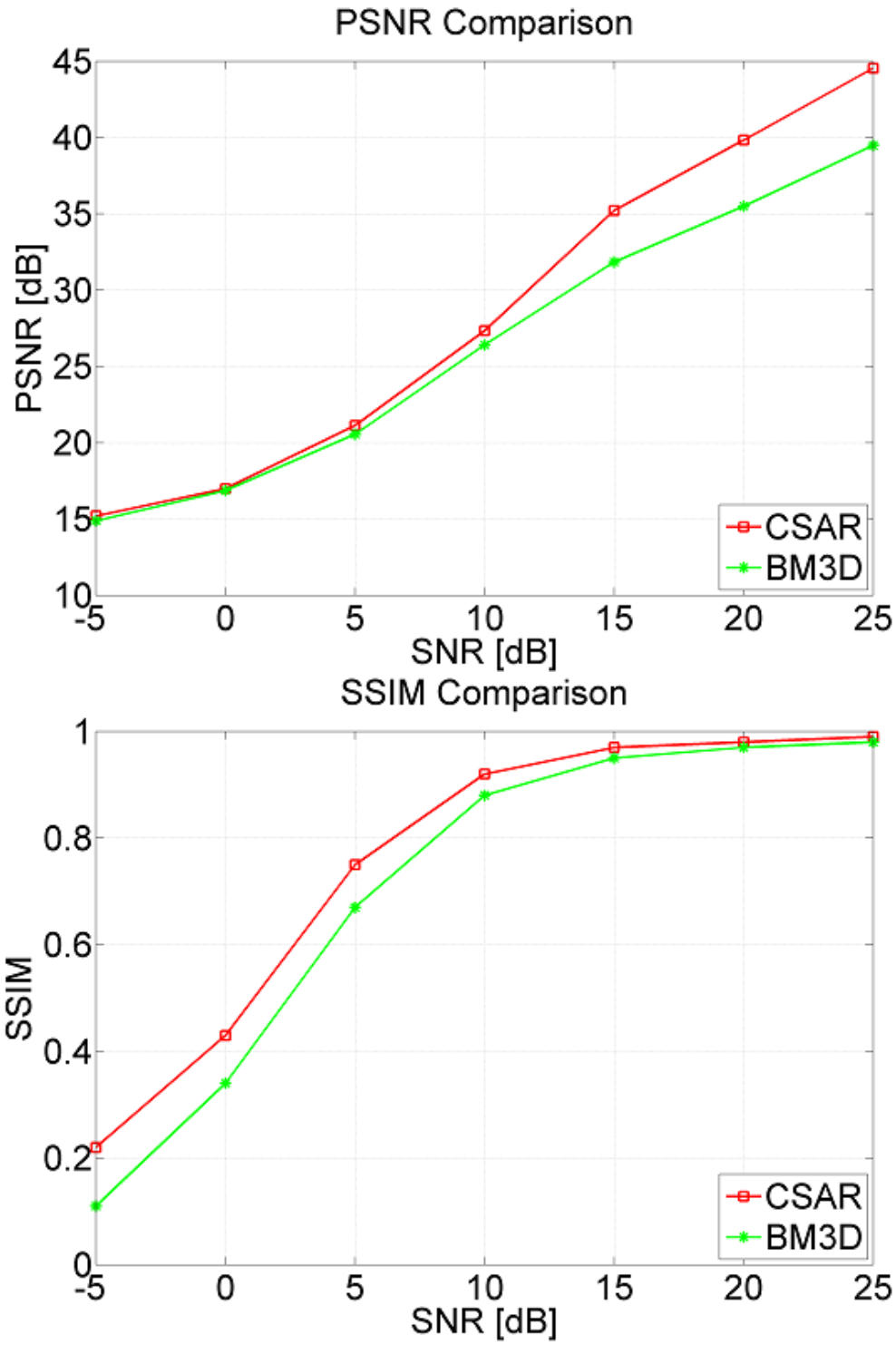

Figure 7.10: A graphical comparison of BM3D and CSAR algorithm's based denoising results of Barbara standard test image.

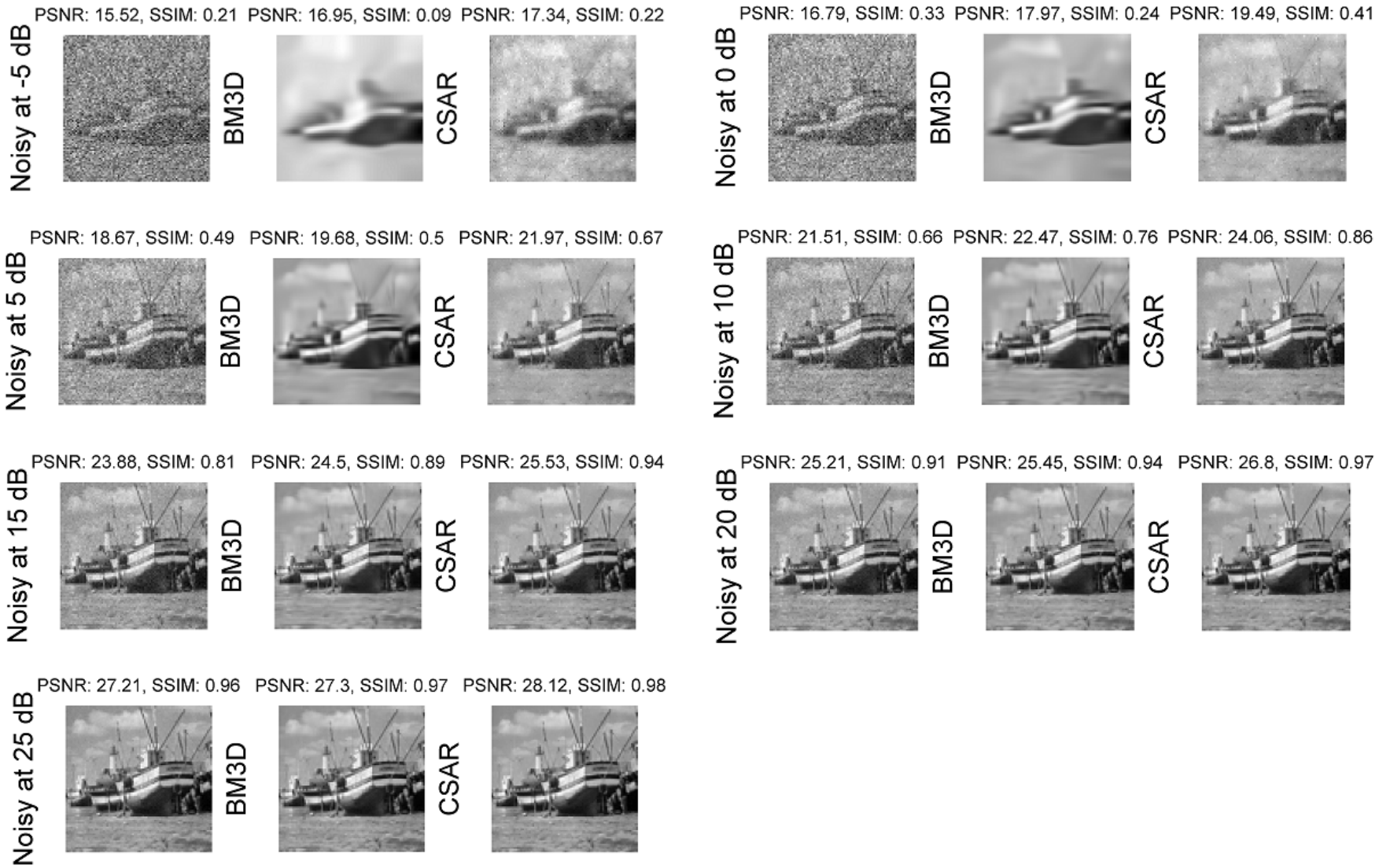

Figure 7.11: A comparison of BM3D and CSAR algorithm's based denoising results of Boat standard test image over an extensive SNR range of -5 dB to 25 dB.

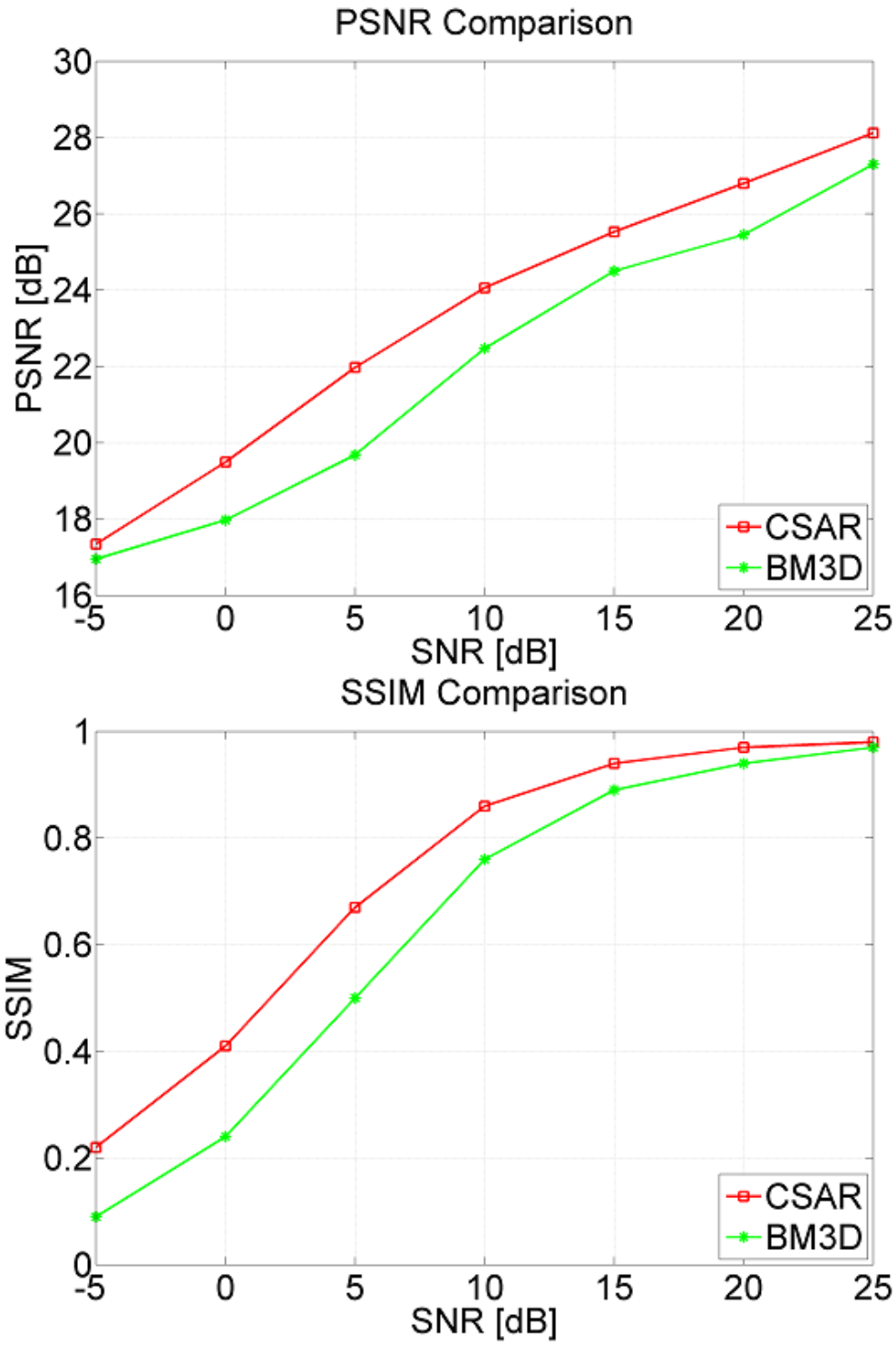

Figure 7.12: A graphical comparison of BM3D and CSAR algorithm's based denoising results of Boat standard test image.

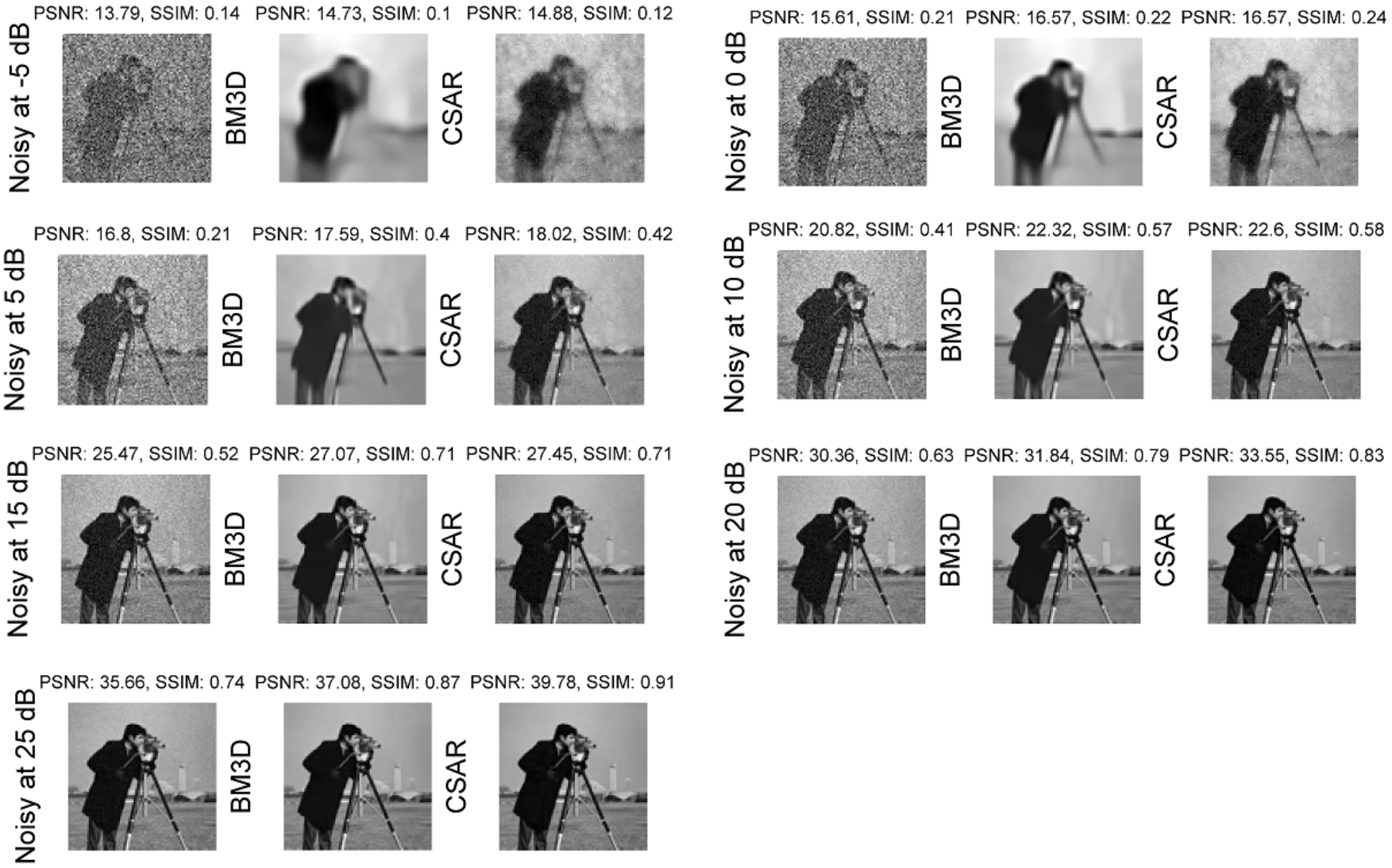

Figure 7.13: A comparison of BM3D and CSAR algorithm's based denoising results of Cameraman standard test image over an extensive SNR range of -5 dB to 25 dB.

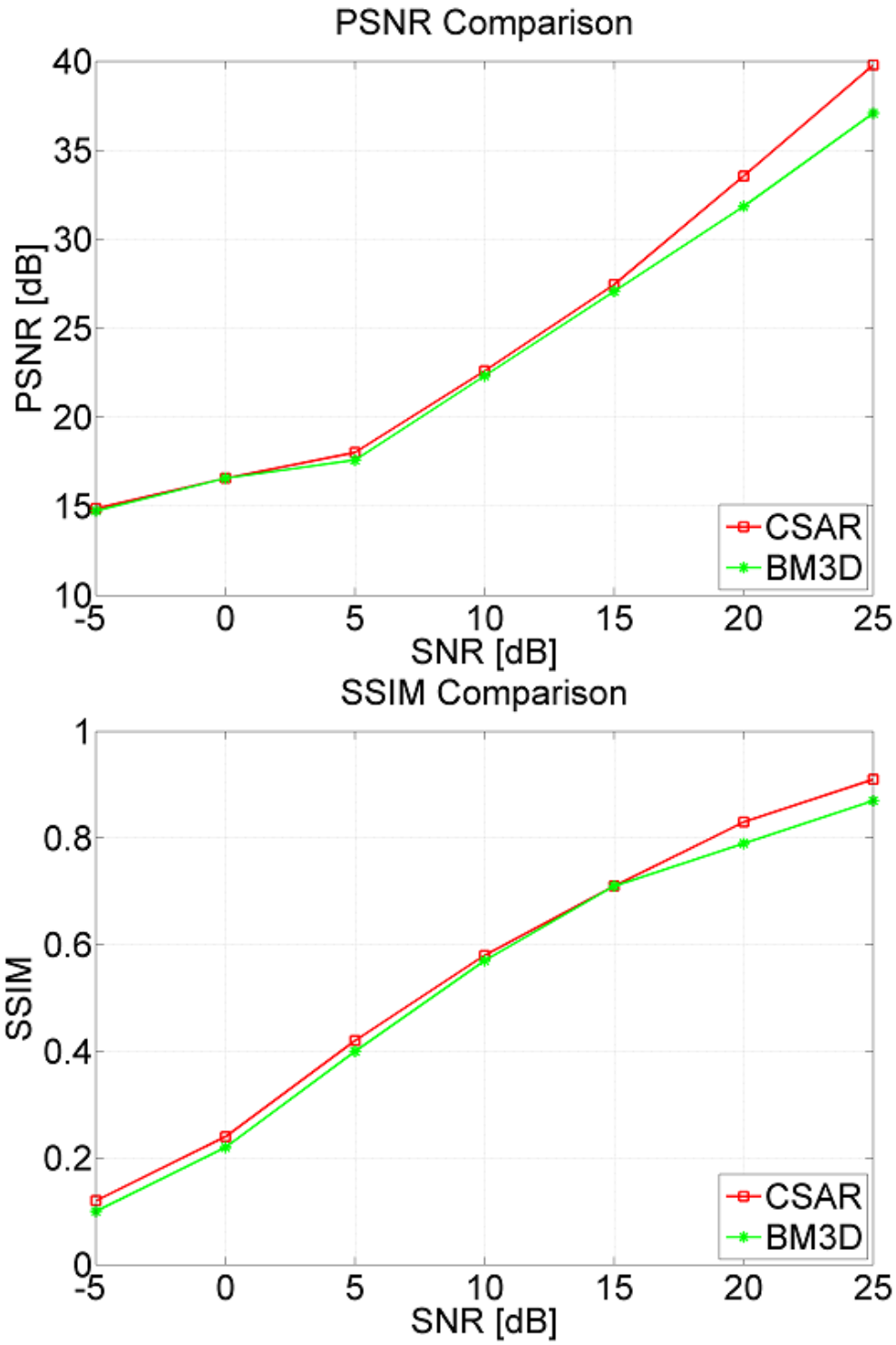

Figure 7.14: A graphical comparison of BM3D and CSAR algorithm's based denoising results of Cameraman standard test image.

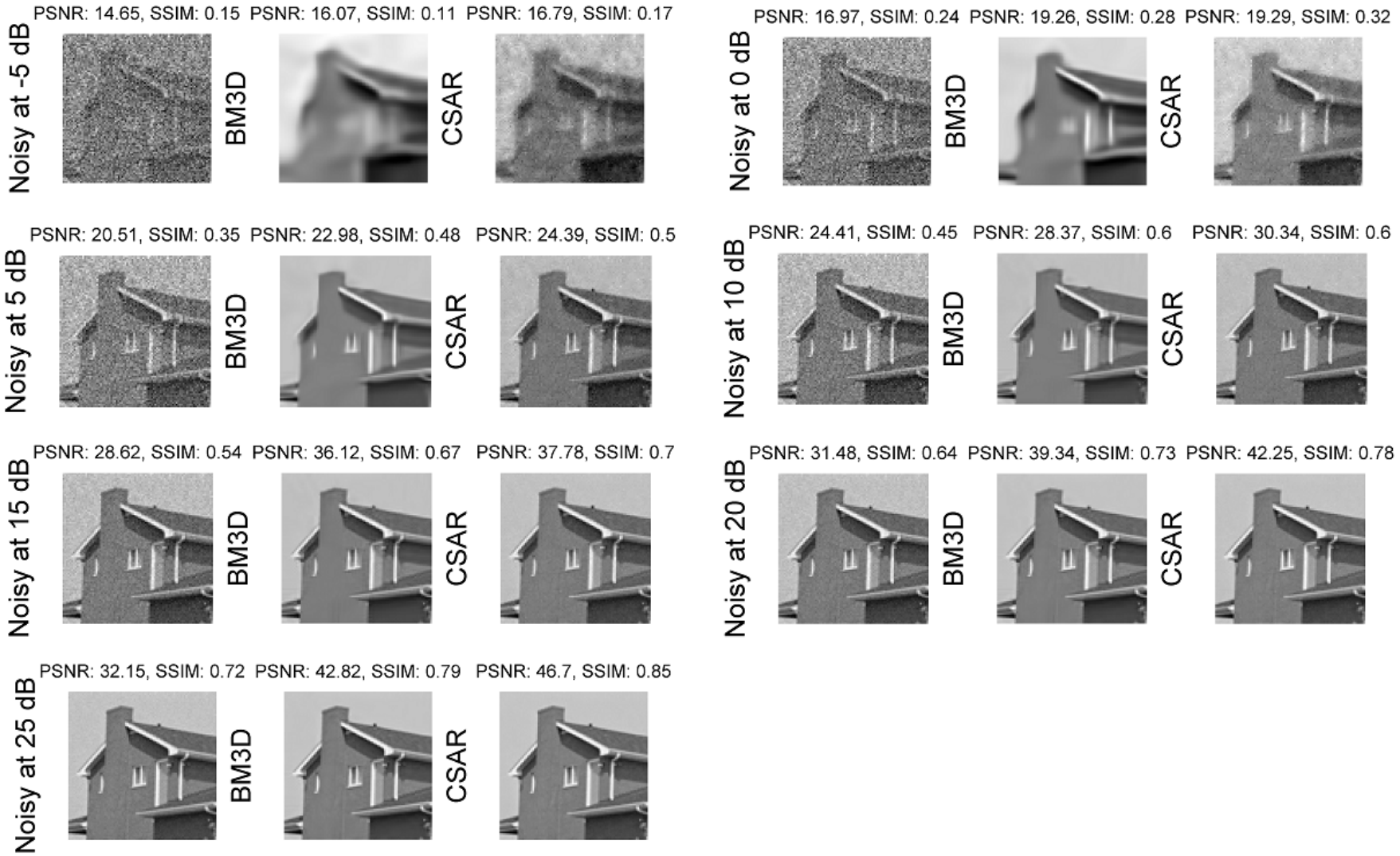

Figure 7.15: A comparison of BM3D and CSAR algorithm's based denoising results of House standard test image over an extensive SNR range of -5 dB to 25 dB.

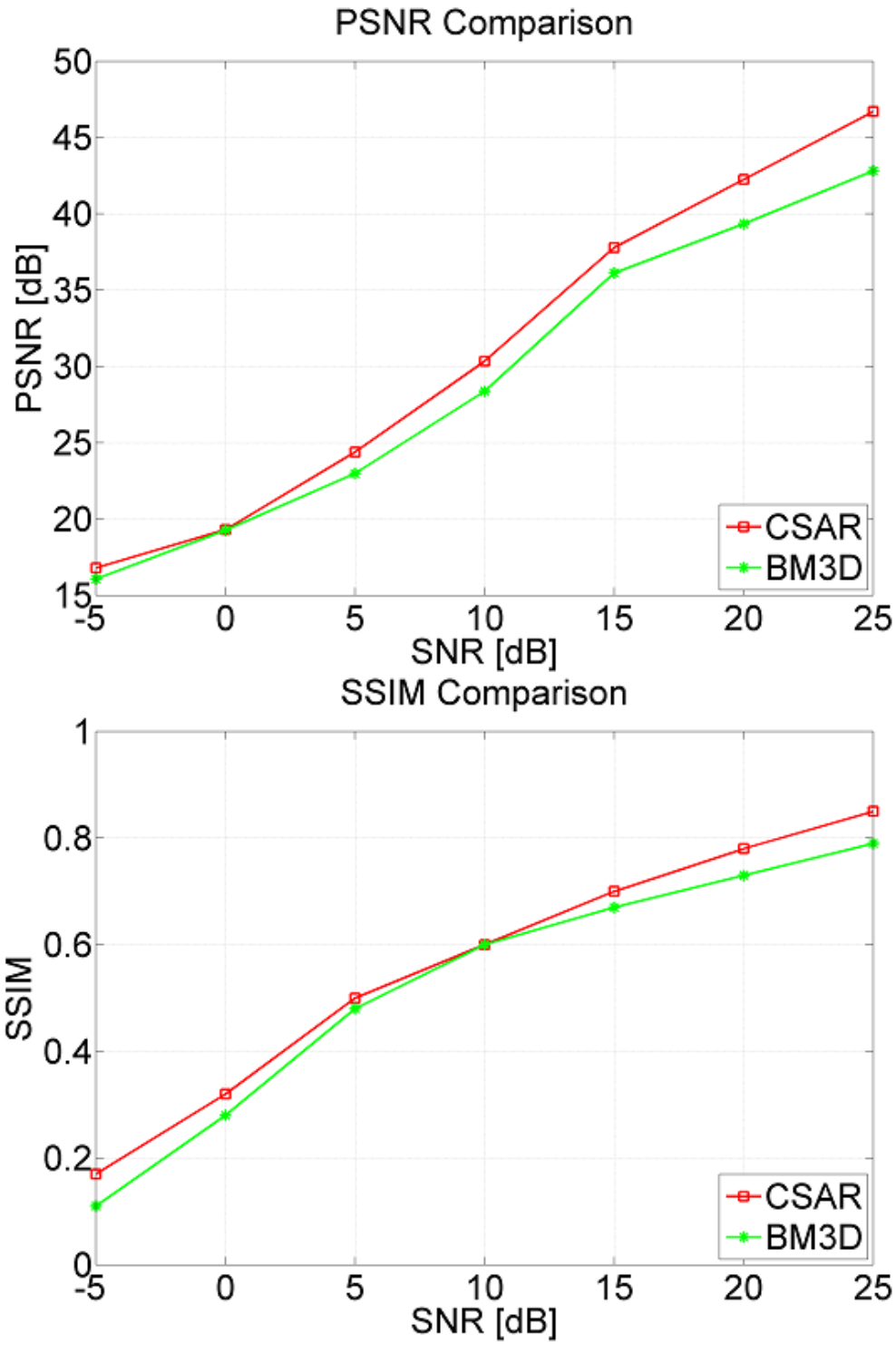

Figure 7.16: A graphical comparison of BM3D and CSAR algorithm's based denoising results of House standard test image.

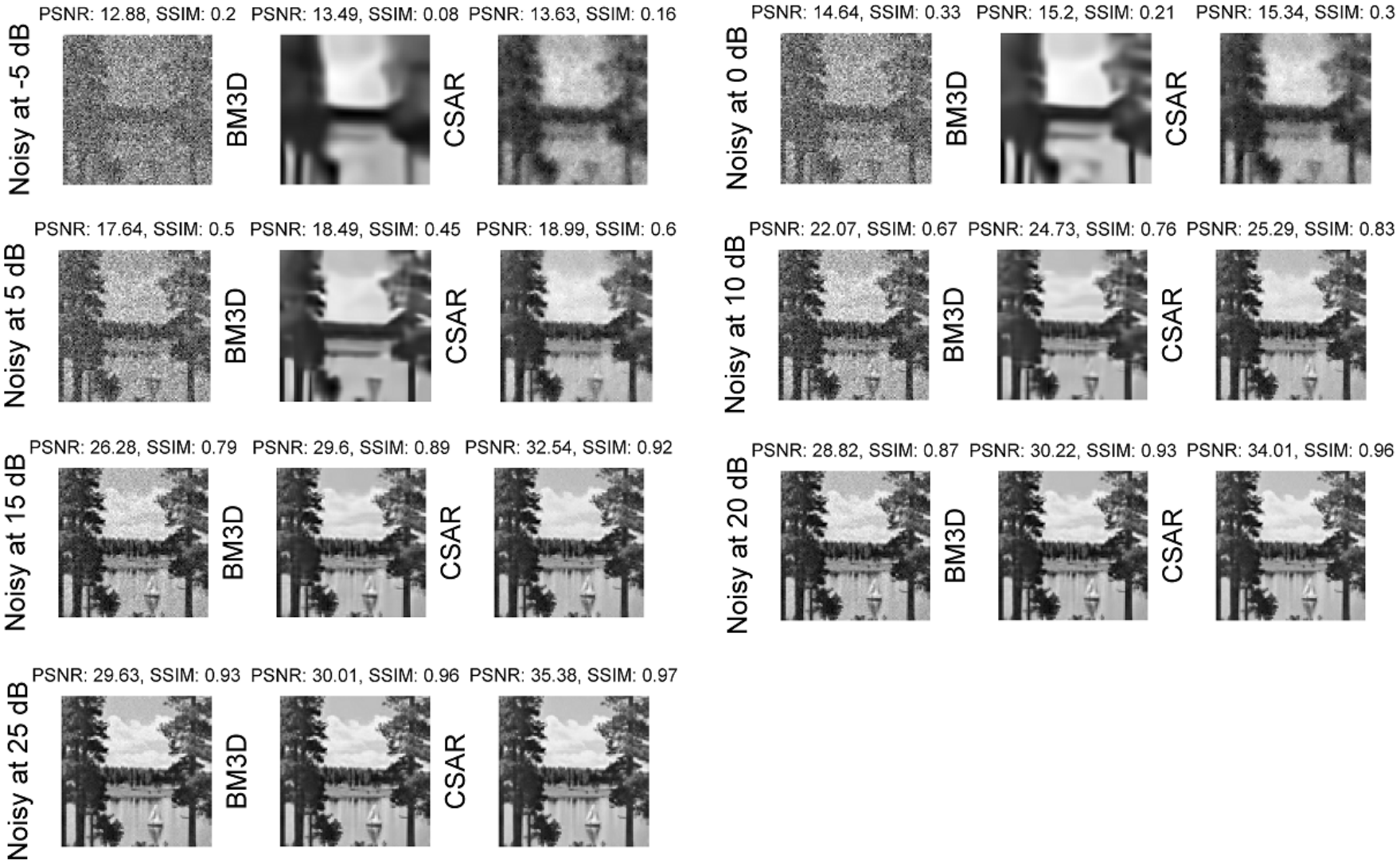

Figure 7.17: A comparison of BM3D and CSAR algorithm's based denoising results of Lake standard test image over an extensive SNR range of -5 dB to 25 dB.

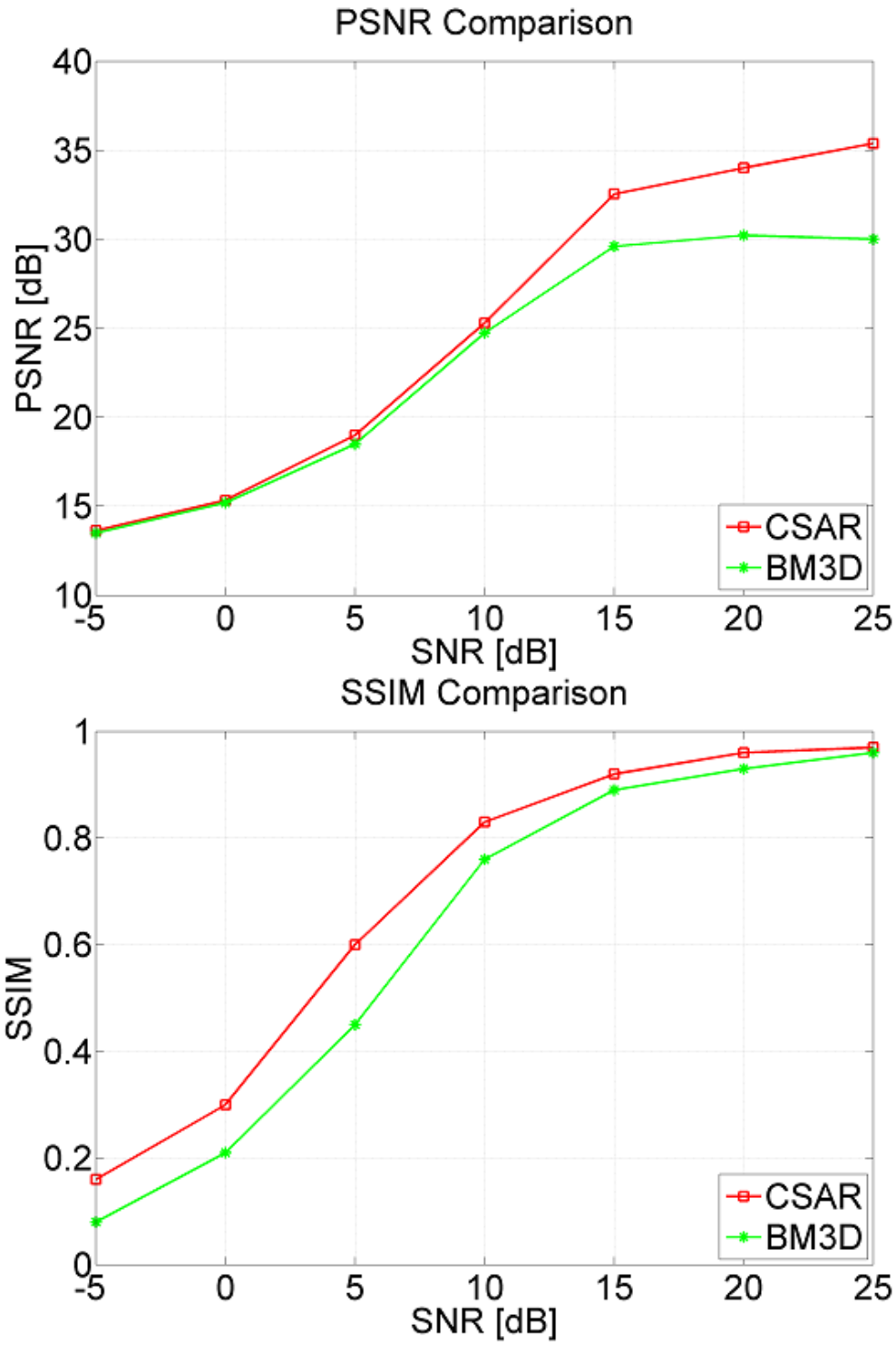

Figure 7.18: A graphical comparison of BM3D and CSAR algorithm's based denoising results of Lake standard test image.

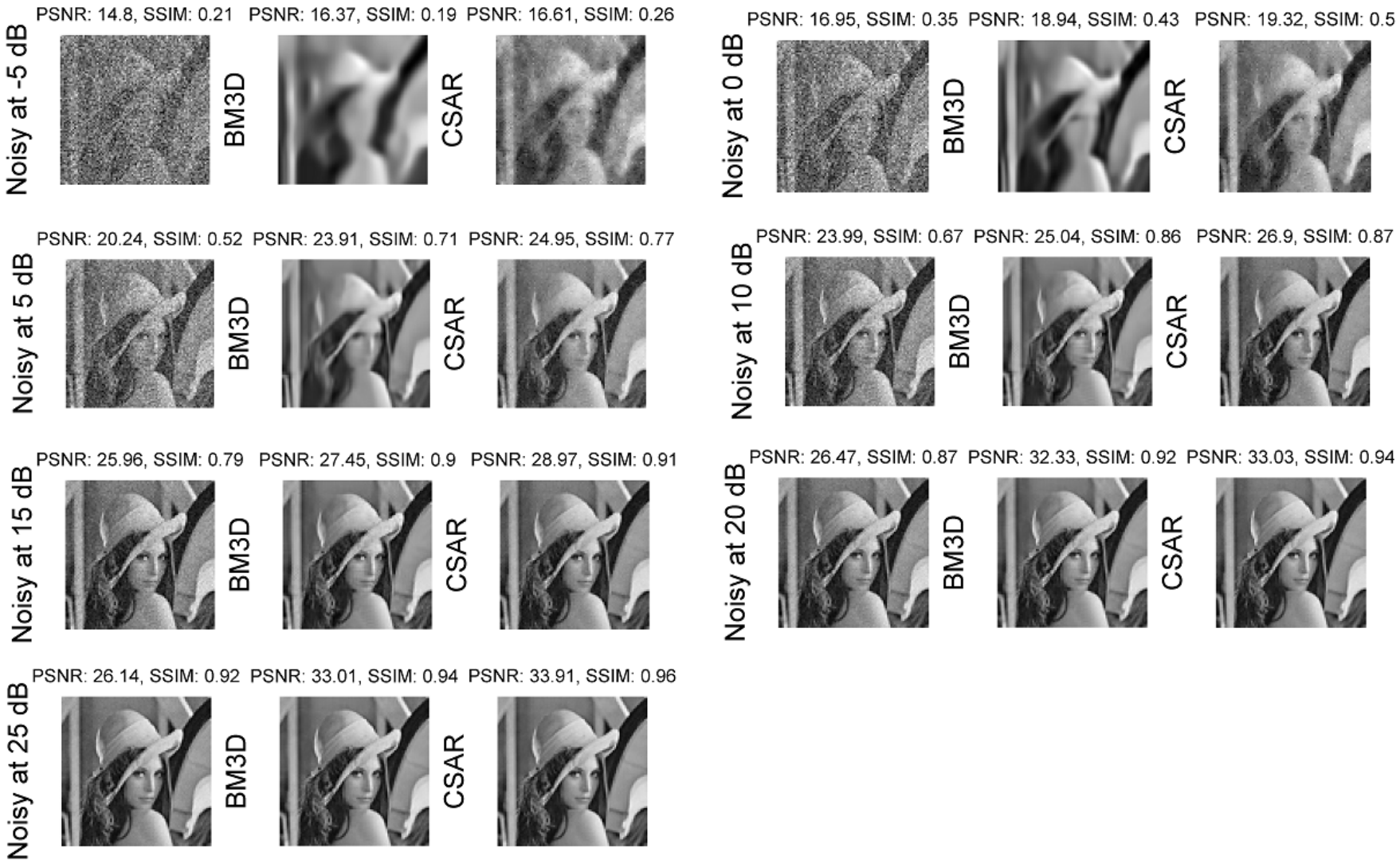

Figure 7.19: A comparison of BM3D and CSAR algorithm's based denoising results of Lena standard test image over an extensive SNR range of -5 dB to 25 dB.

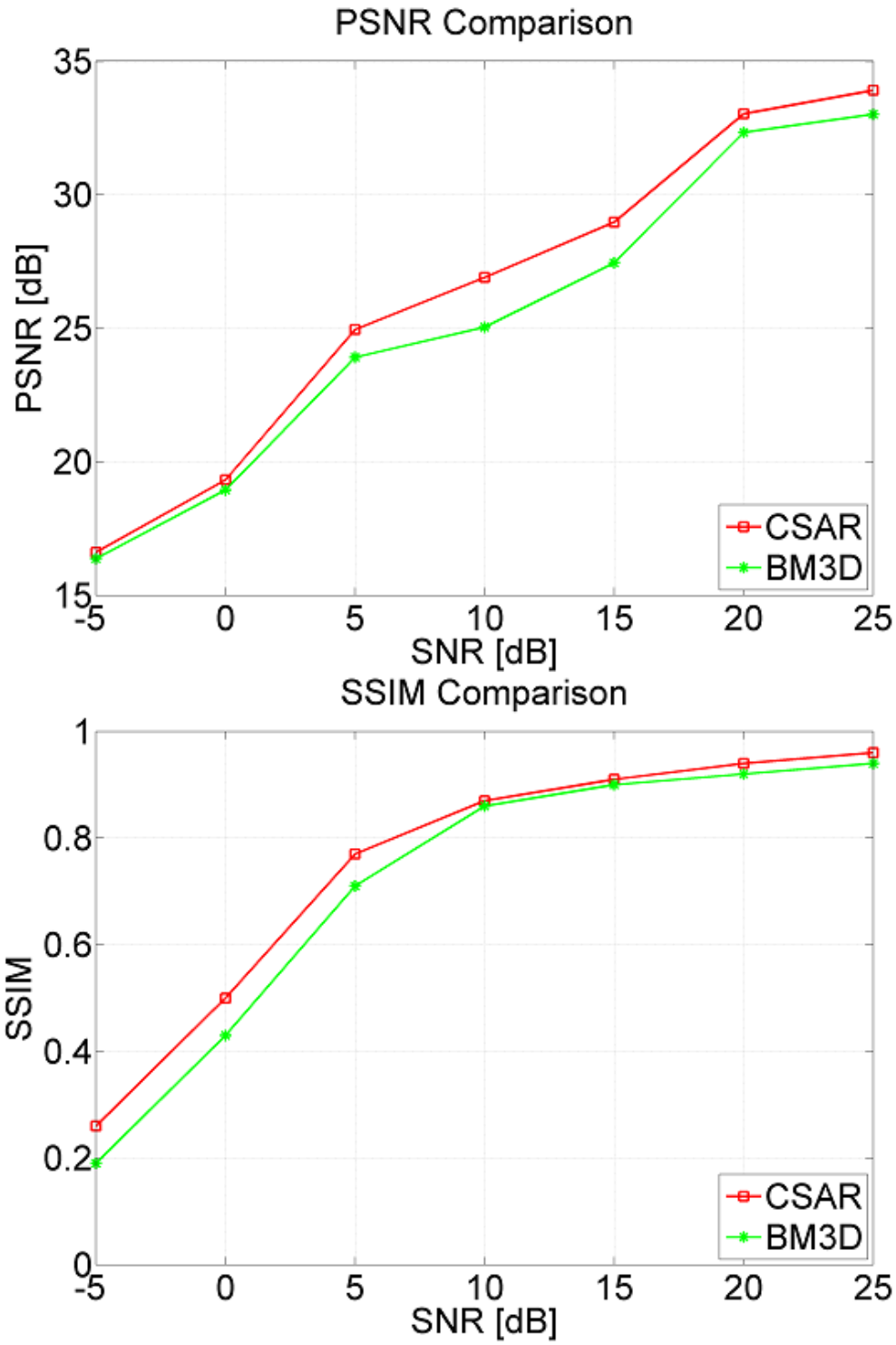

Figure 7.20: A graphical comparison of BM3D and CSAR algorithm's based denoising results of Lena standard test image.

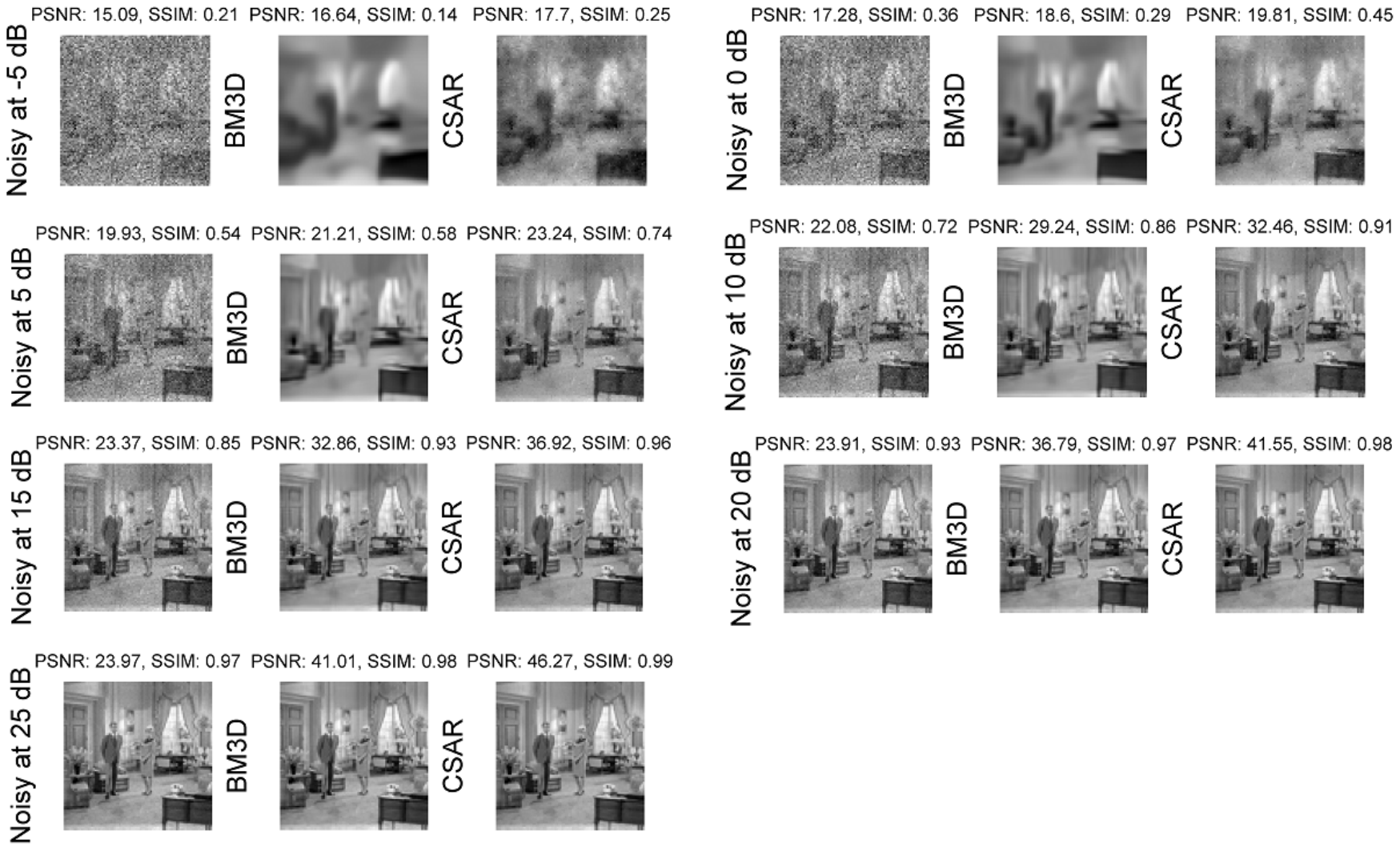

Figure 7.21: A comparison of BM3D and CSAR algorithm's based denoising results of Living room standard test image over an extensive SNR range of -5 dB to 25 dB.

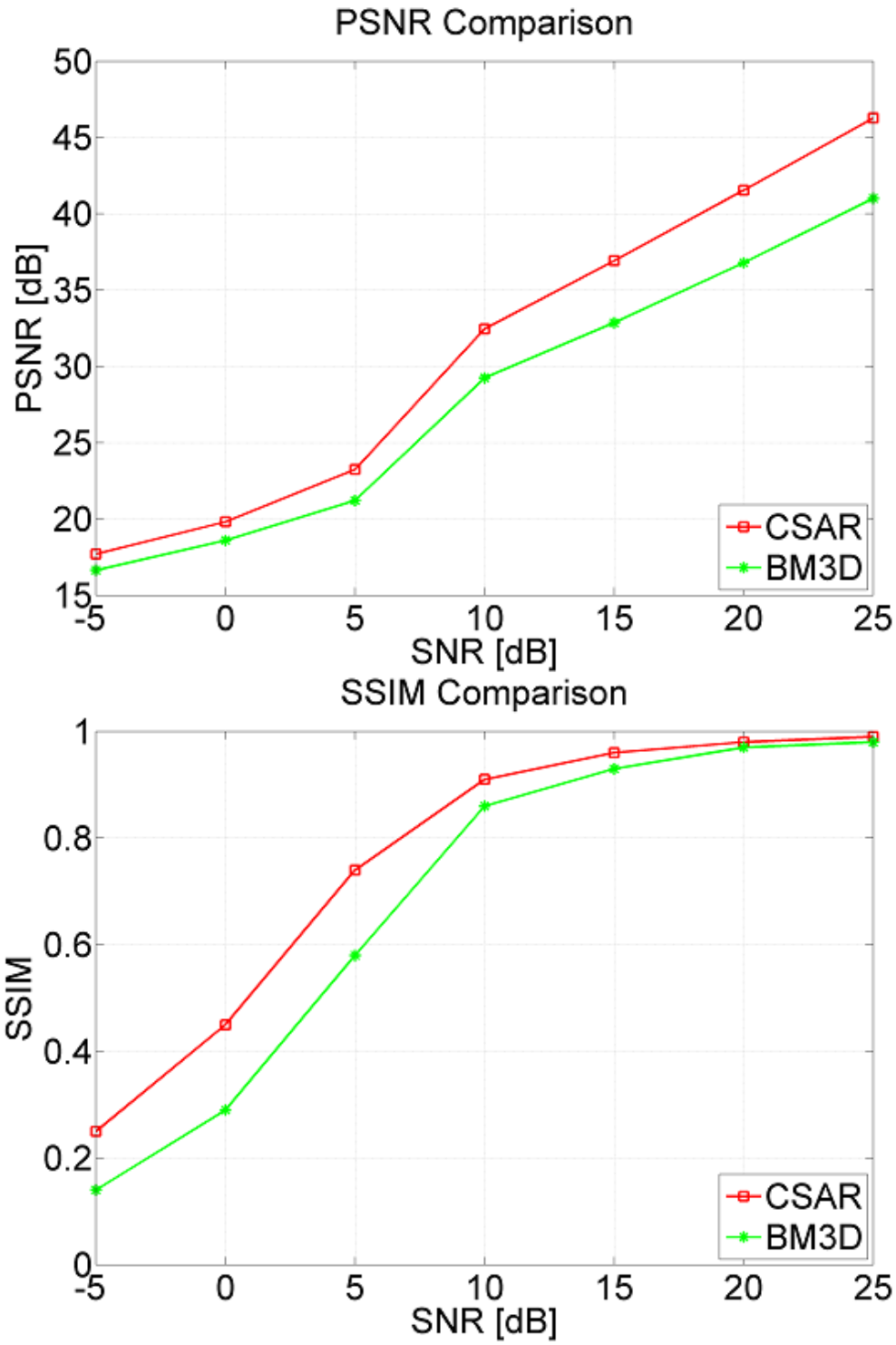

Figure 7.22: A graphical comparison of BM3D and CSAR algorithm's based denoising results of Living room standard test image.

Figure 7.23: A comparison of BM3D and CSAR algorithm's based denoising results of Man standard test image over an extensive SNR range of -5 dB to 25 dB.

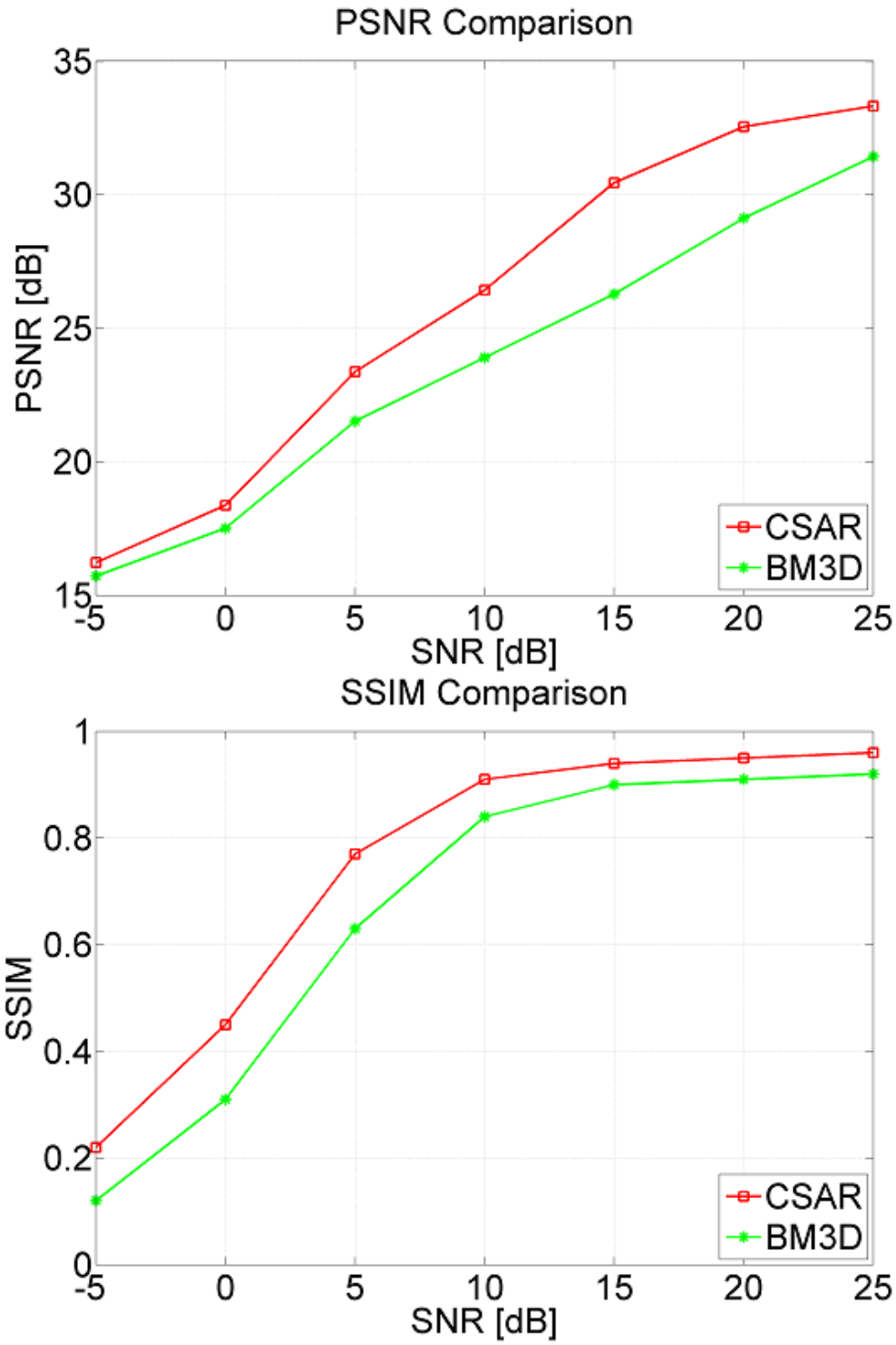

Figure 7.24: A graphical comparison of BM3D and CSAR algorithm's based denoising results of Man standard test image.

7.2 Computational Complexity

The computational complexity of our proposed image denoising algorithm is dominated by that of the sparse recovery algorithm that we use, which fortunately has a low computational complexity when compared to other similar existing algorithms for sparse recovery. With the dimensions of our problem at hand, the complexity for estimating one $\mathbf{h}_k$ via the algorithm SABMP is of order $\mathcal{O}(MN^2P)$ where P is the expected number of non-zeros that is generally a very small number. Lastly, to estimate all of the K patches and for L various iterations for different patch sizes, the computational complexity will gauge to an order of $\mathcal{O}(KLMN^2P)$.

7.3 Results of ACSAR

In this section, we present the experimental results of our proposed image denoising algorithm and compare the results with three existing state-of-the-art denoising methods: NL-means [31], K-SVD [39] and BM3D [48]. The comparison takes place over a number of different sceneries to show the performance gain of our algorithm. For the said purpose, we use standard test images used commonly in the image processing community. We also present the results of other natural images from the database available online on SIPI[1] to validate the applicability and efficiency of our method globally irrespective of a specific scenario.

In these experiments, we perform the image denoising over a range of noise levels covering low noise to extremely high noise regime. In particular, these

[1]http://sipi.usc.edu/database/.

high noise levels make the competition much more challenging by confusing signal components with those of noise components and showcase the limitations of the existing methods where these fail to perform well specifically in preserving structure and details. The entries of dictionary in our case comprises of wavelet as well as DCT basis. For different noise levels, we use an SNR ranging from -5 dB to 25 dB. Further, we use patch size of 3, 5, 7 and 9, i.e, $L = 4$, and the denoising results based on these are averaged in the end.

7.3.1 General Comparisons

Consider Fig. 7.26 where we present the results of denoising 256×256 standard *Mandrill* using the state-of-the-art methods and our proposed method. The results are for different noise levels as shown. Since, this image is a detailed rich image because of its structure, it serves as one of the best images for comparison. As can be seen in this figure, state-of-the-art algorithms, because of the way they operate, go for blurring out the detailed structure of an image especially in case of high noise. On the contrary, our method accurately tackles the noise components in the detail rich and complex parts of the image.

Avoiding such blurring out of the details is one of the key issues. This is important and can have critical consequences in many applications, e.g. bio-medical application where let's say the task is to detect tumors. In that case, the detection may severely go wrong due to blurring and hence, can be life threatening. For example, compare the nostrils, facial hair and white parallel lines in the mandrill

image, as shown in Fig. 7.25, which got blurred out by other competing methods but are recovered to a very good extent by our method.

A similar comparison of denoising 256×256 *Barbara* image has been shown in Fig. 7.27 that depicts successful recovery of image details. Further in Fig. 7.28, we compare the denoising results of *Lena* and *Man* at both high and low noise levels to showcase that our algorithm perform equally well at low noise tenure. Please note that in this figure, we have compared the results with BM3D only as it outperforms all the existing methods. These results clearly validate the efficiency of our proposed method hence, outperforming the existing state-of-the-art methods.

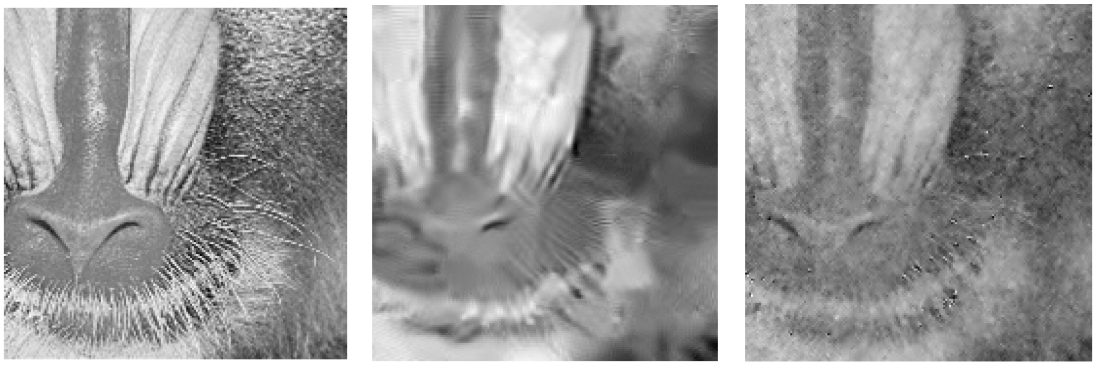

(a) (b) (c)

Figure 7.25: Zoomed versions of the (a) *Mandrill* image denoised by (b) BM3D and (c) proposed ACSAR method at SNR_{dB}/σ = -5/103.

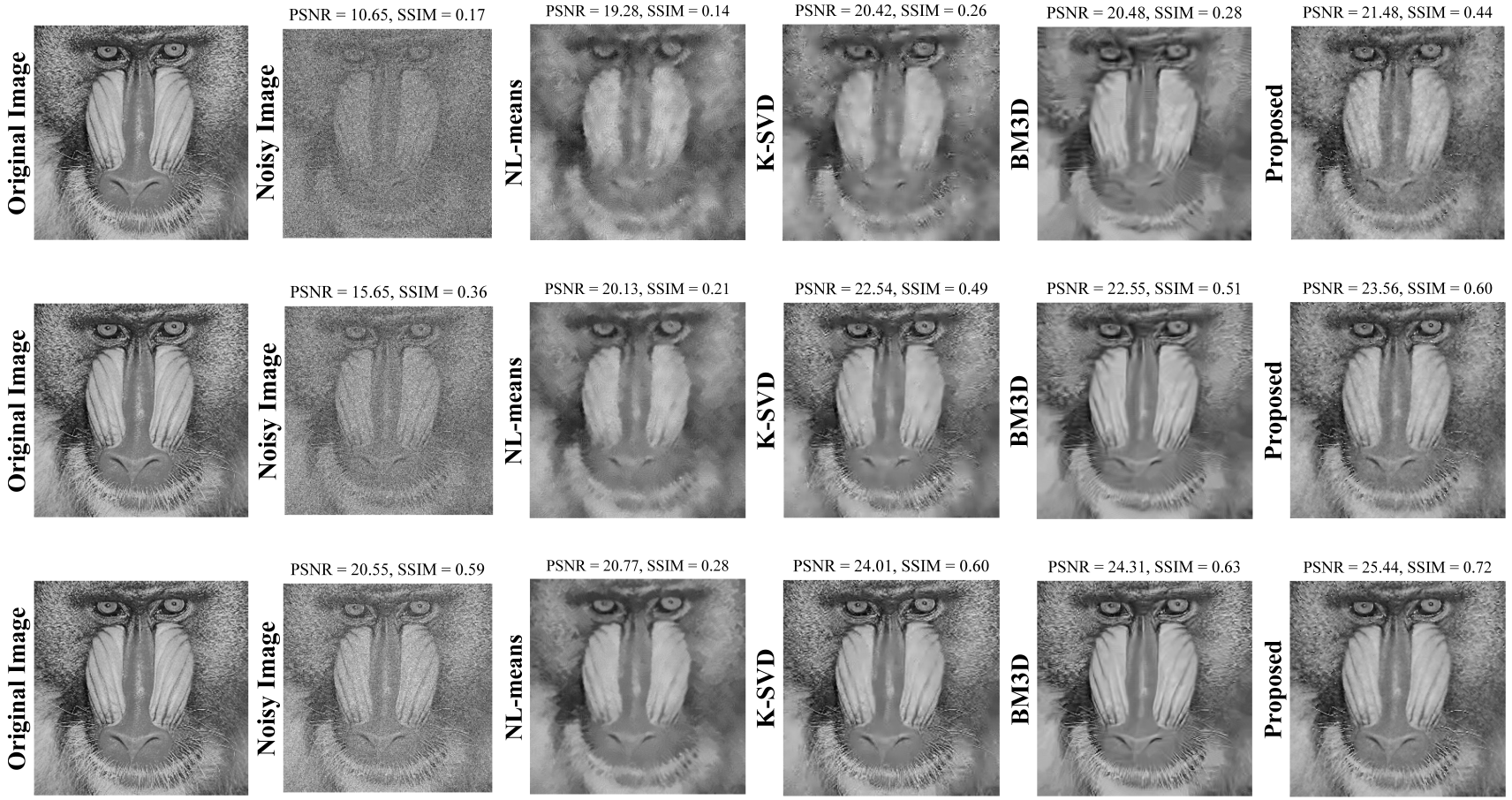

Figure 7.26: Denoising *Mandrill*: 1st row at SNR_{dB}/σ = -5/103, 2nd row at $\text{SNR}_{dB}/\sigma = 0/58$, 3rd row at $\text{SNR}_{dB}/\sigma = 5/58$.

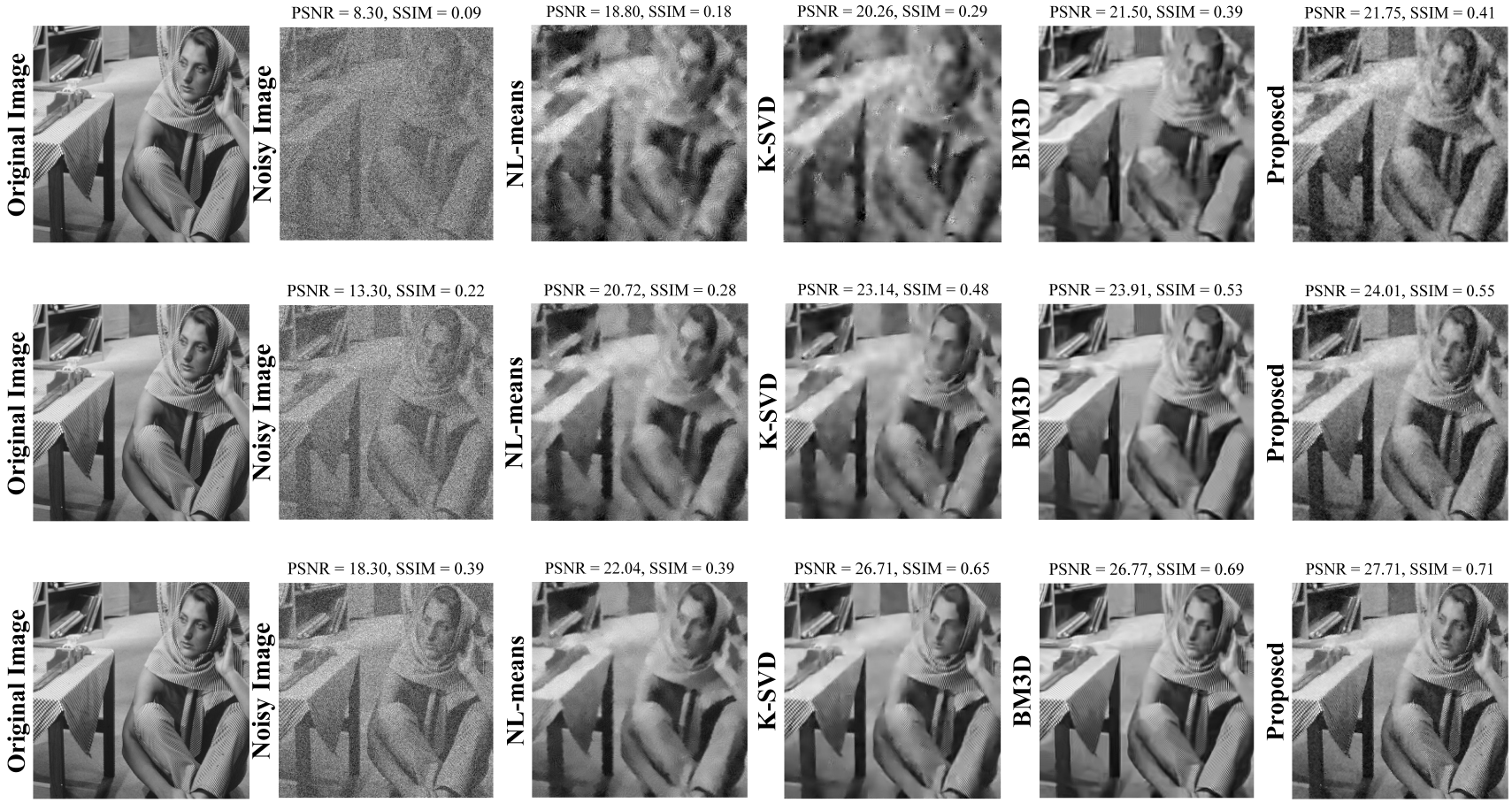

Figure 7.27: Denoising *Barbara*: 1st row at SNR_{dB}/σ = -5/103, 2nd row at $\mathrm{SNR}_{dB}/\sigma = 0/58$, 3rd row at $\mathrm{SNR}_{dB}/\sigma = 5/58$.

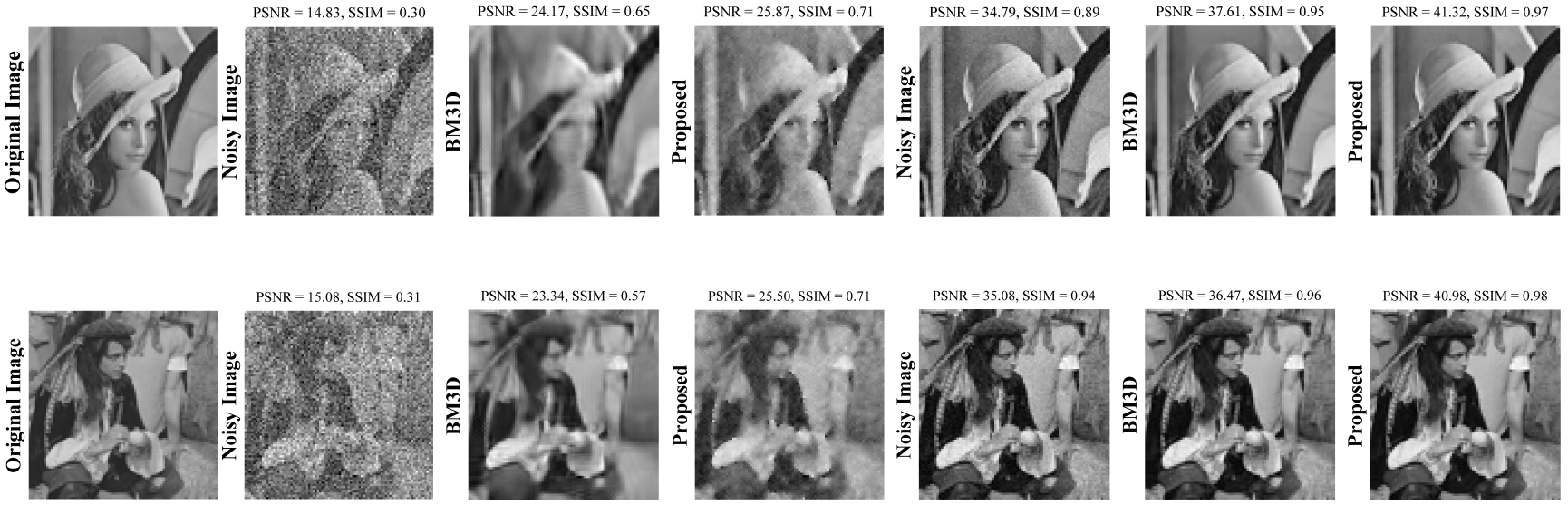

Figure 7.28: 1st row left to right: original *Lena* image, noisy and denoised by BM3D and proposed ACSAR method at SNR = 0 dB, and noisy and denoised by BM3D and proposed ACSAR method at SNR = 20 dB. 2nd row left to right: original *Man* image, noisy and denoised by BM3D and proposed ACSAR method at SNR = 0 dB, and noisy and denoised by BM3D and proposed ACSAR method at SNR = 20 dB.

In Fig. 7.29, we compare the denoising results of grayscale *Cameraman* and *Peppers* image in terms of PSNR and SSIM. The images were corrupted by a range of different noise levels from SNR = -5 dB to SNR = 25 dB and the corresponding results are plotted. In both of these mostly used images, we have shown that our proposed algorithm outperforms the existing methods over a range of SNRs. Specifically, since the *Peppers* image has a lot of flat regions that ultimately favors the competing algorithms, as these tend to blur out the smooth and flat parts of the image, we have outperformed these algorithms even in such a scenario. The PSNR and SSIM in both the images and at any noise level is better than that of the existing methods. We recommend the readers to zoom into the electronic files of this article for a much better comparison of the images shown.

For a detailed comparison of the denoising performance over various grayscale images widely used in image restoration literature and over a range of noise levels, we summarize the PSNR ans SSIM results in Table 7.2. Since BM3D outperforms both NL-means and K-SVD, therefore we only compare our results with that of BM3D in this table. Moreover in table 7.3 and 7.4, we also present the results of denoising grayscale texture and aerial images from SIPI database to prove that our algorithm can be applied globally to any image. From the provided table, it is clear that our proposed image denoising algorithm outperforms the state-of-the-art algorithm in each scenario and has proven itself to be a much better and efficient algorithm for image denoising.

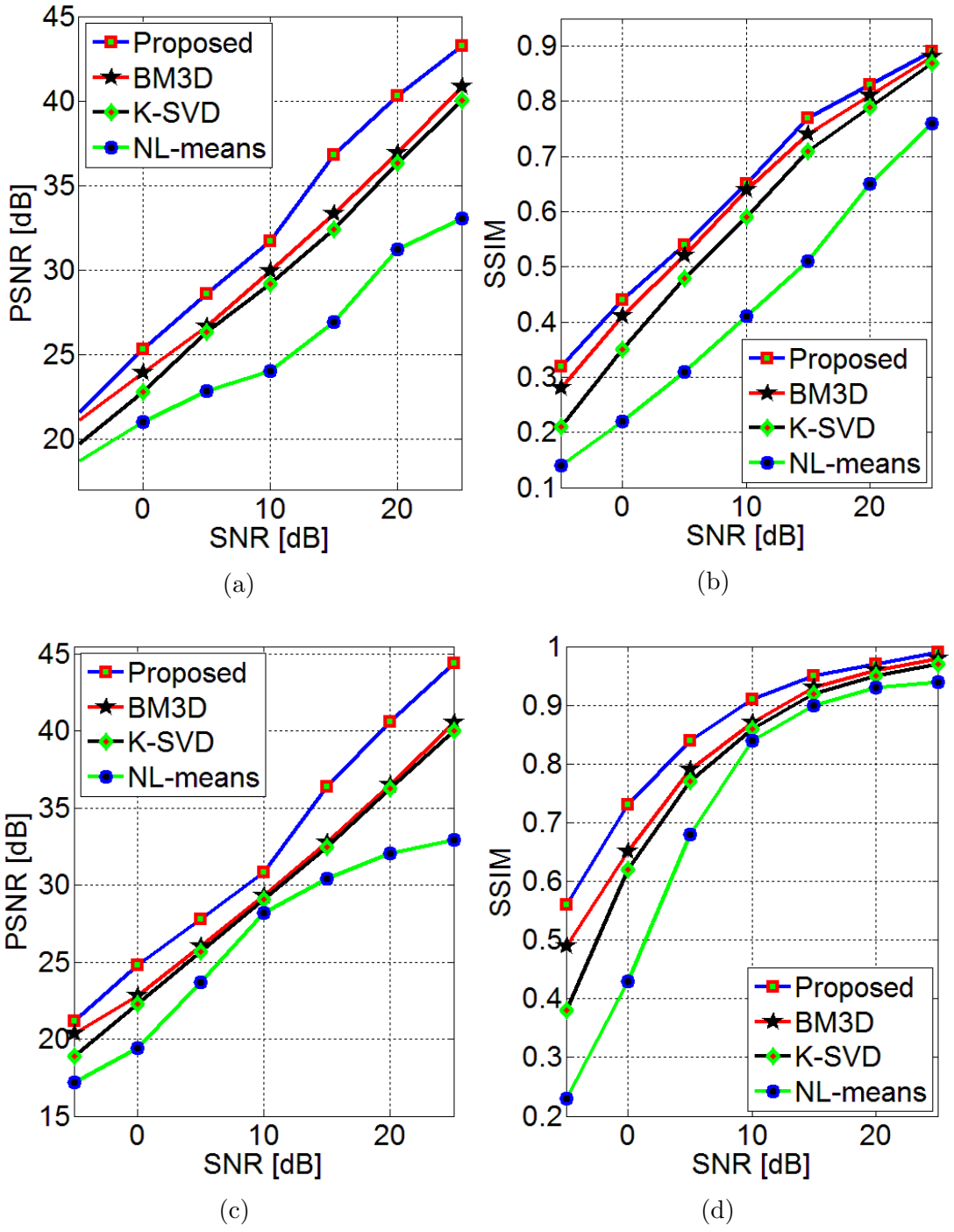

Figure 7.29: Denoising comparison: (a) *Cameraman* PSNR, (b) *Cameraman* SSIM, (c) *Peppers* PSNR and (d) *Peppers* SSIM

SNR [dB] / σ		Living Room	Lena	Barbara	House	Man	Mandrill	Boat
-5/103	BM3D	22.15/0.42	21.53/0.50	21.50/0.39	23.26/0.34	21.21/0.43	20.48/0.28	22.17/0.35
	Proposed	**23.27/0.54**	**22.47/0.55**	**21.75/0.41**	**23.61/0.36**	**22.45/0.55**	**21.48/0.44**	**23.13/0.48**
0/58	BM3D	24.16/0.57	24/17/0.65	23.91/0.53	26.15/0.45	23.34/0.57	22.55/0.51	24.16/0.50
	Proposed	**26.12/0.69**	**25.87/0.71**	**24.01/0.55**	**27.00/0.47**	**25.50/0.71**	**23.56/0.60**	**26.03/0.64**
5/33	BM3D	26.98/0.74	27.48/0.78	26.77/0.69	29.83/0.55	26.20/0.73	24.31/0.63	26.90/0.67
	Proposed	**28.31/0.74**	**28.77/0.81**	**27.71/0.71**	**29.84/0.56**	**28.04/0.81**	**25.44/0.72**	**28.38/0.75**
10/18	BM3D	30.12/0.86	30.72/0.87	29.80/0.79	33.17/0.62	29.19/0.84	27.83/0.80	29.94/0.81
	Proposed	**33.26/0.91**	**33.07/0.88**	**31.60/0.82**	**34.14/0.63**	**32.56/0.91**	**30.19/0.89**	**32.91/0.87**
15/10	BM3D	33.75/0.93	34.02/0.92	32.92/0.85	36.57/0.67	32.59/0.92	31.81/0.90	33.27/0.90
	Proposed	**37.57/0.96**	**37.39/0.94**	**35.74/0.89**	**38.59/0.71**	**36.93/0.96**	**36.59/0.96**	**36.84/0.94**
20/6	BM3D	37.67/0.97	37.71/0.95	36.24/0.90	39.90/0.74	36.47/0.96	36.20/0.96	36.78/0.95
	Proposed	**41.40/0.98**	**41.32/0.97**	**39.81/0.94**	**42.37/0.78**	**40.08/0.98**	**40.66/0.98**	**40.11/0.97**
25/3	BM3D	41.90/0.98	41.51/0.97	39.96/0.94	43.14/0.80	40.77/0.98	40.86/0.98	40.28/0.97
	Proposed	**44.42/0.99**	**44.81/0.98**	**43.44/0.97**	**45.52/0.85**	**44.37/0.99**	**43.92/0.99**	**42.38/0.98**

Table 7.2: Denoising comparison of grayscale images using proposed ACSAR method and BM3D both in terms of PSNR and SSIM

Image Name		$\mathcal{N}(0,50)$	$\mathcal{N}(0,40)$	$\mathcal{N}(0,30)$
1.1.01	BM3D	20.00/0.24	20.48/0.35	21.65/0.52
	Proposed	**21.92/0.55**	**22.58/0.61**	**23.56/0.68**
1.1.02	BM3D	20.08/0.46	20.91/0.59	22.38/0.71
	Proposed	**21.80/0.62**	**22.62/0.69**	**23.68/0.76**
1.1.03	BM3D	23.10/0.16	23.48/0.22	24.12/0.32
	Proposed	**24.30/0.42**	**24.89/0.46**	**25.64/0.53**
1.1.07	BM3D	25.31/0.10	25.55/0.13	25.77/0.16
	Proposed	**25.91/0.35**	**26.51/0.39**	**27.22/0.44**
1.2.01	BM3D	18.18/0.39	19.03/0.56	20.68/0.72
	Proposed	**20.38/0.65**	**21.25/0.72**	**22.33/0.78**
1.2.05	BM3D	18.28/0.49	19.10/0.62	20.84/0.76
	Proposed	**20.23/0.68**	**21.11/0.74**	**22.19/0.80**
1.2.07	BM3D	17.80/0.29	18.67/0.48	20.38/0.68
	Proposed	**20.02/0.61**	**20.88/0.68**	**22.00/0.76**
1.2.13	BM3D	17.96/0.69	18.84/0.76	20.63/0.85
	Proposed	**20.22/0.81**	**21.43/0.85**	**22.96/0.90**
1.3.01	BM3D	20.94/0.18	21.48/0.30	22.40/0.44
	Proposed	**22.52/0.45**	**23.10/0.51**	**23.97/0.60**
1.3.04	BM3D	21.55/0.31	22.30/0.44	23.43/0.57
	Proposed	**23.91/0.65**	**24.78/0.70**	**25.72/0.75**

Table 7.3: Denoising texture images from SIPI database using BM3D and proposed method under $\mathbf{W} \sim \mathcal{N}(\mathbf{0}, \sigma_w \mathbf{I})$

7.3.2 Various Resolution Images

In this section, we present the denoising comparison of various resolution images as opposed to the traditional comparison methods where only single image size is used throughout the experimentations. As we believe, this is very important to validate the effectiveness of any algorithm, i.e. how better can any algorithm, let's say as in our case, tackle noise at different image sizes. For this purpose, we take grayscale 86×86, 128×128 and 256×256 size *Barabara* and *Mandrill* images and denoise them using BM3D and the proposed method at different noise levels.

Image Name		$\mathcal{N}(0,50)$	$\mathcal{N}(0,40)$	$\mathcal{N}(0,30)$
2.1.01	BM3D	20.11/0.36	20.55/0.42	21.26/0.51
	Proposed	**21.47/0.57**	**21.95/0.62**	**22.46/0.67**
2.1.02	BM3D	20.00/0.35	20.53/0.43	21.22/0.51
	Proposed	**21.07/0.52**	**21.50/0.56**	**22.00/0.62**
2.1.05	BM3D	20.22/0.48	20.72/0.54	21.67/0.61
	Proposed	**21.13/0.59**	**21.69/0.64**	**22.32/0.69**
2.1.06	BM3D	20.83/0.21	21.00/0.26	21.25/0.33
	Proposed	**21.38/0.38**	**21.56/0.41**	**21.75/0.45**
2.1.12	BM3D	18.31/0.11	18.43/0.15	18.57/0.20
	Proposed	**18.57/0.30**	**18.68/0.33**	**18.80/0.36**
2.2.07	BM3D	26.44/0.32	27.17/0.37	28.06/0.43
	Proposed	**27.48/0.45**	**28.43/0.51**	**29.53/0.57**
2.2.11	BM3D	24.47/0.12	24.95/0.19	25.58/0.27
	Proposed	**26.04/0.42**	**26.78/0.48**	**27.71/0.55**
2.2.13	BM3D	24.65/0.23	25.12/0.30	25.89/0.38
	Proposed	**26.17/0.53**	**27.23/0.60**	**28.52/0.67**
2.2.14	BM3D	24.96/0.22	25.43/0.29	26.11/0.37
	Proposed	**26.43/0.47**	**27.20/0.53**	**28.17/0.60**
2.2.17	BM3D	23.09/0.21	23.60/0.27	24.32/0.35
	Proposed	**24.81/0.46**	**25.46/0.51**	**26.26/0.57**

Table 7.4: Denoising aerial images from SIPI database using BM3D and proposed method under $\mathbf{W} \sim \mathcal{N}(\mathbf{0}, \sigma_w \mathbf{I})$

The results of denoising *Mandrill* image at different resolutions and at SNR = -5, 0, 5 and 10 dB is shown in Fig. 7.30 as bar plots. This figure shows that the proposed method not only outperforms state-of-the-art denoising algorithms like NL-means, K-SVD and BM3D at large image size but is also capable of removing noise components effectively at small image sizes. The first row in this figure corresponds to the resultant PSNR achieved by denoising at SNR = -5, 0, 5 and 10 dB, while the second row shows the corresponding SSIM results.

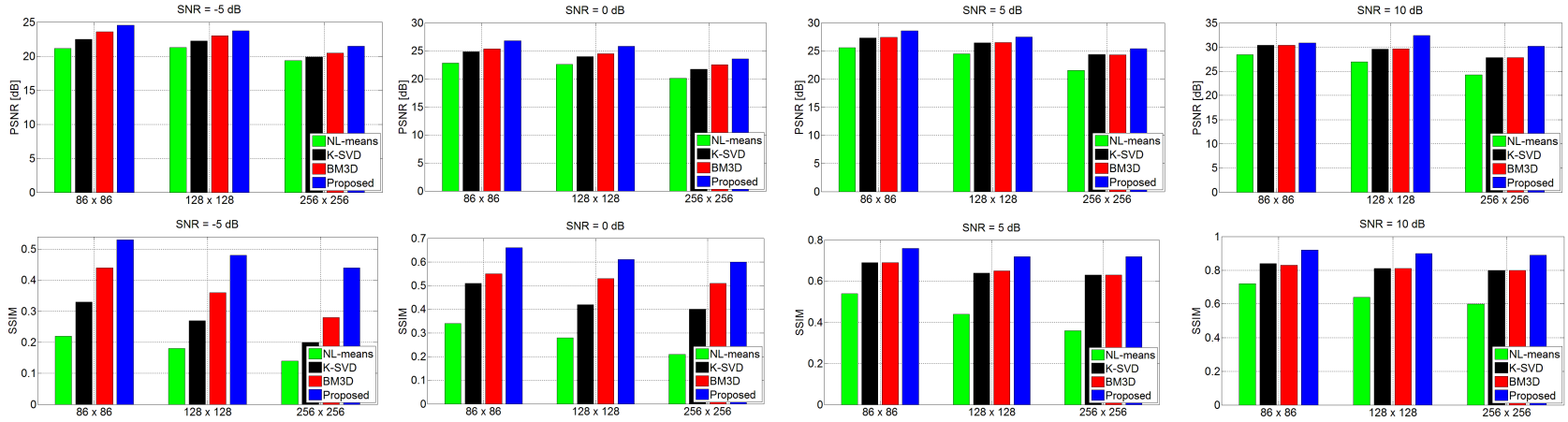

Figure 7.30: Comparison of denoising 86×86, 128×128 and 256×256 size grayscale *Mandrill* images in terms of PSNR (1st row) and SSIM (2nd row) using NL-means, K-SVD, BM3D and proposed ACSAR method.

Similarly in Fig. 7.31, we present the denoising comparison of 86×86, 128×128 and 256×256 size *Barabara* images over an SNR ranging from very high noise i.e., -5 dB, to low noise i.e., 25 dB. A pictorial representation of the denoised images has been shown in Fig. 7.32 to depict the limitation of existing algorithms. As discussed already, even state-of-the-art method like BM3D tend to blur out the images especially at low resolution images and high noise. For instance, observe the first row of this figure where the facial details of the *Mandrill* image has been blurred out while the details are preserved in results by our method. A similar problem is detected for the *Barbara* where e.g. the hands, facial details and the table legs get disappeared but exist in our denoised results. The results for 256×256 has already been shown previously in Fig. 7.26. As can be clearly concluded from these figures that the proposed ACSAR method shows an effective performance in all the scenarios and leads the PSNR and SSIM points table by quite a good margin.

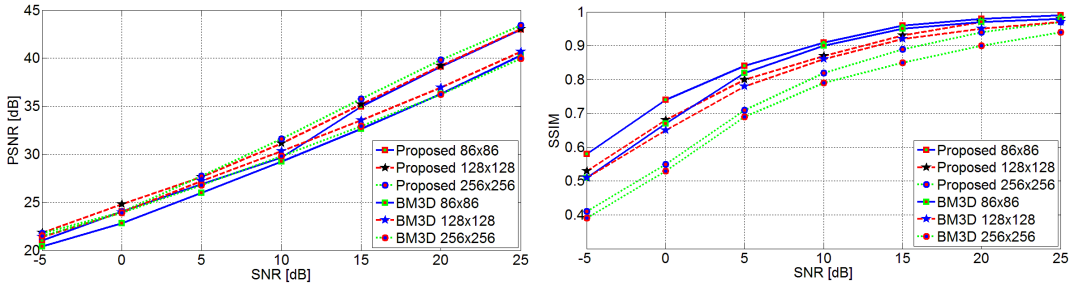

Figure 7.31: Denoising comparison of 86×86, 128×128 and 256×256 size grayscale *Barbara* images in terms of PSNR and SSIM using BM3D and proposed ACSAR method.

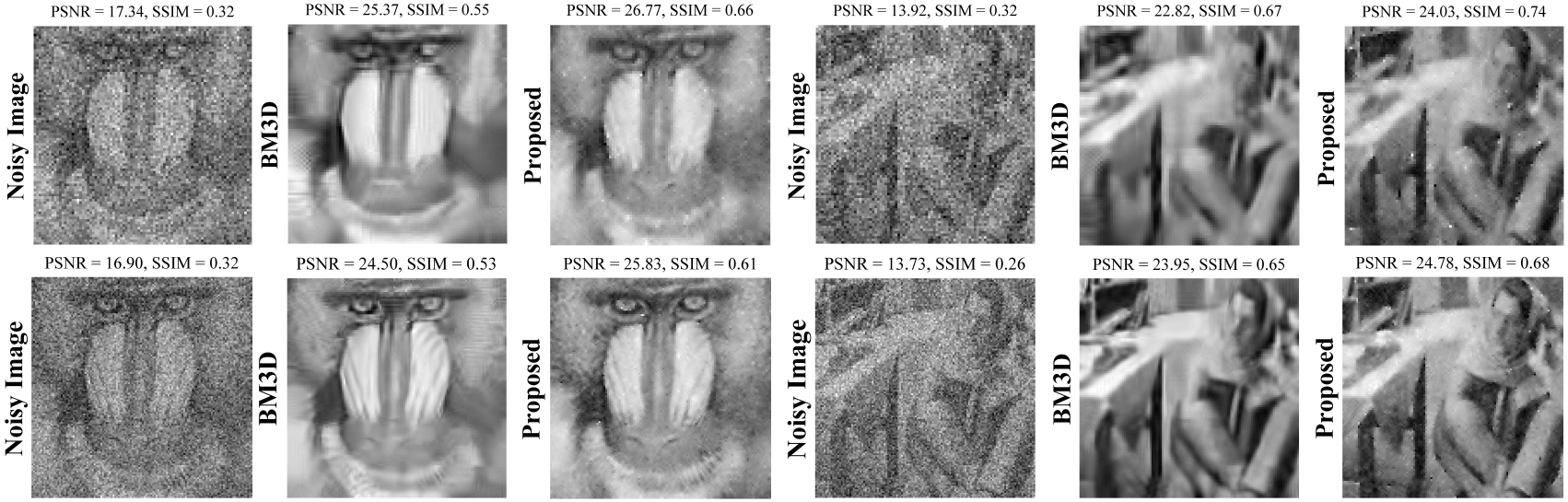

Figure 7.32: Denoising results of *Barbara* and *Mandrill* at SNR = 0 dB: 1st row 86×86, 2nd row 128×128 size images

7.3.3 Color-Image Denoising

In this section, we present the denoising results of the extended version of our image denoising algorithm on various color images over different noise scenarios. The standard color images were taken and Gaussian noise was added in the same fashion as we did for grayscale images. Since the color images has three different R,G,B channels that together contribute to present the colors in an image, these channels provide a more efficient platform to perform collaboration.

To take advantage of the channel correlation, we collaborate across the channels to provide us a much better refined sparse estimate. This is done by considering a patch and finding similar patches not only within the channel of reference, but also across the other channels and then, the collaboration is performed.

The effectiveness of this improved collaboration step for color images has been shown in Fig. 7.33 where we have tested our color image denoising algorithm on various images and under various high noise levels. As shown, the images, even under severe noise contamination, are recovered to a very good extent. We have also showed that the proposed method is valid for not only natural images, but is also equally efficient for synthetic images as shown in the third row of the figure under observation.

In addition to the color images shown in Fig. 7.33, we summarize the denoising results of other color images in table 7.5 to show the performance gain as compared to the color version of the BM3D algorithm, i.e. C-BM3D [**?**]. The stated results demonstrate the efficacy of the proposed method over a wide range of im-

ages and prove that the proposed method can be used globally in any scenario outperforming existing state-of-the-art algorithms.

Image Name		$\sigma = 50$	$\sigma = 40$	$\sigma = 30$
Jet	C-BM3D	23.47/0.75	24.68/0.79	26.40/0.86
	Proposed	**26.26/0.79**	**27.63/0.83**	**29.80/0.87**
Lake	C-BM3D	21.52/0.83	22.83/0.87	24.37/0.90
	Proposed	**26.01/0.92**	**27.71/0.94**	**30.18/0.96**
Mandrill	C-BM3D	22.48/0.77	23.36/0.81	24.69/0.85
	Proposed	**24.37/0.82**	**25.83/0.86**	**28.13/0.90**
Peppers	C-BM3D	21.88/0.91	23.40/0.94	24.95/0.95
	Proposed	**27.44/0.97**	**29.11/0.98**	**31.52/0.99**
Girl	C-BM3D	24.40/0.80	25.97/0.0.85	27.71/0.90
	Proposed	**29.81/0.93**	**31.49/0.95**	**33.79/0.97**
Woman	C-BM3D	24.73/0.79	26.01/0.82	27.46/0.88
	Proposed	**28.90/0.85**	**30.26/0.88**	**32.25/0.92**

Table 7.5: Results of denoising color images using proposed method under $\mathbf{W} \sim \mathcal{N}(\mathbf{0}, \sigma_w \mathbf{I})$

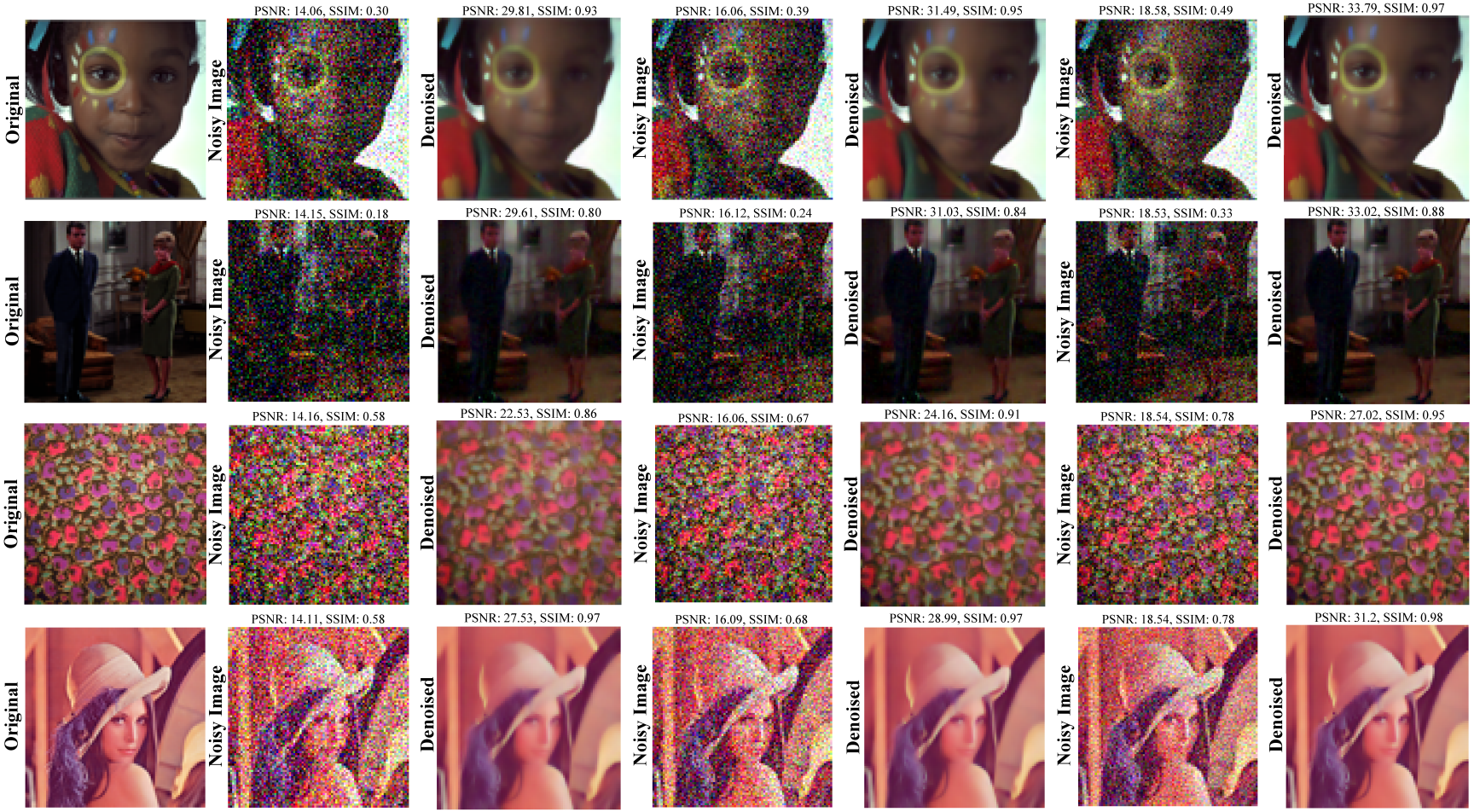

Figure 7.33: Denoising color images by the proposed color denoising method. 1st column: original images, 2nd and 3rd columns: noisy and denoised images at $\mathcal{N}(0, 50)$, 4th and 5th columns: noisy and denoised images at $\mathcal{N}(0, 40)$, 6th and 7th columns: noisy and denoised images at $\mathcal{N}(0, 30)$,

CHAPTER 8

CONCLUSIONS AND FUTURE WORK

In this thesis, we proposed novel patch-based image denoising algorithms utilizing collaborative filtering in the sparse domain. The methods utilized a collaborative approach in the transformed domain using similarly structured patches. The probabilities of taps being active were computed and then refined via collaboration among similar patches. This approach tremendously isolated the noisy components and thus improved the sparse estimates thereby producing high quality reconstructed image.

For a further improvement in the denoised image and to preserve all the details without blurring, we deployed a region growing based specially developed post-processor that further refines the edge details as well as the smooth regions. We presented our denoising algorithms for both grayscale and color images. Comparison results from extensive experiments and under a number of scenarios proved

that our proposed image denoising algorithms outperform the existing state-of-the-art methods by a very good margin both subjectively and objectively, i.e. in terms of PSNR and SSIM.

As a future work, we propose to use the patches in their original rectangular patch form instead of vectorizing them. This will ensure the efficient use of neighborhood correlation and will avoid destroying of continuity when a patch is vectorized. Consequently, the field of tensor analysis and algebra will have to be explored. This field discusses processing of rectangular patches and designing the appropriate dictionary to represent those patches. Another interesting future direction can be to collaborate a reference patch with both its geographical close patches as well as similarity based close patches.

A more appealing future direction can be the extension of this work over the video denoising. As opposed to images, the collaboration among patches to denoise a reference patch can be done not only considering the similar patches in a single channel and frame but it can also incorporate the similarity from other channels and even similar video frames. Since the similar patches in different frames are supposed to have a similar support, averaging those very patches will produce improvements in denoising and may lead to significant contributions in this field.

REFERENCES

[1] R. C. Gonzalez and R. E. Woods, *Digital Image Processing (3rd Edition)*. Upper Saddle River, NJ, USA: Prentice-Hall, Inc., 2006.

[2] K. Castleman, *Digital Image Processing*, ser. Prentice Hall international editions. Prentice-Hall, 1995. [Online]. Available: https://books.google.com.sa/books?id=i20dAQAACAAJ

[3] H. H. Arsenault, C. Gendron, and M. Denis, "Transformation of film-grain noise into signal-independent additive gaussian noise," *J. Opt. Soc. Am.*, vol. 71, no. 1, pp. 91–94, Jan 1981. [Online]. Available: http://www.osapublishing.org/abstract.cfm?URI=josa-71-1-91

[4] I. Ram, M. Elad, and I. Cohen, "Image processing using smooth ordering of its patches," *Image Processing, IEEE Transactions on*, vol. 22, no. 7, pp. 2764–2774, July 2013.

[5] P. Campisi and K. Egiazarian, *Blind image deconvolution: theory and applications*. CRC press, 2007.

[6] M. Elad and M. Aharon, "Image denoising via sparse and redundant representations over learned dictionaries," *Image Processing, IEEE Transactions on*, vol. 15, no. 12, pp. 3736–3745, Dec 2006.

[7] P. Qiu and P. S. Mukherjee, "Edge structure preserving 3d image denoising by local surface approximation," *IEEE Transactions on Pattern Analysis and Machine Intelligence*, vol. 34, no. 8, pp. 1457–1468, Aug 2012.

[8] H. Yue, X. Sun, J. Yang, and F. Wu, "Image denoising by exploring external and internal correlations," *IEEE Transactions on Image Processing*, vol. 24, no. 6, pp. 1967–1982, June 2015.

[9] G. Ghimpeeanu, T. Batard, M. Bertalmo, and S. Levine, "A decomposition framework for image denoising algorithms," *IEEE Transactions on Image Processing*, vol. 25, no. 1, pp. 388–399, Jan 2016.

[10] J. Boulanger, C. Kervrann, and P. Bouthemy, "Space-time adaptation for patch-based image sequence restoration," *IEEE Transactions on Pattern Analysis and Machine Intelligence*, vol. 29, no. 6, pp. 1096–1102, June 2007.

[11] G. Gilboa, "Nonlinear scale space with spatially varying stopping time," *IEEE Transactions on Pattern Analysis and Machine Intelligence*, vol. 30, no. 12, pp. 2175–2187, Dec 2008.

[12] N. Dowson and O. Salvado, "Hashed nonlocal means for rapid image filtering," *IEEE Transactions on Pattern Analysis and Machine Intelligence*, vol. 33, no. 3, pp. 485–499, March 2011.

[13] P. Chatterjee and P. Milanfar, "Patch-based near-optimal image denoising," *IEEE Transactions on Image Processing*, vol. 21, no. 4, pp. 1635–1649, April 2012.

[14] N. Pierazzo, M. Lebrun, M. E. Rais, J. M. Morel, and G. Facciolo, "Non-local dual image denoising," in *IEEE International Conference on Image Processing (ICIP)*, Oct 2014, pp. 813–817.

[15] S. H. Chan, E. Luo, and T. Q. Nguyen, "Adaptive patch-based image denoising by em-adaptation," in *IEEE Global Conference on Signal and Information Processing (GlobalSIP)*, Dec 2015, pp. 810–814.

[16] A. Buades, J. L. Lisani, and M. Miladinovi, "Patch-based video denoising with optical flow estimation," *IEEE Transactions on Image Processing*, vol. 25, no. 6, pp. 2573–2586, June 2016.

[17] L. Lu, W. Jin, and X. Wang, "Non-local means image denoising with a soft threshold," *IEEE Signal Processing Letters*, vol. 22, no. 7, pp. 833–837, July 2015.

[18] J. Xu, L. Zhang, W. Zuo, D. Zhang, and X. Feng, "Patch group based nonlocal self-similarity prior learning for image denoising," in *IEEE International Conference on Computer Vision (ICCV)*, Dec 2015, pp. 244–252.

[19] I. Ram, I. Cohen, and M. Elad, "Patch-ordering-based wavelet frame and its use in inverse problems," *IEEE Transactions on Image Processing*, vol. 23, no. 7, pp. 2779–2792, July 2014.

[20] V. Papyan and M. Elad, "Multi-scale patch-based image restoration," *IEEE Transactions on Image Processing*, vol. 25, no. 1, pp. 249–261, Jan 2016.

[21] V. Badrinarayanan, I. Budvytis, and R. Cipolla, "Semi-supervised video segmentation using tree structured graphical models," *IEEE Transactions on Pattern Analysis and Machine Intelligence*, vol. 35, no. 11, pp. 2751–2764, Nov 2013.

[22] K. Cao, E. Liu, and A. K. Jain, "Segmentation and enhancement of latent fingerprints: A coarse to fine ridgestructure dictionary," *IEEE Transactions on Pattern Analysis and Machine Intelligence*, vol. 36, no. 9, pp. 1847–1859, Sept 2014.

[23] J. Kwon and K. M. Lee, "Highly nonrigid object tracking via patch-based dynamic appearance modeling," *IEEE Transactions on Pattern Analysis and Machine Intelligence*, vol. 35, no. 10, pp. 2427–2441, Oct 2013.

[24] R. Amit, G. Mishne, and R. Talmon, "Improving resolution in supervised patch-based target detection," in *2016 IEEE International Conference on Acoustics, Speech and Signal Processing (ICASSP)*, March 2016, pp. 1994–1998.

[25] H. C. Shin, M. R. Orton, D. J. Collins, S. J. Doran, and M. O. Leach, "Stacked autoencoders for unsupervised feature learning and multiple organ detection in a pilot study using 4d patient data," *IEEE Transactions on*

Pattern Analysis and Machine Intelligence, vol. 35, no. 8, pp. 1930–1943, Aug 2013.

[26] I. Diamant, A. Hoogi, C. Beaulieu, M. Safdari, E. Klang, M. Amitai, H. Greenspan, and D. Rubin, "Improved patch based automated liver lesion classification by separate analysis of the interior and boundary regions," *IEEE Journal of Biomedical and Health Informatics*, vol. PP, no. 99, pp. 1–1, 2015.

[27] L. Sun, J. Chen, D. Zeng, and X. Ding, "A novel nonlocal mri reconstruction algorithm with patch-based low rank regularization," in *IEEE Global Conference on Signal and Information Processing (GlobalSIP)*, Dec 2015, pp. 398–402.

[28] P. Getreuer, "Rudin-Osher-Fatemi Total Variation Denoising using Split Bregman," *Image Processing On Line*, vol. 2, pp. 74–95, 2012.

[29] C. Kervrann and J. Boulanger, "Optimal spatial adaptation for patch-based image denoising," *IEEE Transactions on Image Processing*, vol. 15, no. 10, pp. 2866–2878, Oct 2006.

[30] J.-H. Chang and Y.-C. Wang, "Propagated image filtering," in *IEEE Conference on Computer Vision and Pattern Recognition*, June 2015, pp. 10–18.

[31] A. Buades, B. Coll, and J.-M. Morel, "A non-local algorithm for image denoising," in *IEEE Computer Society Conference on Computer Vision and Pattern Recognition*, vol. 2, June 2005, pp. 60–65.

[32] N. Qi, Y. Shi, X. Sun, W. Ding, and B. Yin, "2d nonlocal sparse representation for image denoising," in *Visual Communications and Image Processing (VCIP)*, Dec 2015, pp. 1–4.

[33] J.-L. Starck, E. Candes, and D. Donoho, "The curvelet transform for image denoising," *IEEE Transactions on Image Processing*, vol. 11, no. 6, pp. 670–684, Jun 2002.

[34] D. Gnanadurai and V. Sadasivam, "Image de-noising using double density wavelet transform based adaptive thresholding technique," *International Journal of Wavelets, Multiresolution and Information Processing*, vol. 03, pp. 141–152, 2005. [Online]. Available: http://www.worldscientific.com/doi/abs/10.1142/S0219691305000701

[35] H. qiao Li, S.-Q. Wang, and C. zhi Deng, "New image denoising method based wavelet and curvelet transform," in *WASE International Conference on Information Engineering*, vol. 1, July 2009, pp. 136–139.

[36] A. Rajwade, A. Rangarajan, and A. Banerjee, "Image denoising using the higher order singular value decomposition," *IEEE Transactions on Pattern Analysis and Machine Intelligence*, vol. 35, no. 4, pp. 849–862, April 2013.

[37] N. Pierazzo, M. Rais, J. Morel, and G. Facciolo, "Da3d: Fast and data adaptive dual domain denoising," in *IEEE International Conference on Image Processing*, Sept 2015, pp. 432–436.

[38] H. Liu, R. Xiong, J. Zhang, and W. Gao, "Image denoising via adaptive soft-thresholding based on non-local samples," in *IEEE Conference on Computer Vision and Pattern Recognition (CVPR)*, June 2015, pp. 484–492.

[39] M. Elad and M. Aharon, "Image denoising via sparse and redundant representations over learned dictionaries," *IEEE Transactions on Image Processing*, vol. 15, no. 12, pp. 3736–3745, 2006.

[40] J. Mairal, M. Elad, and G. Sapiro, "Sparse representation for color image restoration," *IEEE Transactions on Image Processing*, vol. 17, no. 1, pp. 53–69, Jan 2008.

[41] J. Mairal, G. Sapiro, and M. Elad, "Learning multiscale sparse representations for image and video restoration," *Multiscale Modeling & Simulation*, vol. 7, no. 1, pp. 214–241, 2008. [Online]. Available: http://dx.doi.org/10.1137/070697653

[42] M. Lebrun and A. Leclaire, "An Implementation and Detailed Analysis of the K-SVD Image Denoising Algorithm," *Image Processing On Line*, vol. 2, pp. 96–133, 2012.

[43] G. Yu, G. Sapiro, and S. Mallat, "Image modeling and enhancement via structured sparse model selection," in *IEEE International Conference on Image Processing*, Sept 2010, pp. 1641–1644.

[44] Q. Guo, C. Zhang, Y. Zhang, and H. Liu, "An efficient svd-based method for image denoising," *IEEE Transactions on Circuits and Systems for Video Technology*, vol. 26, no. 5, pp. 868–880, May 2016.

[45] C. Knaus and M. Zwicker, "Progressive image denoising," *IEEE Transactions on Image Processing*, vol. 23, no. 7, pp. 3114–3125, July 2014.

[46] H. Talebi and P. Milanfar, "Global image denoising," *IEEE Transactions on Image Processing*, vol. 23, no. 2, pp. 755–768, Feb 2014.

[47] T. Dai, C.-B. Song, J.-P. Zhang, and S.-T. Xia, "Pmpa: A patch-based multiscale products algorithm for image denoising," in *IEEE International Conference on Image Processing*, Sept 2015, pp. 4406–4410.

[48] K. Dabov, A. Foi, V. Katkovnik, and K. Egiazarian, "Image denoising by sparse 3-d transform-domain collaborative filtering," *IEEE Transactions on Image Processing*, vol. 16, no. 8, pp. 2080–2095, Aug 2007.

[49] A. Levin and B. Nadler, "Natural image denoising: Optimality and inherent bounds," in *IEEE Conference on Computer Vision and Pattern Recognition (CVPR)*, June 2011, pp. 2833–2840.

[50] P. Chatterjee and P. Milanfar, "Is denoising dead?" *IEEE Transactions on Image Processing*, vol. 19, no. 4, pp. 895–911, April 2010.

[51] M. Masood and T. Al-Naffouri, "Sparse reconstruction using distribution agnostic bayesian matching pursuit," *IEEE Transactions on Signal Processing*, vol. 61, no. 21, pp. 5298–5309, Nov 2013.

[52] K. He and J. Sun, "Image completion approaches using the statistics of similar patches," *IEEE Transactions on Pattern Analysis and Machine Intelligence*, vol. 36, no. 12, pp. 2423–2435, Dec 2014.

[53] H. Liu, R. Xiong, S. Ma, X. Fan, and W. Gao, "Gradient based image/video softcast with grouped-patch collaborative reconstruction," in *IEEE Visual Communications and Image Processing Conference*, Dec 2014, pp. 141–144.

[54] M. Wang, J. Yu, and W. Sun, "Group-based hyperspectral image denoising using low rank representation," in *IEEE International Conference on Image Processing (ICIP)*, Sept 2015, pp. 1623–1627.

[55] W. Yang, J. Liu, S. Yang, and Z. Quo, "Image super-resolution via nonlocal similarity and group structured sparse representation," in *IEEE Visual Communications and Image Processing*, Dec 2015, pp. 1–4.

[56] K. Bahrami, F. Shi, x. zong, H. W. Shin, H. An, and D. Shen, "Reconstruction of 7t-like images from 3t mri," *IEEE Transactions on Medical Imaging*, vol. PP, no. 99, pp. 1–1, 2016.

[57] M. M. Van Hulle, *Self-organizing Maps*. Berlin, Heidelberg: Springer Berlin Heidelberg, 2012, pp. 585–622. [Online]. Available: http://dx.doi.org/10.1007/978-3-540-92910-9_19

[58] A. Gersho, "On the structure of vector quantizers," *IEEE Transactions on Information Theory*, vol. 28, no. 2, pp. 157–166, Mar 1982.

[59] F. Höppner, *Fuzzy cluster analysis: methods for classification, data analysis and image recognition.* John Wiley & Sons, 1999.

[60] A. K. Jain, M. N. Murty, and P. J. Flynn, "Data clustering: a review," *ACM computing surveys (CSUR)*, vol. 31, no. 3, pp. 264–323, 1999.

[61] G. Liu, H. Zhong, and L. Jiao, "Comparing noisy patches for image denoising: A double noise similarity model," *IEEE Transactions on Image Processing*, vol. 24, no. 3, pp. 862–872, March 2015.

[62] K. Panetta, L. Bao, and S. Agaian, "Sequence-to-sequence similarity-based filter for image denoising," *IEEE Sensors Journal*, vol. 16, no. 11, pp. 4380–4388, June 2016.

Vitae

- Muzammil Behzad
- Born in Islamabad, Pakistan on October 22^{nd}, 1990.
- Received Bachelor of Science (BS) in Electrical Engineering from COMSATS Institute of Information Technology, Islamabad, Pakistan in June 2013.
- Research Associate in COMSATS Institute of Information Technology, Islamabad, Pakistan from September 2013 to August 2014.
- Joined the Electrical Engineering Department at King Fahd University of Petroleum and Minerals (KFUPM) for Fully Funded MS Electrical Engineering in August 2014.
- Email: {*muzammil.behzad@*}*ieee.org,gmail.com*
- Website: `http://muzammilbehzad.com/`

List of Publications

- **M. Behzad**, M. Masood, T. Ballal, M. Shadaydeh and T. Al-Naffouri, "Image denoising via collaborative support-agnostic recovery", U.S. Patent [under preparation].

- **M. Behzad**, M. Masood, T. Ballal, M. Shadaydeh and T. Al-Naffouri, "Image denoising via correlation based improved collaborative support-agnostic recovery", *IEEE Transactions on Pattern Analysis and Machine Intelligence* [under preparation].

- **M. Behzad**, M. S. Javaid, M. A. Paracha and S. Khan, "Distributed PCA and Consensus Based Energy Efficient Routing Protocol for WSNs", *Journal of Information Science and Engineering* [Initially Submitted: December 2015 - First Revision Submitted April 2016 Positive Results in First Round].

- **M. Behzad**, M. Masood, T. Ballal, M. Shadaydeh and T. Al-Naffouri, "Image denoising via collaborative support-agnostic recovery", *The 42nd IEEE International Conference on Acoustics, Speech and Signal Processing (ICASSP)*, New Orleans, USA, 2017 [Accepted To Appear].

- **M. Behzad**, M. Masood, T. Ballal, M. Shadaydeh and T. Al-Naffouri, "Image denoising via collaborative support-agnostic recovery", Available Online: `https://arxiv.org/abs/1609.02932`.

- M. Behzad and Y. Ge, "Performance Optimization in Wireless Sensor Networks: A Novel Collaborative Compressed Sensing Approach", *The 31st IEEE International Conference on Advanced Information Networking and Applications (AINA)*, Tamkang University, Taipei, Taiwan, 2017 [Accepted To Appear].

- **M. Behzad**, N. Javaid, A. Sana, M. T. A. Khan, N. Saeed, Z. A. Khan, U. Qasim, "TSDDR: Threshold Sensitive Density Controlled Divide and Rule Routing Protocol for Wireless Sensor Networks", *The 9th IEEE International Conference on Broadband and Wireless Computing, Communication and Applications (BWCCA)*, Guangzhou, China, 2014.

- F. Saleem, Y. Moeen, **M. Behzad**, M. A. Hasnat, Z. A. Khan, U. Qasim, N. Javaid, "IDDR: Improved Density Controlled Divide-and-Rule Scheme for Energy Efficient Routing in Wireless Sensor Networks", *The 9th International Conference on Future Networks and Communications (FNC)*, Niagara Falls, Canada, 2014.

- **M. Behzad**, A. Sana, M. A. Khan, Z. Walayat, U. Qasim, Z. A. Khan, N. Javaid, "Design and Development of a Low Cost Ubiquitous Tracking System", *The 9th International Conference on Future Networks and Communications (FNC)*, Niagara Falls, Ontario, Canada, 2014.

- A. Umar, M. A. Hasnat, **M. Behzad**, I. Baseer, Z. A. Khan, U. Qasim, N. Javaid, "On Enhancing Network Reliability and Throughput for Critical-

Range Based Applications in UWSNs", *The 9th International Conference on Future Networks and Communications (FNC)*, Niagara Falls, Ontario, Canada, 2014.

- M. M. Sandhu, M. Akbar, **M. Behzad**, N. Javaid, Z. A. Khan, U. Qasim, "REEC: Reliable Energy Efficient Critical data routing in wireless body area networks", *The 9th IEEE International Conference on Broadband and Wireless Computing, Communication and Applications (BWCCA)*, Guangzhou, China, 2014.

- M. M. Sandhu, M. Akbar, **M. Behzad**, N. Javaid, Z. A. Khan, U. Qasim, "Mobility Model for WBAN", *The 9th IEEE International Conference on Broadband and Wireless Computing, Communication and Applications (BWCCA)*, Guangzhou, China, 2014.